MICROSTRUCTURAL COMPARISON OF POSITIVE FLOAT AND TRICKLE DISCHARGE OPERATIONS ON THE POSITIVE ELECTRODES OF SUBMARINE STORAGE BATTERIES WITH LEAD-CALCIUM ALLOY GRIDS

Michael Thomas Coyle

NAVAL POSTGRADUATE SCHOOL
Monterey, California

THESIS

MICROSTRUCTURAL COMPARISON OF
POSITIVE FLOAT AND TRICKLE DISCHARGE
OPERATIONS ON THE POSITIVE ELECTRODES
OF SUBMARINE STORAGE BATTERIES
WITH LEAD-CALCIUM ALLOY GRIDS

by

Michael Thomas Coyle

September 1976

Thesis Advisor: A. J. Perkins

REPORT DOCUMENTATION PAGE

READ INSTRUCTIONS BEFORE COMPLETING FORM

1. REPORT NUMBER

2. GOVT ACCESSION NO.

3. RECIPIENT'S CATALOG NUMBER

4. TITLE (and Subtitle)
Microstructural Comparison of Positive Float and Trickle Discharge Operations on the Positive Electrodes of Submarine Storage Batteries with Lead-Calcium Alloy Grids

5. TYPE OF REPORT & PERIOD COVERED
Master's Thesis; September 1976

6. PERFORMING ORG. REPORT NUMBER

7. AUTHOR(s)
Michael Thomas Coyle

8. CONTRACT OR GRANT NUMBER(s)

9. PERFORMING ORGANIZATION NAME AND ADDRESS
Naval Postgraduate School
Monterey, California 93940

10. PROGRAM ELEMENT, PROJECT, TASK AREA & WORK UNIT NUMBERS

11. CONTROLLING OFFICE NAME AND ADDRESS
Naval Postgraduate School
Monterey, California 93940

12. REPORT DATE
September 1976

13. NUMBER OF PAGES
176

14. MONITORING AGENCY NAME & ADDRESS(if different from Controlling Office)

15. SECURITY CLASS. (of this report)
Unclassified

15a. DECLASSIFICATION/DOWNGRADING SCHEDULE

16. DISTRIBUTION STATEMENT (of this Report)
Approved for public release; distribution unlimited.

17. DISTRIBUTION STATEMENT (of the abstract entered in Block 20, if different from Report)

18. SUPPLEMENTARY NOTES

19. KEY WORDS (Continue on reverse side if necessary and identify by block number)

Dendritic network	Grid surface corrosion layer
Float	Battery
Trickle-discharge	Lead-acid battery
Active material morphology	Battery capacity

20. ABSTRACT (Continue on reverse side if necessary and identify by block number)

Lead-calcium alloy grid batteries are utilized as the backup emergency power supply on non-diesel-electric submarines. Sudden and premature capacity losses have been experienced when these batteries are operated in a float mode while in standby conditions, hence a continuous drain, or trickle discharge, is maintained in lieu of float. This requires periodic battery charges to restore full capacity.

(20. ABSTRACT Continued)

The microstructural effects of float and trickle discharge operation on positive plates from small cells, manufactured from full size submarine battery plates, are studied using a scanning electron microscope. This is complemented with light microscopy observations and x-ray diffraction analysis. A patterned dendritic network of spiny crystals was discovered to be prevalent in the trickle-discharged plates. This network was seen on the grid surface corrosion layer and on a dense layer found in the internal active material. It is postulated that this network may be related to lead-sulfate dissolution upon recharge.

Microstructural Comparison of Positive Float and Trickle Discharge Operations on the Positive Electrodes of Submarine Storage Batteries with Lead-Calcium Alloy Grids

by

Michael Thomas Coyle
Lieutenant Commander, United States Navy
B.S., United States Naval Academy, 1965

Submitted in partial fulfillment of the requirements for the degree of

MASTER OF SCIENCE IN MECHANICAL ENGINEERING

from the

NAVAL POSTGRADUATE SCHOOL
September 1976

ABSTRACT

Lead calcium alloy grid batteries are utilized as the backup emergency power supply on non-diesel-electric submarines. Sudden and premature capacity losses have been experienced when these batteries are operated in a float mode while in standby conditions, hence a continuous drain, or trickle discharge, is maintained in lieu of float. This requires periodic battery charges to restore full capacity. The microstructural effects of float and trickle discharge operation on positive plates from small cells, manufactured from full size submarine battery plates, are studied using a scanning electron microscope. This is complemented with light microscopy observations and x-ray diffraction analysis. A patterned dendritic network of spiny crystals was discovered to be prevalent in the trickle-discharged plates. This network was seen on the grid surface corrosion layer and on a dense layer found in the internal active material. It is postulated that this network may be related to lead-sulfate dissolution upon recharge.

TABLE OF CONTENTS

LIST OF TABLES

LIST OF FIGURES

#63 - Exterior of grid with active material broken away. Some dendritic network is visible on the corrosion layer. Spiny crystals are also evident. 6 cycle positive plate operated in the float routine at lowered cell voltage, plate is fully charged, 2650x ----------111

#64 - Exterior of grid with active material broken away. Spiny crystals are evident in the corrosion layer. 6 cycle PbCa positive plate operated in the float routine at lowered cell voltage, plate is fully charged, 6900x ----------112

#65 - Active material, 6 cycle PbCa positive plate, operated in float routine, plate is fully charged, 690x ----------113

#66 - Active material, 12 cycle PbCa positive plate operated in the float routine, plate is fully charged, 695x ----------114

#67 - Active material, 16 cycle PbCa positive plate operated in the float routine, plate is fully charged, 680x ----------115

#68 - Active material, 16 cycle PbCa positive plate operated in the float routine, plate is fully charged. Substructure of active material showing pebbly grains, 6400x ----------117

#69 - Active material, 10 cycle PbCa positive plate operated in the trickle discharge routine, plate is fully charged. Substructure of active material showing spiny crystals and some pebbly grains, 5700x ----------118

#70 - Exterior of grid with active material broken away showing break in the dense corrosion layer covering the grid surface. 5 cycle PbCa positive plate operated in the trickle discharge routine, plate is fully charged, 2200x ----------119

#71 - Exterior of grid with active material broken away showing break in the dense corrosion layer covering the grid surface. A narrow crack in the grid metal surface is also evident. 12 cycle PbCa positive plate operated in the float routine, plate is fully charged, 3450x ----------120

ACKNOWLEDGMENT

The author wishes to extend sincere appreciation for assistance from his advisor Professor Jeff Perkins. His guidance in the data interpretation and thought organization in preparing the final manuscript was invaluable.

A special note of gratitude is due to Lt. John Pokorny, a colleague, whose help in building the test cells and maintaining them in operation, despite numerous leaks and corroded terminals, contributed significantly to the amount of data possible to be collected.

Material Science Laboratory Technician, Roy Edwards, deserves a word of thanks for his efforts to maintain the microscopy equipment, for instruction in its use, for photographs of the experimental apparatus and many more day-to-day items too numerous to list. Mechanical Engineering Department Electronics Technician, Tom Christian, warrants praise for the equipment he designed and built in support of float operation and constant current capacity test discharge.

Last, but certainly not least, the author is indebted to his wife for assistance in data collection, manuscript review, and mainly for patience and understanding.

I. INTRODUCTION

A storage battery is a device which supplies direct current electrical energy as a result of spontaneous internal chemical action, and has the ability to be recharged from an external power source; this reverses the chemical reaction of discharge, and the storage battery regains its potential to supply electrical energy.

A. HISTORICAL BACKGROUND

The contemporary storage battery evolved from Alessandro Volta's discovery of the galvanic battery in 1800 and subsequent research by several experimenters in the field of electrochemistry [1].

The principle of the lead storage battery was first discovered in 1850 by Wilhelm Siemens, and, independently, by Sinsteden [2]. In 1860 Gaston Planté presented the first lead-acid storage battery to the French Academy of Sciences. This battery resulted from his work on electrolytic polarization [1]. Planté's battery consisted of two sheets of lead separated by strips of rubber and rolled into the form of a spiral. The electrolyte was dilute (about 10%) sulfuric acid. Initially Planté formed his plates (i.e. – increased their capacity by electrochemically forming lead dioxide (PbO_2) at the positive plate and sponge lead at the negative plate) using primary batteries.

This process consumed many of these cells and took as long as one year to develop a battery's capacity.

In 1881 Faure patented a process for pasting the surface of the lead plates with a lead compound which could be readily formed into the active material of the battery. However, the adherence of the active materials to the solid lead plates was poor.

In 1882 Sellon patented a grid structure for holding the paste. The grid material was an alloy of lead and antimony. This grid is the basic design for the grids of today's lead acid storage battery.

B. THEORY AND CONSTRUCTION OF A LEAD-ACID BATTERY

The smallest complete unit of a battery is the cell (i.e., one cell could constitute a "battery"). It may consist of one or several sets of positive and negative plates. It is normal practice for lead-acid storage battery cells to have one more negative plate than the number of positive plates. For example, the TLX-39-B submarine storage battery cell contains twenty negative plates and nineteen positive plates for a total of thirty-nine. In addition to the plates, the cell contains the electrolyte, a solution capable of carrying an electric current. In the lead-acid cell the electrolyte is aqueous sulfuric acid.

Although the battery delivers and receives electrical energy via the discharge and charge processes, the energy

that is "stored" is chemical energy. The reversible conversion of this chemical energy is governed by the following reactions:

$$Pb + PbO_2 + 2H_2SO_4 \underset{\text{Charge}}{\overset{\text{Discharge}}{\rightleftharpoons}} 2H_2O + 2PbSO_4 \qquad (1)$$

On discharge, lead (Pb) is converted to lead sulfate ($PbSO_4$) at the negative plate, and lead dioxide (PbO_2) is converted into $PbSO_4$ at the positive plate. In turn, the electrolyte becomes more dilute as SO_4^{--} ions go into forming $PbSO_4$. When the battery is charged, the reverse process takes place as Pb and PbO_2 are reformed at the negative and positive plates respectively; and the acid becomes more concentrated.

The following electrochemical reactions depict the plate behavior during charge and discharge:

Positive Plate

$$PbO_2 + 4H^+ + SO_4^{=} + 2e^- \underset{\text{Charge}}{\overset{\text{Discharge}}{\rightleftharpoons}} PbSO_4 + 2H_2O \qquad (2)$$

$$E_o = 1.685 \text{ v}$$

Negative Plate

$$Pb + SO_4^{=} \underset{\text{Charge}}{\overset{\text{Discharge}}{\rightleftharpoons}} PbSO_4 + 2e^- \qquad (3)$$

$$E_o = -0.356 \text{ v}$$

The potentials indicated represent values on an oxidation potential scale relative to the H^+/H_2 electrode (i.e., the reaction: $H_2 \rightarrow 2H^+ + 2e^-$ at $E_o = 0.0$ V). During discharge the negative or lead electrode oxidizes to form lead sulfate ($PbSO_4$), while the positive or lead dixoide (PbO_2) electrode is reduced to $PbSO_4$. Thus the negative plate is operating as an anode during discharge, giving up electrons to the external circuit.

The following sketch visualizes the processes described above:

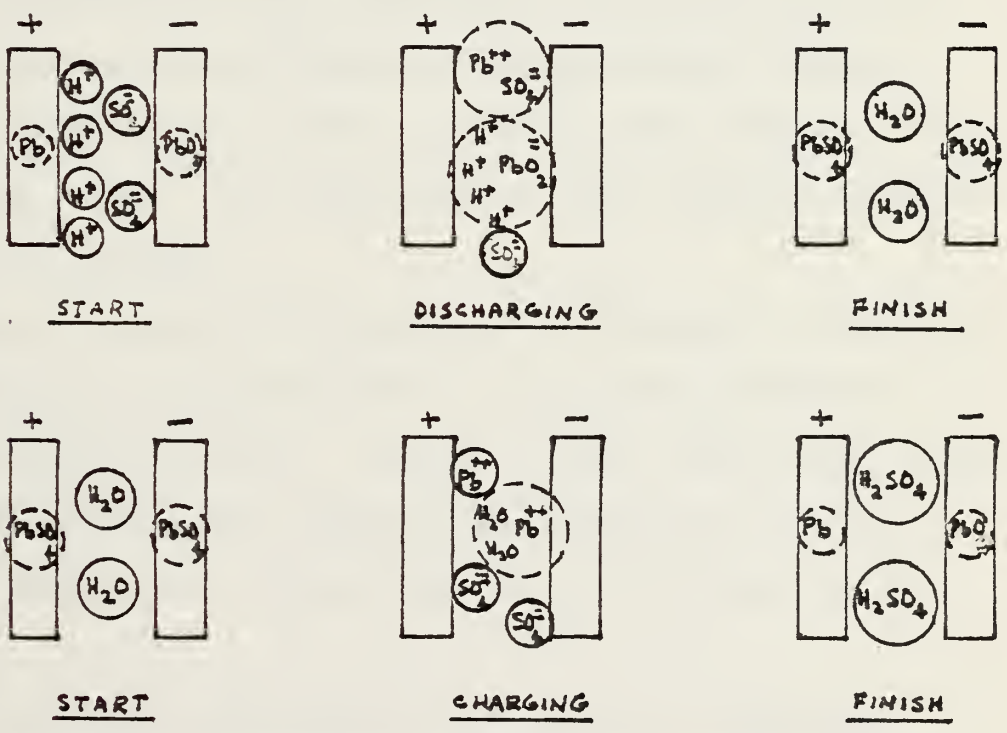

Fig. 1 — Visualization of the discharge/charge reaction

Positive plate grids in submarine batteries are made of lead based alloys containing either 4-8% antimony (for diesel-electric submarines) or up to .085% calcium (for non-diesel submarine application). These plates contain lead dioxide as the charged electrode active material.

Negative plate grids may be either pure lead, lead alloyed with 4% antimony (diesel electric submarines), or lead alloyed with up to .085% calcium (non-diesel electric submarines). The charged electrode contains sponge lead as the active material.

The purpose of using lead based alloys for the plate grids is because of the need to increase their rigidity and also to promote the ease of casting the intricate shapes used in the grids. As noted earlier, the earliest alloying element was antimony.

Lead and antimony form an alloy system with a eutectic composition at 87 per cent lead — 13 per cent antimony, melting at 247°C (477°F). Figure 2 shows the microstructure of a lead-antimony grid used in the battery of a diesel-electric submarine. Figure 3 is the Pb - Sb binary phase diagram.

The corrosion resistance of the alloy is improved by the addition of a small percentage of arsenic; usually about .05%.

The presence of antimony in the alloy has some major disadvantages; especially for standby service in the closed

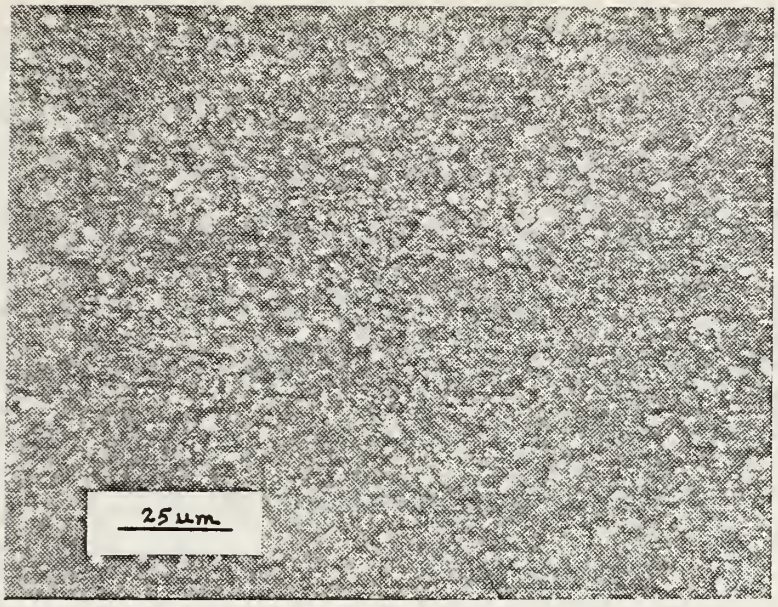

Figure 2. Microstructure of a 0-cycle PbSb grid bar from a diesel electric submarine battery, 600x

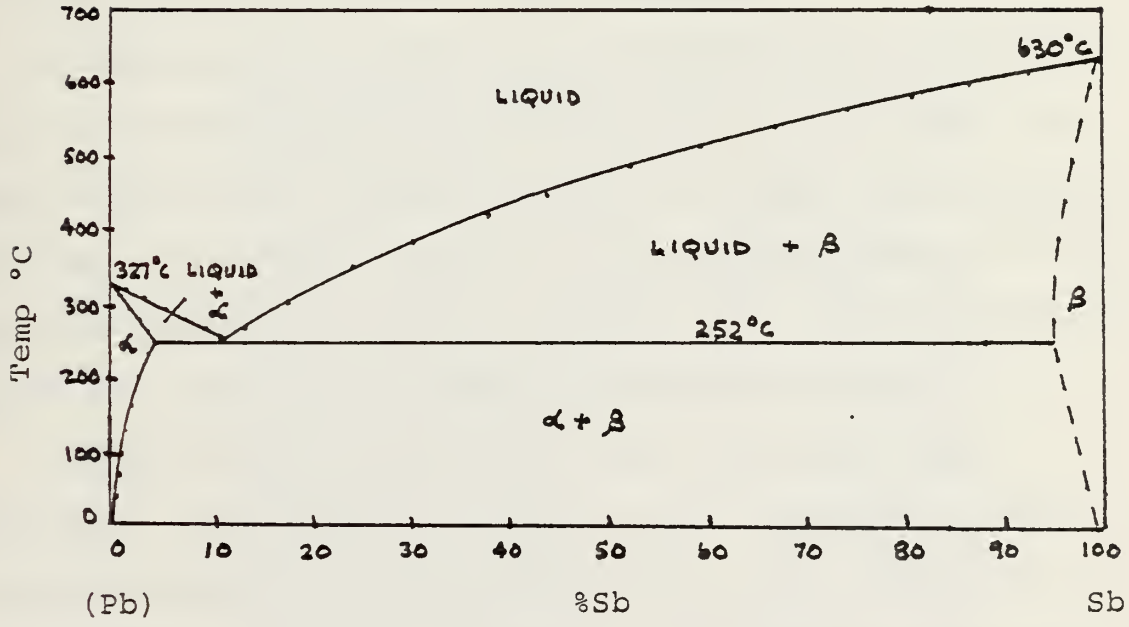

Figure 3. Binary phase diagram of lead and antimony [2]

atmosphere of a non-diesel electric submarine. Antimony is leached from the grid metal, causing an increased rate of self discharge at both the negative and positive plates. Antimony also has a low hydrogen over voltage; its accumulation on the surface of the negative electrode interferes with charging because hydrogen will be liberated instead of the reduction of $PbSO_4$. In addition, toxic arsine gas is continuously generated during operation as is SbH_3 (stibine gas) when the battery is on charge.

As a consequence of these shortcomings associated with the use of antimony, calcium has been found to be a successful rival. In 1936 Haring of the Bell Telephone Laboratories patented the use of calcium lead as a grid material after a study of all the alkali earth materials.

Calcium has a limited solid solubility in lead of 0.52 at.% (0.10 wt%) at 328° C and 0.052 at. % (0.01 wt%) at room temperature. Figure 4 shows the binary phase diagram of lead and calcium. Figure 5 is a photomicrograph of the microstructure of a lead-calcium grid bar from the positive plate of a non-diesel electric submarine battery.

Despite very limited solubility, the alloy shows excellent precipitation hardening and exhibits a tensile strength close to that of 12% antimony alloy. With such a small amount of alloying addition, lead-calcium alloy has a microstructure similar to pure lead; but, because of the precipitation hardening that has occurred, it is much harder;

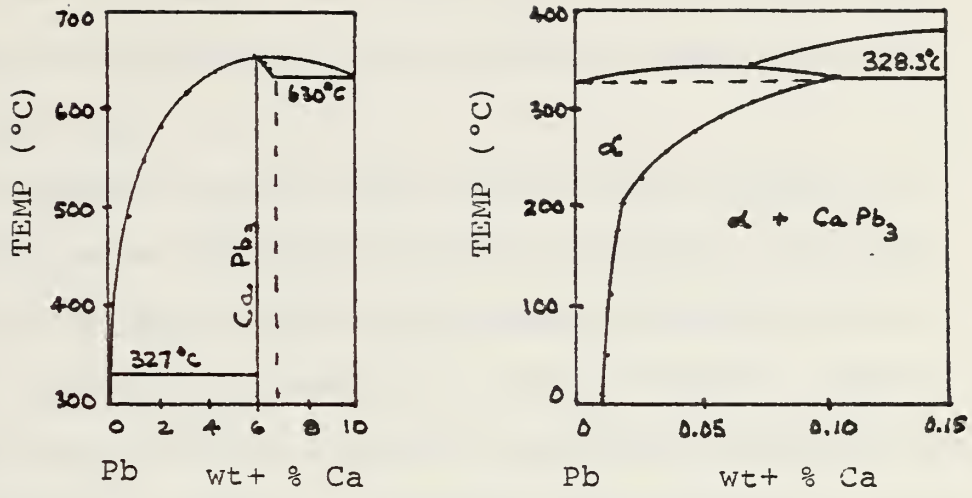

Figure 4 — Binary phase diagram of lead and calcium. [2]

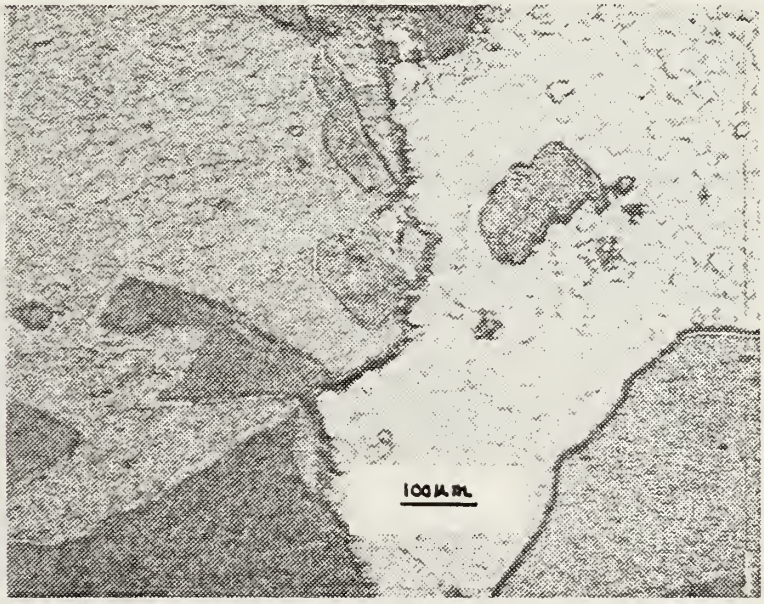

Figure 5 — Microstructure of 0-cycle Pb - Ca grid bar from a non-diesel electric submarine battery, 100x

has superior tensile strength; and shows less tendency to recrystallize at room temperature. When proper casting conditions are used, the lead-calcium alloy shows less tendency to corrode by inter-granular attack than does pure lead [9].

In addition to the lower rate of self-discharge by lead-calcium as compared with lead-antimony, the lead calcium alloy has a higher hydrogen overvoltage which causes less hydrogen generation during charge. Lead-calcium alloy is also a better electrical conductor than lead-antimony. Table 1, obtained from Reference 4, compares two stationary batteries which were identical except for grid alloy.

Table I

Float Behavior of Stationary Batteries

	New 1000 AH Cells Floated @ 77° F.	
	Calcium	Antimony
Float Voltage - Normal - Volts/Cell	2.17	2.17
Float Current - Milliamperes	40	200
Hydrogen Evolution, cc/hr./cell	4.56	91
Total Water Use, cc/yr./cell	130	630
Watering Interval, Years, Max.	10	2

Lead-calcium alloy grids are not without problems, however. Service failures due to abnormal growth have occurred in pressure cast lead-calcium alloy positive grids when used for float applications. More will be said about float operation later in this paper. Other problems noted in cycling have been premature grid corrosion, softening of the active material, and sharply reduced capacity without visible sign of change [9].

The active material (i.e., that which undergoes reversible electro-chemical reactions) in the fully charged positive electrode is lead dioxide (PbO_2). PbO_2 is a non-stoichiometric compound, a powerful oxidizing agent, which is insoluble in sulfuric acid H_2SO_4 [9]. It exists in two polymorphic forms; the orthorhombic low temperature α-form (columbite type) and the tetragonal high temperature β-form (plattnerite) [9,11].

The bare grid is initially pasted with a mixture of lead oxides, basic lead sulfates, sulfuric acid, and water. Following pasting, the plates are assembled into cells, filled with a dilute sulfuric acid, and given a "forming" charge which electro-chemically produces PbO_2 via anodization.

The active material in the negative electrode is sponge lead. The paste used for these plates is similar to that used in the positive with the exception that it contains barium sulfate and other organic materials such as lignin which optimize surface area and increase porosity. During

formation these plates are made the cathode and the lead oxides are reduced to sponge lead.

Other cell components include separators and retainers. The separators are microporous insulators used to separate and electrically isolate the positive and negative plates. They are freely permeable to the electrolyte but have no openings which would permit trees of active material to grow between the plates and cause internal short circuits. Retainers are fiberglass mats which are placed between the separator and the positive plate. They serve to prevent shedding of the positive active material.

The limitations associated with the electrode reactions of the lead-acid cell are primarily those of mass transport and ionic diffusion. The electro-chemical reaction of discharge results in a deposition of crystals of $PbSO_4$ on the surface and in the pores of the solid electrodes. This causes a decrease in pore diameter that in turn interferes with free access of electrolyte into the plate interior. The H_2SO_4 within the pores of the plates becomes diluted and the relatively slow rate of diffusion from the bulk of the electrolyte further limits plate reaction. In addition, the $PbSO_4$ forms on the surface of the active materials. Since it is a nonconductor, this reduces the amount of area available for electrochemical reactions. The discharge process does not consume all of the active material; hence the residual, unused active material serves

as an electrically conducting network in the plates and provides a readily available site for the recharge process [9].

II. DEFINING THE PROBLEM

The purpose of the main storage battery in submarines is to provide electrical and propulsion power when the engines are not available. In diesel-electric submarines, the battery is the principal power supply when submerged and a secondary source when the submarine is on the surface or snorkeling so that the engines may be used. In non-diesel-electric submarines, the battery is a secondary energy source to back up the power plant [3].

For reasons noted previously, the lead-calcium grid alloy has been chosen as the type of storage battery to be used in non-diesel-electric submarines. Due to high reliability of the primary power source for these ships, their batteries see only limited use. Typical service conditions are characterized by long periods of standby operation punctuated by infrequent, high-rate discharges which consume a fraction of the total capacity. These discharges are followed by rapid, modified-constant potential charges as specified in Ref. 3.

In many respects, this type of service life is similar to that of the reserve power supplies in telephone central stations. It was in this use that lead-calcium was first introduced as the positive plate grid material and is today its major application.

The focus of the problem is the maintenance of the battery in the standby mode. In telephone service and in other services where a battery is installed in parallel with a primary power source across the load, a float condition is specified. Float is the maintenance of a battery at a constant voltage slightly above its open circuit potential. The purpose of this operation is to maintain a fully charged battery as a standby emergency power source requiring a minimum of attention. The positive plates properly float at a constant polarization just slightly above its open circuit value, where the grid corrosion rate is low. In floating lead calcium cells, the line voltage can vary over a large range; but these variations are not reflected in large surges of current or changes in positive plate polarization. The negative plate voltages will change with line fluctuations, and may safely be subjected to considerable changes in polarization [12]. Polarization refers to changes in cell voltage caused by current passing through the cell. It is measured with respect to a fixed reference electrode.

References 12 and 13 discuss requirements for proper float operation. All floating cells must have nearly the same developed plate surface areas in order to float together simultaneously. Smaller negative plate areas result in the cells polarizing at float voltage not sufficiently high enough to keep the positive plates above open circuit potential; hence, the positives would spend much time partially

discharged leading to growth of large electrically passivating $PbSO_4$ crystals. Several cells floating together would be governed by the cell with the smallest negative plate area. On the other hand, if negative plate area were too large, positive plate polarization variations would occur leading to increased grid corrosion.

Since float is the optimum standby condition for these batteries, this method of operation was specified when lead-calcium grid batteries were introduced into non-diesel-electric submarine service. However, some batteries experienced rapid loss of capacity when operated on the full float routine. Inasmuch as this capacity loss was unexpected and its occurrence could not be predicted, float operation was terminated; and a modified standby operation of "trickle-discharging" was specified by technical authority [3].

Trickle discharging is a very slow drain, nominally 5 amperes for a 5000 ampere-hour capacity battery. Its use has resulted in retention of high capacity throughout the useful life; however, it does have the following operational disadvantages:

a. Useful battery cycle life is wasted (for the TLX-39B battery trickle discharging will consume 47.5 discharge-charge cycles of 5000 ampere-hours capacity during the manufacturers guaranteed life of 66 months; the manufacturer also guarantees 165 cycles) [35].

b. Periodic battery charges are required in order to restore the battery to full capacity.

c. Water additions are needed more frequently.

d. Positive grid corrosion is increased.

This problem was studied extensively by Burbank and Wales [5,12,14,15]. They tested full scale submarine cells and small cells fabricated from submarine battery plates. Capacity loss was noted to be accompanied by softening of the positive plate active material which shed badly during gassing periods. In addition, they noted no electrochemical or microscopic evidence of a barrier layer as had been suggested to them by contemporary battery manufacturers. Reference 5 also contains a summary from an at sea test conducted aboard USS Skipjack (SSN-585). It concluded that, in shipboard use, the battery was receiving adequate charge and floating normally most of the time. Demands were not excessive, nor was there any evidence that the service could be counted as a cause of failure.

Burbank's testing routine consisted of daily shallow discharges with float recharge, and capcity was measured every two weeks by capacity discharges at the six-hour rate. On occasions when this routine was interrupted, float was continued until testing began again. In other work, [11], Burbank noted that the major difference between failing and successful submarine type Pb - Ca positive plates in float service was a startling contrast in the morphology of PbO_2 as examined by electron microscopy. Positive

battery plates that contained mostly nondescript pebble-like nodular PbO_2 particles were found to soften and fail. Plates made up of PbO_2 particles that were prismatic needles with many branches, possibly twinned, maintained capacity and retained a firm texture.

Tudor, Weisstuch, and Davang [16] concluded that the failure of thin-plate (0.43cm) Pb - Ca grid positive plates was caused by a rapid formation of a $PbSO_4$ barrier layer surrounding the grids, with positive plate shedding being only a minor factor. They did conclude, however, that thick plate (0.64cm) Pb - Ca grid cells lost capacity slowly, initially as a result of softening and shedding of positive active material; and as effective positive plate thickness decreased, grid sulfation became an additional factor reducing capacity.

The testing routine employed in Tudor et. al.'s research consisted of:

1. Charge at 2.25 v/cell with
2. A one-hour shallow discharge at approximately the six-hour rate each working day followed by
3. A two hour constant current charge at 2-3 amps, then return to charge at 2.25 v/cell. Every two weeks the cells received a capacity discharge at the same rate as above to 1.75 v/cell; followed by overnight constant current charge to gassing (16 hour rate).

Ruetschi [17] concluded that the reasons for failure of calcium-alloy positive plates after relatively short

periods of float was connected with a problem of contact between the grid and active material. He postulated that at float voltages PbO forms in the corrosion layer close to the grid and that this eventually serves to isolate the active material from the grid. In related work on industrial and automotive batteries, Mao, Larson and Rao [10] noted that pressure cast lead-calcium alloy positive grids for float applications can cause some unexpected service failures due to abnormal growth. Simon [18] conducted optical microscopic examination of commercial battery plates obtained from several manufacturers and representing various stages in manufacturing and use. He observed a "reticulate" network, which he concluded was composed of α - PbO_2; and noted that this structure resulted in improved capacity and prevented softening and shedding of active material in plates which had been floated for long periods. He conjectured that this network is continuous through the plate and tends to act as a supporting grid for the remainder of the active material.

Although floated Pb - Ca alloy grid batteries have displayed a tendency to prematurely lose capacity, it has been noted that this capacity is recoverable by reverting to shallow, low-rate discharges (i.e., trickle discharge). Reference 19 discusses a Pb - Ca alloy positive grid battery that had been on a modified float schedule for approximately 17 months, at which time capacity had dropped to 36% of initial capacity. The battery was then placed on a trickle

discharge routine for ten months and capacity increased to 87%. Burbank and Wales [5] also noted recovery of capacity by shifting to a shallow, low-rate discharge.

The exact mechanisms by which submarine lead-calcium alloy grid batteries lose capacity on float and how trickle discharging functions to preserve this capacity is obviously not well understood. It is also possible, as suggested by Simon in Ref. 18, that a similar capacity loss has been present and undetected in lead-antimony batteries.

The purpose of this research is to study lead calcium grid batteries in float and trickle discharge operation, as well as a lead antimony grid battery on float, and to compare trends in microstructural behavior. It is intended that the operating conditions will simulate service which would be similar to that found in submarine use. Utilization of the scanning electron microscope (SEM) will be the principal analytical method, augmented by optical microscopy and x-ray analysis.

III. EXPERIMENTAL PROCEDURES

A. BATTERY CONSTRUCTION

A full size lead-antimony grid diesel-electric submarine battery cell (TPX-61E) was obtained from Mare Island Naval Shipyard. This cell was dry and ready for filling and initial charging. In addition, nine formed plates (3 positive and 6 negative) from a lead-calcium grid, non-diesel-electric submarine battery (TLX-39B) were obtained from Gould, Inc. These plates were cut into approximately 11.5 cm by 13 cm sections for use in small three plate (2 negative and 1 positive) cells for laboratory testing. Dimensions varied slightly between PbCa and PbSb plates due to locations of grid bars. PbCa positive plates were 0.48-0.50 cm thick, while the PbSb positives were 0.42-0.45 cm.

Cell jars were manufactured from .25 inch (.635 cm) plexiglass; inner dimensions were 15.5 cm high by 12.75 cm wide by 5 cm deep. Suitably sized separators (11.7 cm by 13.9 cm) were cut from the full size ribbed, porous, hard rubber separators contained in the TPX-61E cell. These separators were used in both the PbCa and PbSb miniature cells. Fiberglass mats from the full sized cell were cut and placed against the positive plates. In addition, positive and negative plate binding strips cut from the full sized cell were used. Figures 6 and 7 show the assembly of these cells.

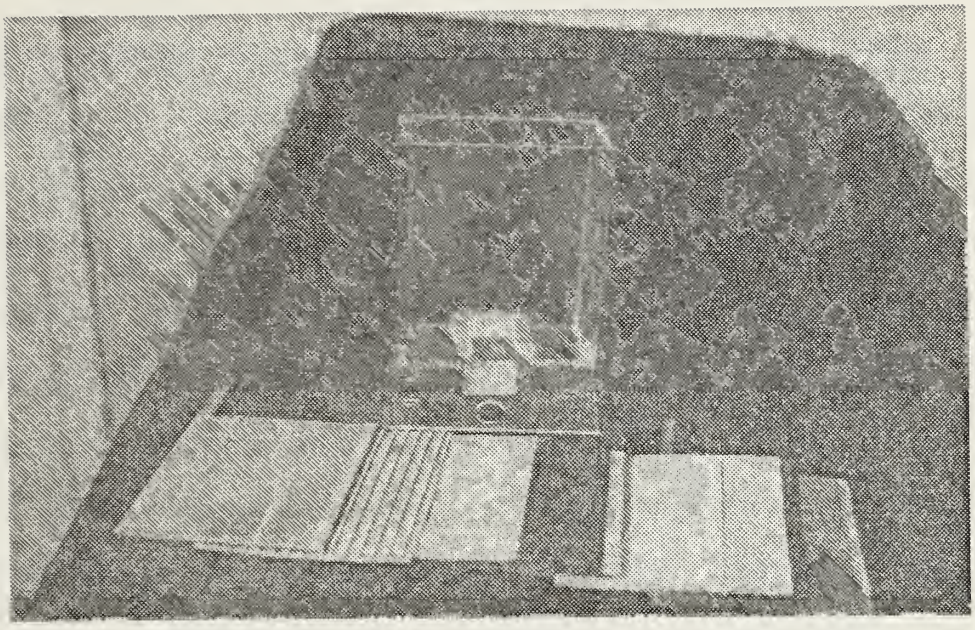

Figure 6 – The components of a PbCa cell in the disassembled condition

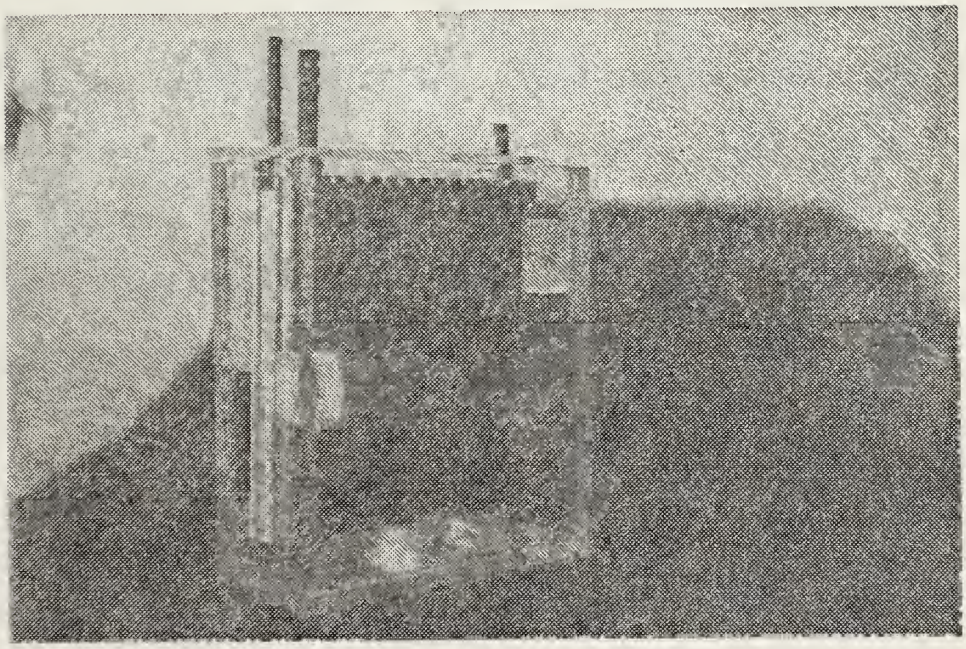

Figure 7 – The assembled PbCa cell

It should be noted that the microporous separators were installed in a reverse position from that specified in Ref. 20. This was not done intentionally, however, once it was discovered it was decided to continue with this installation in order to have consistent results. Pokorny [32], in associated work, evaluated the effect of the separator reversal and determined that it had no detectable effect on capacity. This was probably due to an excess loading of electrolyte to active material and the use of fiberglass retainer mats next to the positive plate.

Cell electrolyte was prepared in accordance with Ref. 3 using analytical reagent H_2SO_4, specific gravity 1.84. The specific gravity of the electrolyte was nominally maintained between 1.295 and 1.275 for the PbCa cells and between 1.275 and 1.255 for the PbSb cells specified in Ref. 3.

The plates were rigidly installed in the cells using scraps of plexiglass. Plexiglass covers, 0.125 inches (0.32 cm) thick, were glued on top of the jar. These covers had three small holes drilled for the one positive and two negative plate terminal posts, and had one service opening, 2 cm in diameter.

The cells were then connected using bus bars manufactured from scraps of lead obtained from cutting the full size plates. The bus bars were fastened to the terminal posts using stainless steel screws (2-56/64). In order to facilitate the operational routines, three cells were

connected together to form a battery. These batteries were designated as follows:

PbCa #1	(Trickle Discharge)
PbCa #2	(Float)
PbSb	(Float)

During the course of testing, five cells were operated in each battery, for various lengths of service cycles. This was accomplished by two cell replacements per battery.

Figure 8 shows a typical three cell battery assembly, and Figure 9 shows all three batteries in operation.

B. OPERATION

The cells were filled with prepared electrolyte in concentrations specified for the respective batteries (1.255 for the TLX-39B PbCa and 1.235 for the TPX-61E PbSb). Prior to the initial charge, the batteries were allowed to stand approximately fifteen hours in order to cool [20, 22]. The initial constant current charge rate for the PbCa cells was 0.51 amps based on suggestions provided by the manufacturer [21]. The PbSb cells were charged for the first time at 0.66 amps. The initial charge duration was set at a minimum of 65 hours and continued until cell voltages and specific gravities stabilized.

Following the initial charge, several conditioning discharge/charge cycles were conducted in order to develop cell capacity. In addition, the first cycles conducted on

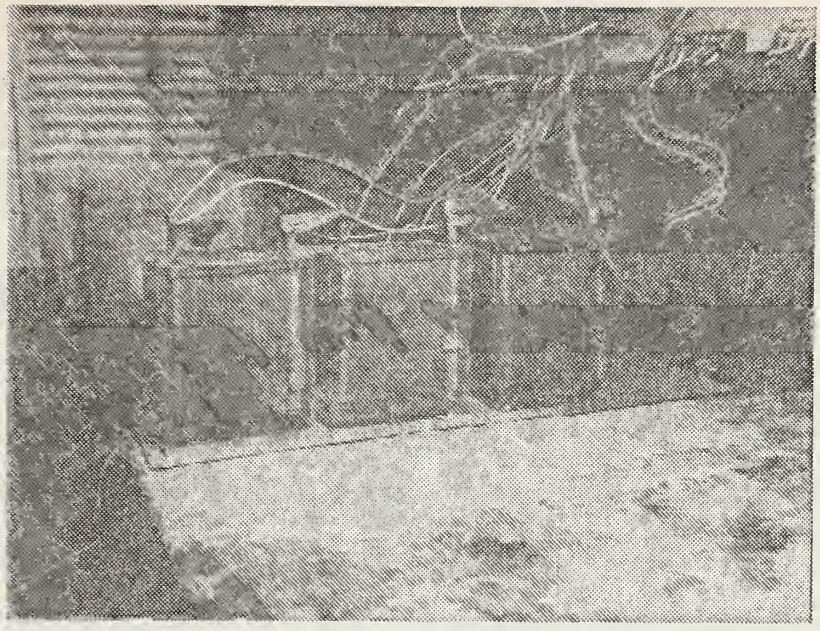

Figure 8 — Typical three cell battery assembly.

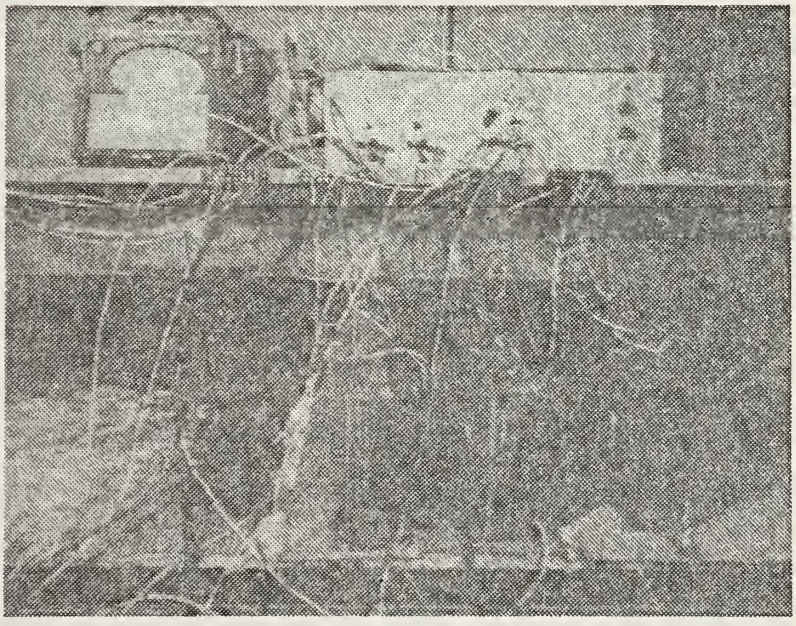

Figure 9 — All three batteries in operation (PbCa #2, PbCa #1, PbSb).

PbCa #1 were used to determine parameters such as finishing rate, capacity test discharge rates, and the trickle discharge rate. Parameters for the PbSb cells had been determined by Pokorny in related work [32].

Following initial testing, the three-cell batteries were placed on routines of four days float (PbCa #2 and PbSb) or trickle discharge (PbCa #1) with a capacity test discharge followed by a charge on the fifth day. PbCa #1 was given a charge prior to each capacity test discharge.

PbCa #1 was trickle discharged between discharge/charge cycles at about 50 milliamperes (+5ma,-0ma) which corresponds to approximately 0.33 ma/cm^2 based on the planar surface area (13 cm by 11.5 cm) of each face of a positive plate. The discharge rate was regulated by a small slide wire resistor.

PbCa #2 and PbSb were floated during standby periods using a dual, independent power supply (see Appendix A) manufactured specifically for this purpose by Mr. Tom Christian of the U.S. Naval Postgraduate School. Each power supply had a range of 25 VDC with a maximum current of 75 milliamperes. These equipment limitations were well in excess of float requirements since the cells were not put on float until the completion of a constant potential charge.

The individual cell float voltage ranges selected were 2.32 - 2.36 for PbCa #2 and 2.25 - 2.29 for PbSb. These values were selected based on the specific gravity ranges of these batteries. This procedure worked well until cell

replacement was conducted. The new cell float voltages ran much lower than those of the older cells, and float voltage imbalances were experienced until several cycles had been conducted on the replacements. Appendix B shows how float voltages varied. Since the dual power supply voltage was relatively free from perturbations, only small, slow float voltage transients occurred. Periodic plate voltage measurements referenced to a cadmium electrode showed these fluctuations to be absorbed by the negative plates.

As noted earlier, capacity test discharges were conducted about every fifth day. PbCa #2 and PbSb were put on discharge directly from a float condition, whereas PbCa #1 was charged from its partially discharged (trickle discharged) state prior to test discharge. Discharges were automatically terminated when battery voltage dropped to 4.8 volts. This was accomplished by another control circuit manufactured by Mr. Christian (Appendix A). Discharges were monitored by a two-channel Honeywell-Electronix 194 strip recorder. One channel was set up on the total battery voltage and the other on one of the three operating cells, usually the one previously determined to be the limiting cell. In addition, a two channel Hewlett-Packard Model 7100B strip chart recorder was used periodically to monitor one cell's positive and negative plate voltages referenced to a cadmium electrode. This was done in order to confirm that the positive plate capacity was limiting the discharge.

Initially it was intended to discharge the PbCa batteries at the three hour rate and the PbSb at the six-hour rate as specified in Ref. 3. These rates were determined based on initial test discharges using Peukert's equation as indicated in Ref. 1, and were set at 4.5 amps (30 ma/cm^2) for the PbCa and 3.4 amps (22.7 ma/cm^2) for the PbSb. In actuality, the PbCa rate was too low and the PbSb rate too high; however, they were close enough to satisfy the test objectives.

As noted earlier, total battery voltage was used as the limiting parameter on discharge vice cell voltage. This resulted in occasional deep discharges in individual cells. While this is not the optimum situation, it was necessary based on test equipment limitations. Appendix C contains a record of the test discharges.

In order to have a valid basis for comparing the service lifetime of cells subjected to either trickle discharge or float routine, an operational cycle was determined as follows:

- for the floated cells an operational cycle consisted of a period of float (nominally four days) followed by a capacity test discharge and recharge.
- for the trickle-discharged cells it was a period of trickle-discharge (nominally four days) followed by a battery charge, capacity test-discharge, and recharge.

Battery charges were conducted in accordance with Ref. 3. All charges were of the constant-potential mode with some overcharge. The potential chosen was limited to a value such that hydrogen and oxygen gas generation did not take place. This voltage was dependent on temperature, and tables for determining its value are located in Ref. 3 under the title of temperature-voltage-gassing (TVG). The nominal TVG cell voltage for 80° F is 2.38. Prior to the completion of charge, the battery voltage was allowed to rise at a constant current, or finishing rate, until it reached the maximum temperature corrected voltage as specified in Table 9623-13 of Ref. 3. At 80° F this voltage was 2.66 volts per cell. The finishing rates chosen for these batteries were: 0.8 amps for the PbCa and 1.0 amps for the Pb - Sb. During the overcharge period, while the battery voltage is rising on the finishing rate, hydrogen gas generation takes place at the negative plates and oxygen evolves at the positives. During the constant potential portion of the charge, the charging rate initially rose as the resistive lead sulfate ($PbSO_4$) network opposed the passage of current through the plates. Later, after a conducting path was established in the active material, current gradually dropped until the finishing rate was reached.

Battery charges were performed using a Hewlett-Packard Model 6434B DC Power Supply (0 - 40 VDC; 0 - 25 amps) augmented by a Kepco Model Ck 18-3M DC Power Supply (0 - 18

VDC; 0-3 amps). Both of these power supplies were configured for constant potential operation using remote (battery voltage) sensing. Figure 10 shows these power supplies.

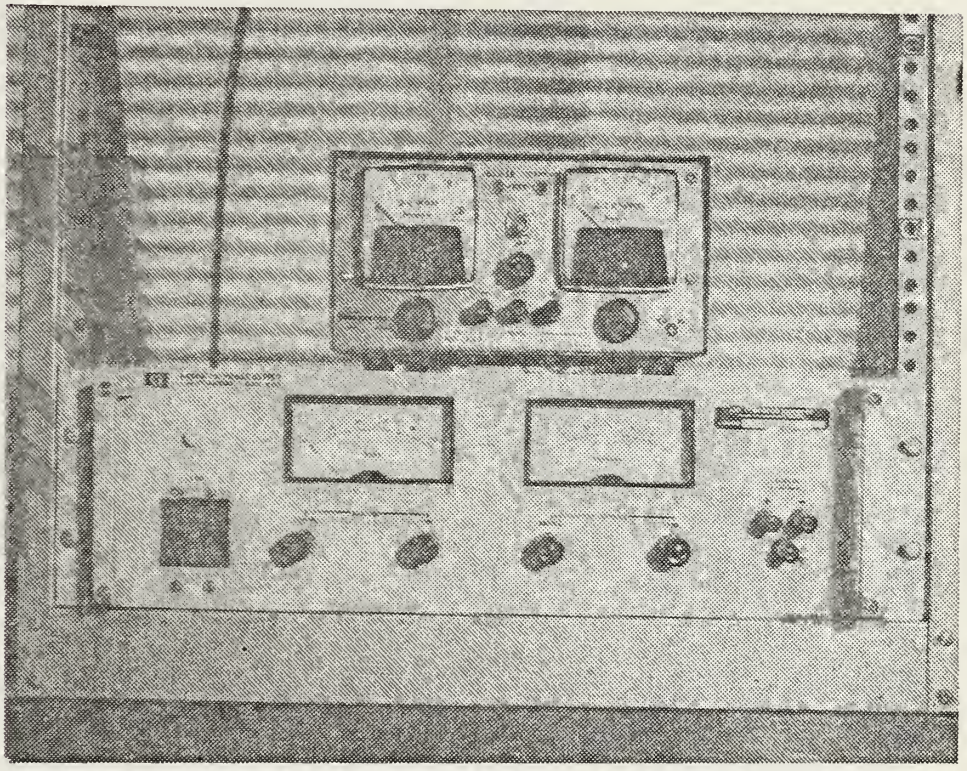

Figure 10 - Kepco Model CK 18-3M and Hewlett-Packard Model 6434B DC Power Supplies.

Electrolyte specific gravities and individual cell voltages were measured daily, following test discharges, and at the completion of battery charges. Appendix B contains a record of the average values of these readings during each cycle. Specific gravities were determined using a standard submarine floating hydrometer kit. Voltages were measured using a DANA Digital Voltmeter and temperatures were obtained using a standard laboratory floating thermometer

(30 - 100° F). Specific gravity readings were corrected for temperature in accordance with Article 9623.305 of Ref. 3.

In order to closely evaluate the microstructural changes in the positive plates during discrete stages of battery life, replacement cells were introduced at certain intervals. The following table shows the various operational cycle histories:

Table II

Cell Life History for Each Battery

PbCa #1		PbCa #2		PbSb	
Cell	Cycles	Cell	Cycles	Cell	Cycles
1	4	1	4	3	4
5	5	5	6	5	4
3	7	2	10	1	9
4	10	4	12	4	9
2	13	3	16	2	13

Since each battery operated with three cells, there were two cell replacements per battery during the test period.

C. ANALYSIS

The major microstructural analysis instrument employed was the S4-10 Stereoscan Scanning Electron Microscope (SEM). The SEM is an extremely useful device for conducting this type of research due to its relatively high useful magnification (about 12,000x), excellent depth of field (about 100

microns at 1000x), and the ease of sample preparation when compared with requirements for light microscopy and transmission electron microscopy (TEM).

The SEM, shown in Figure 11, detects and displays information derived from the action of an electron probe scanning the surface of a specimen. The resultant image has a three-dimensional appearance.

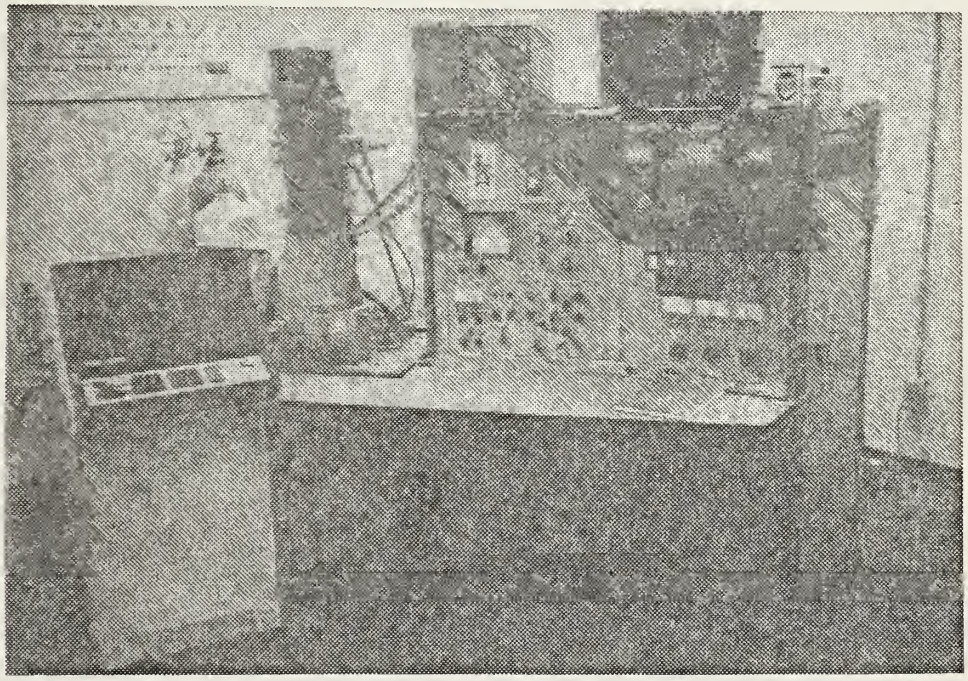

Figure 11 - Cambridge Model S4-10 scanning electron microscope and Princeton-Gamma-Tech PGT-1000 x-ray Analyzer.

The electron probe is formed from a primary beam of electrons, focused to a fine spot on the surface of the specimen by a system of electromagnetic lenses. Low-energy electrons leaving the surface of the specimen due to the action of the electron probe are attracted towards the electron collection system. This consists of an electrostatic focusing electrode and a scintillator optically

coupled to a photomultiplier. Electrons impinging upon the scintillator release photons which travel along a light-guide to the photo-cathode of the photomultiplier. Signals from the photomultiplier are passed through a head amplifier to video amplifier and then to a visual display unit, where the amplified signals modulate the brightness of the cathode ray tube beam. This beam scans the tube face on the display unit in synchronism with the scanning of the specimen by the electron probe. The resultant image has a three-dimensional appearance because contrast is produced by the variation in the number of electrons emitted or reflected from different parts of the specimen. In order that the image can be photographed, a second display unit is provided on which a camera can be mounted [23].

The specimen to be observed is mounted on a metallic stub and cemented with conducting paint. It is then placed on a specimen stage in an evacuated chamber and bombarded with an electron beam as noted above. The operator has the ability to translate the stage in the x, y, and z directions; rotate it 360°; and view the specimen at angles of incidence from about 0° to 90°.

The SEM at the Naval Postgraduate School is coupled to a Princeton-Gamma-Tech (PGT-1000) energy-dispersive x-ray analyzer. This device is capable of elemental analysis through detection of characteristic x-ray energy associated with electron transitions in the outer shells

of material being scanned. No major use was made of this capability, since it was not possible to discriminate between lead and sulfur, which were two of the major elements encountered in plate analysis.

Positive plates were removed from the cell and washed for about five minutes in cold tap water. The washing process involved immersing the plate in a beaker of water for a short period to allow the tap water to displace the electrolyte from its internal pores. Then the plate was laid over the top of the beaker; and, one side at a time, was rinsed by directing a stream of water over the surface. No mechanical cleaning or blotting with paper was attempted. After washing, the plate was allowed to dry for twenty-four hours in an oven set for a temperature range of 65 - 70° C (150 - 158° F). The plates were sectioned using a jewelers saw. The active material was broken away from the grid using needlenose pliars. This allowed direct examination of the grid-active material interface on both the grid and on the active material. In addition, pieces of active material from the planar face of the plate were obtained. The pieces to be observed varied considerably in size but fit easily on the 1.2 cm diameter stubs. Prior to putting the specimen in the SEM, it was examined under a Bausch + Lomb Model SFB-2 Stereozoom Microscope (7x - 30x) in order to identify principal features to serve as reference points while using the SEM.

Photographs were taken with an attached polaroid camera (Tektronix Oscilloscope Camera C-27) configured with a Polaroid 545 Land Camera Film Holder. The film used was Polaroid 4 x 5 Land Film Type 55 (positive/negative).

A limited amount of optical light microscopy was also undertaken using a Bausch + Lomb Dynazoom Bench Metallograph Model 32. The principal features studied using this method were the grid - active material interface and the grid metal microstructure. Samples were cold mounted using a Buehler Plastic Kit (No. 20-3550). Samples containing active material were vacuum impregnated in order to fill the pores using an apparatus built by Mr. Roy Edwards of the Naval Postgraduate School (Figure 12).

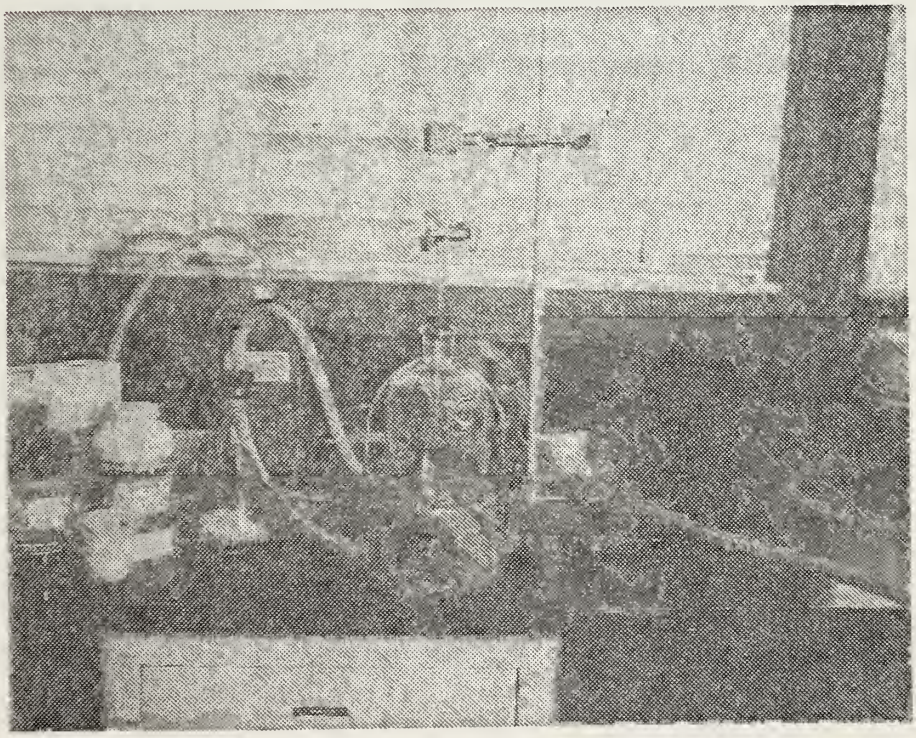

Figure 12 - Vacuum Impregnation Equipment

All specimens were ground with #320 SiC grit paper on a grinding belt then hand sanded on 0 and 3/0 grit paper. The time in each process varied depending on the surface scratches. The specimen was rotated 90° between each step. The grid - active material specimens were dry-polished for several hours, using 1.0 micron, alumina powder, on a vibratory polisher until the desired surface was obtained. Grid bar specimens were polished on two rotary wheels using 0.3 and .05 micron Al_2O_3 slurries. Only the grid bar specimens were etched using an etchant of 2 parts glacial acetic and one part hydrogen peroxide. Etching was done until grains were visible to the naked eye (5 - 10 seconds), then the specimen was washed with tap water, dried with alcohol and hot air, and then examined under the microscope.

Photomicrographs were obtained using the camera attachment on the metallograph. This attachment was configured with a Type 405 Polaroid Land Film Holder.

In order to determine prevalent compounds, x-ray powder diffraction patterns were run on active material samples using a Norelco water-cooled x-ray diffraction unit configured with a wide range goniometer and coupled to a Norelco Data Control and Processor (Figure 13). Samples were prepared from pieces broken out of positive plate active material pellets. It was ground to a fine powder using a mortar and pestle then mounted in a specimen holder.

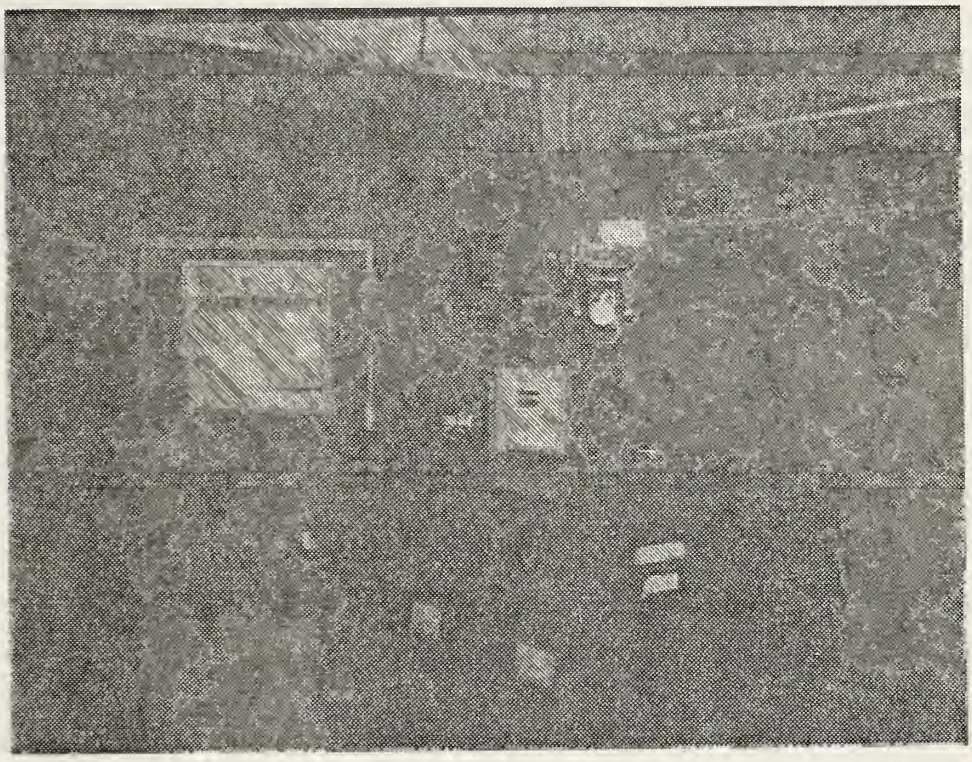

Figure 13 - Norelco water cooled x-ray diffraction unit with wide range goniometer, and data control and processor.

IV. EXPERIMENTAL RESULTS AND DISCUSSION

A. SERVICE PERFORMANCE

The primary measure of service performance was the capacity test discharge. As noted earlier, the rate chosen for the lead-calcium alloy grid batteries was 4.5 amps (30 ma/cm^2), while 3.4 amps (22.7 ma/cm^2) was used for the lead-antimony cells. Appendix C contains the record of capacity test discharges for all three batteries.

Figure 14 graphically depicts the performance of PbCa #1, the trickle discharged battery. In analyzing this data and a similar graph for PbCa #1 (the floated lead calcium battery), it must be recognized that no one cell governed the battery's performance throughout the test period. For PbCa #1, test discharge duration was generally governed by the newest cell. Dashed lines approximate the developing capacity in cells #3, #4, and #5. As can be seen, cell #5 capacity was still increasing after 5 operational cycles. Since cell #3 was taken out of service when #5 was brought on, it was not ascertained whether it's capacity would have leveled out and taken over after the first few cycles on cell #5. Cell #2, which was the oldest in numbers of cycles, was monitored on the final discharge. It only dropped to 1.89 volts at the completion of discharge and appeared to still have capacity remaining based on the slope of the strip recorder plot of voltage versus time.

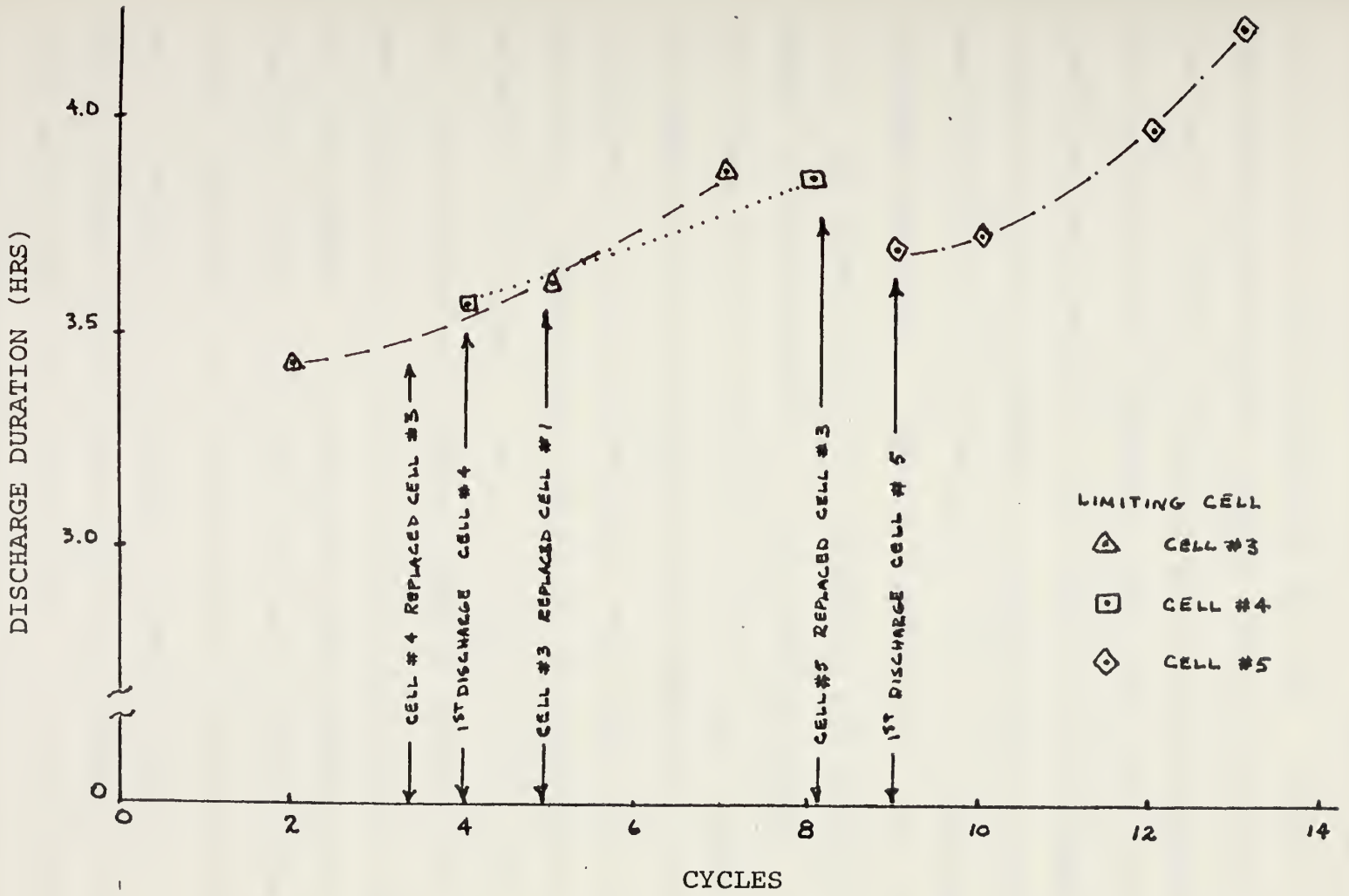

Figure 14 — Capacity vs. Cycles PbCa #1 - Trickle Discharge

In comparison, Figure 15 shows the capacity versus cycles for PbCa #2, the floated lead calcium grid battery. Following the replacement of cell #1, capacity was governed by cell #3 for the remainder of the test. Cells #4 and #5 developed enough capacity during conditioning cycles that they had no effect on limiting test discharge duration. The leveling out of capacity by cell #3 is consistent with predicted performance [1], and agrees with contemporary results obtained by Pokorny in cycling tests of similar lead calcium alloy grid batteries [32]. The difference in discharge durations by PbCa #1 and PbCa #2 is not particularly significant since this parameter was governed by the amount of active material in the positive plates. Although the plates were all fabricated from the same larger plate, the sizes of the grid members varied somewhat in various locations in the full size plate; where they were larger, there was a corresponding reduction in the amount of active material. For example, cell #1 of PbCa #2 had seven thick (0.6 cm) vertical grid members whereas cell #3, from the same battery, had one thick vertical grid and six thin (0.2 cm) members. It is felt that this accounts for the dramatic increase in duration of test discharge when cell #1 was replaced by cell #4 and cell #3 became the limiting cell. The fact that the amount of active material in the positive plate governed the extent of discharge is also confirmed by two other observations: (a.) monitoring of positive and negative plate voltages versus a reference

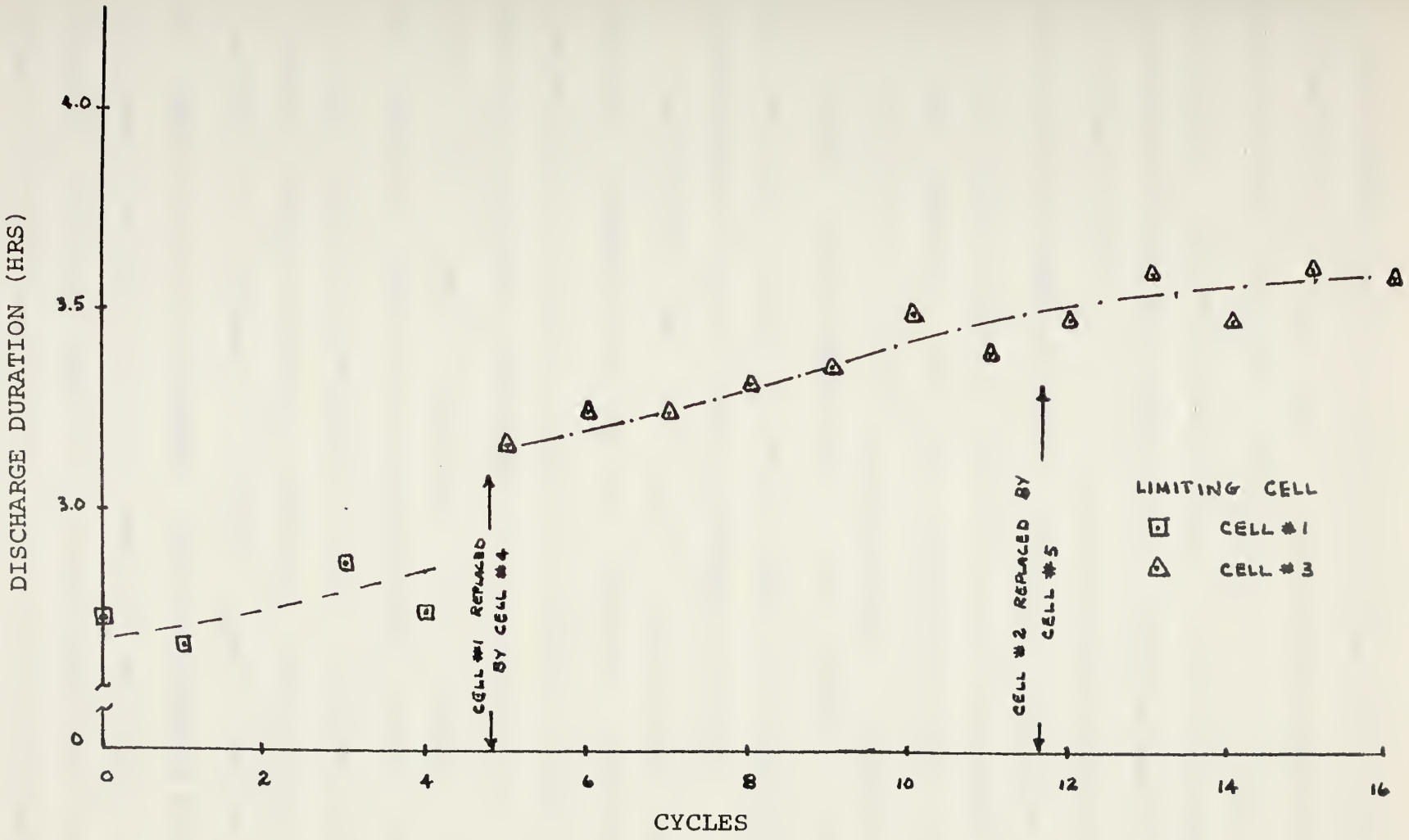

Figure 15 — Capacity vs. Cycles PbCa #2 - Floated

cadmium electrode during discharge showed the positive plate to be limiting, and (b.) electrolyte specific gravities only dropped on the average of 32 points during discharge, much less than the drop on full size submarine batteries during semi-annual test discharges conducted in accordance with Ref. 3. It is conjectured that the latter fact resulted from an excess loading of electrolyte to positive plate volume in the small test cells manufactured for this research. In a full size TLX-39B cell, the ratio of electrolyte to positive plate volume is approximately 2.5 ml/cm^3. In the test cells, it was roughly 11 ml/cm^3. This was done in order to ensure that the electrolyte concentration did not govern discharge duration.

The data for PbSb, the floated lead antimony grid battery, is shown in Figure 16. Although a quantitative comparison to the lead-calcium grid batteries cannot be made due to several differences in parameters (e.g., discharge rates, specific gravities, float voltages), it is of interest to note the behavior of cell #2 which governed discharge duration throughout the test. Following the initial buildup of capacity there was a sharp drop, following cycle #7, followed by a gradual capacity decline for the remaining test discharges. This performance was markedly different from that of either lead-calcium battery. A review of the daily operating log maintained for the battery shows nothing different in the float routine following the cycle #7 test discharge and prior to the discharge for

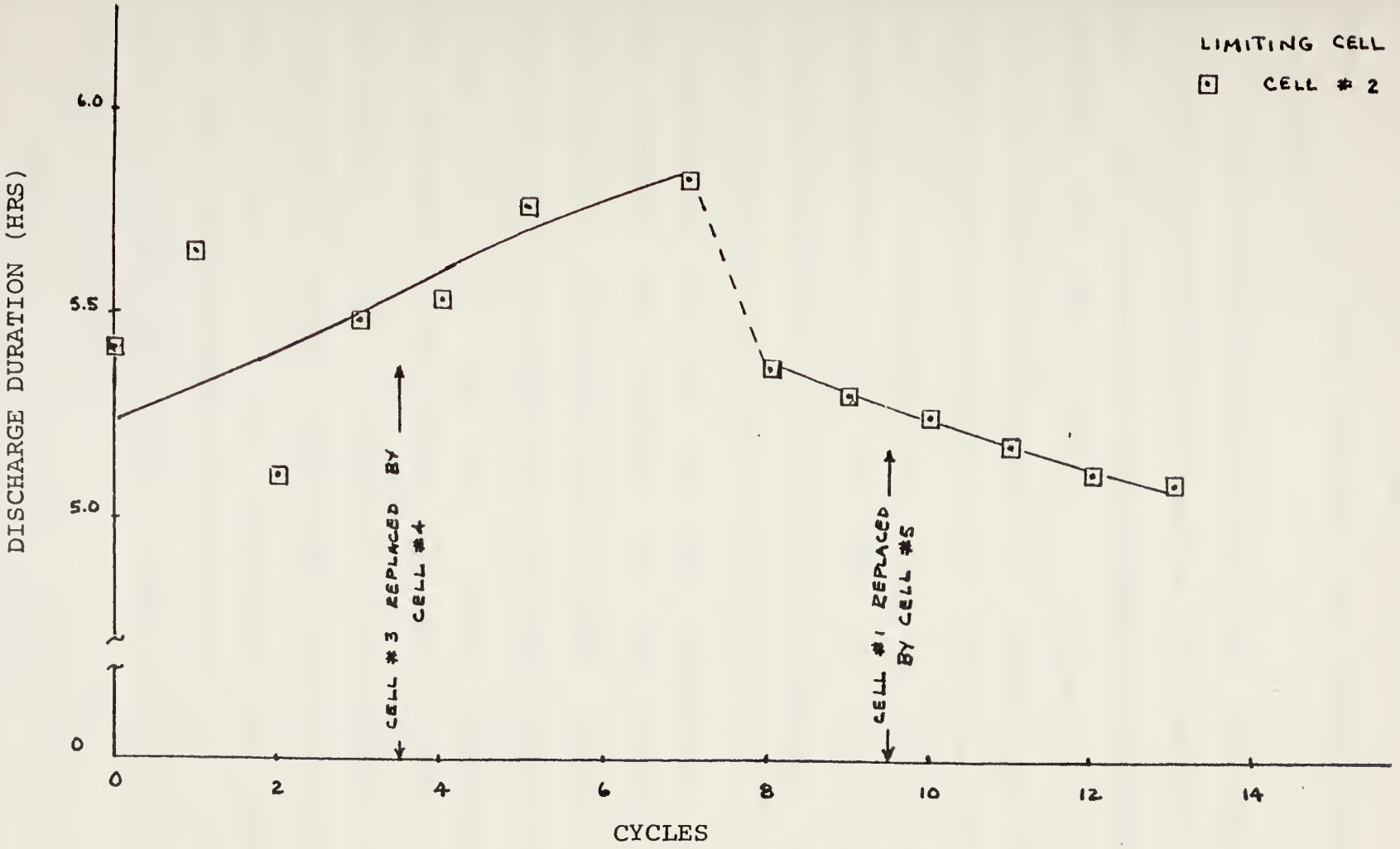

Figure 16 — Capacity vs. Cycles PbSb - Floated

cycle #8. The decline in capacity following cycle #8 is similar to data Burbank recorded for a floated lead-calcium grid battery [15].

In both the floated PbCa #2 and PbSb, cell float voltage imbalances were experienced when new cells replaced older ones. The average cycle float voltages are recorded in Appendix B and shown graphically in Figures 17 and 18. Since the controlling parameter for floating was total battery voltage, this resulted in at least one cell floating outside the allowable float voltage range (2.32 - 2.36 volts for PbCa #2 and 2.25 - 2.29 for PbSb) for several cycles. Voltages eventually tended to equalize indicating a balancing of cell resistance with time. Recognizing the necessity of maintaining compatible cell float voltages, as pointed out by Burbank [12] and Milner [13], this detracted from the validity of the strict float routine. However, it is not unreasonable to expect that the actual service conditions of full float routine for a 126 cell submarine battery see some cells at the extremes experienced in this testing. For example, in Ref. 5, Burbank and Wales present a plot of the record of float voltages made aboard USS Skipjack (SSN-585) during an "at sea" instrumented test. Typical daily cell voltage spans ranged from about 2.15 - 2.38 volts due to variations among effective negative plate areas of the cells in the battery.

The fact that neither PbCa #1 nor PbCa #2 gave evidence of failure (i.e., loss of capacity), makes any conclusions

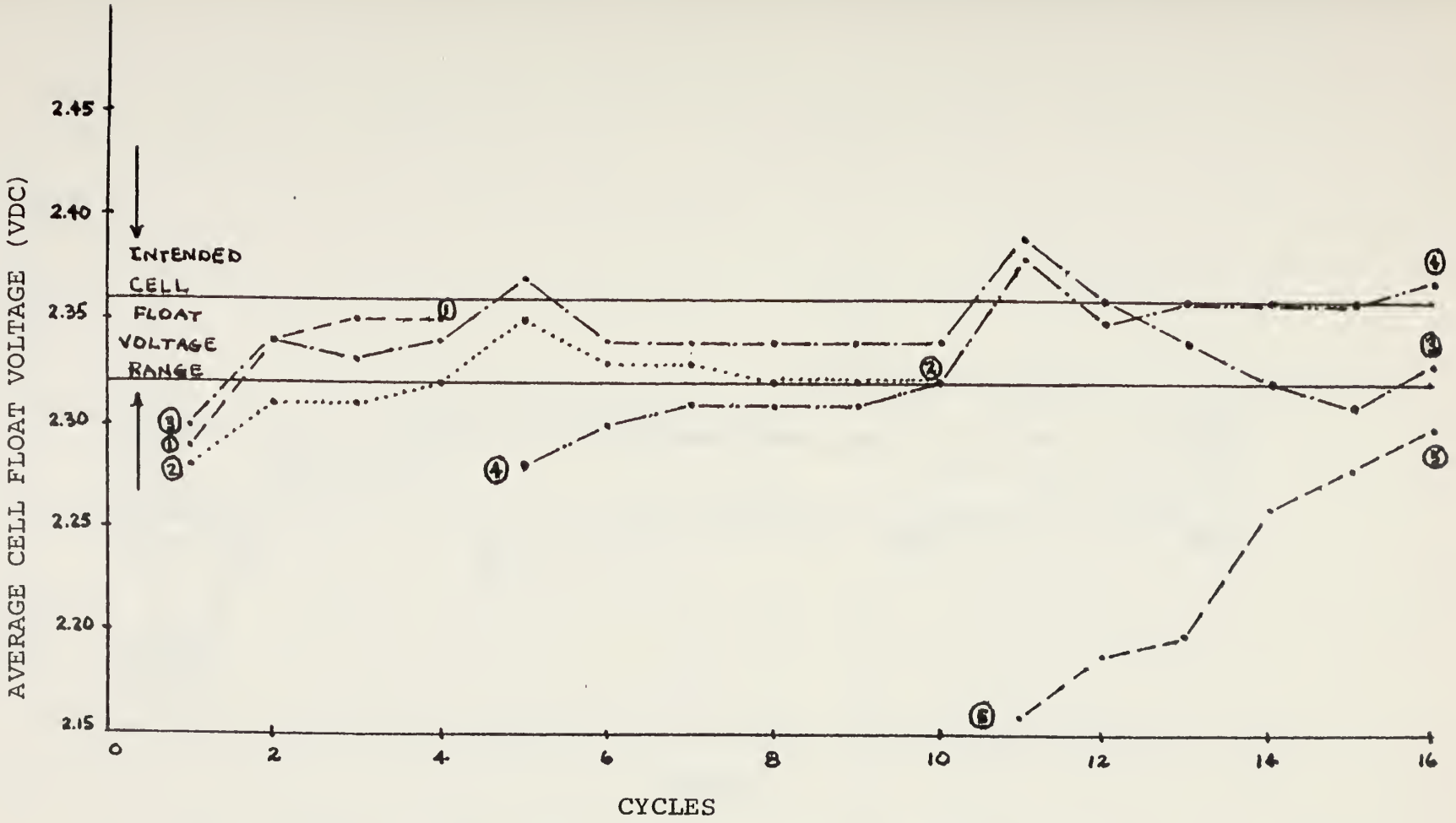

Figure 17 – Average cell float voltages vs. cycles PbCa #2

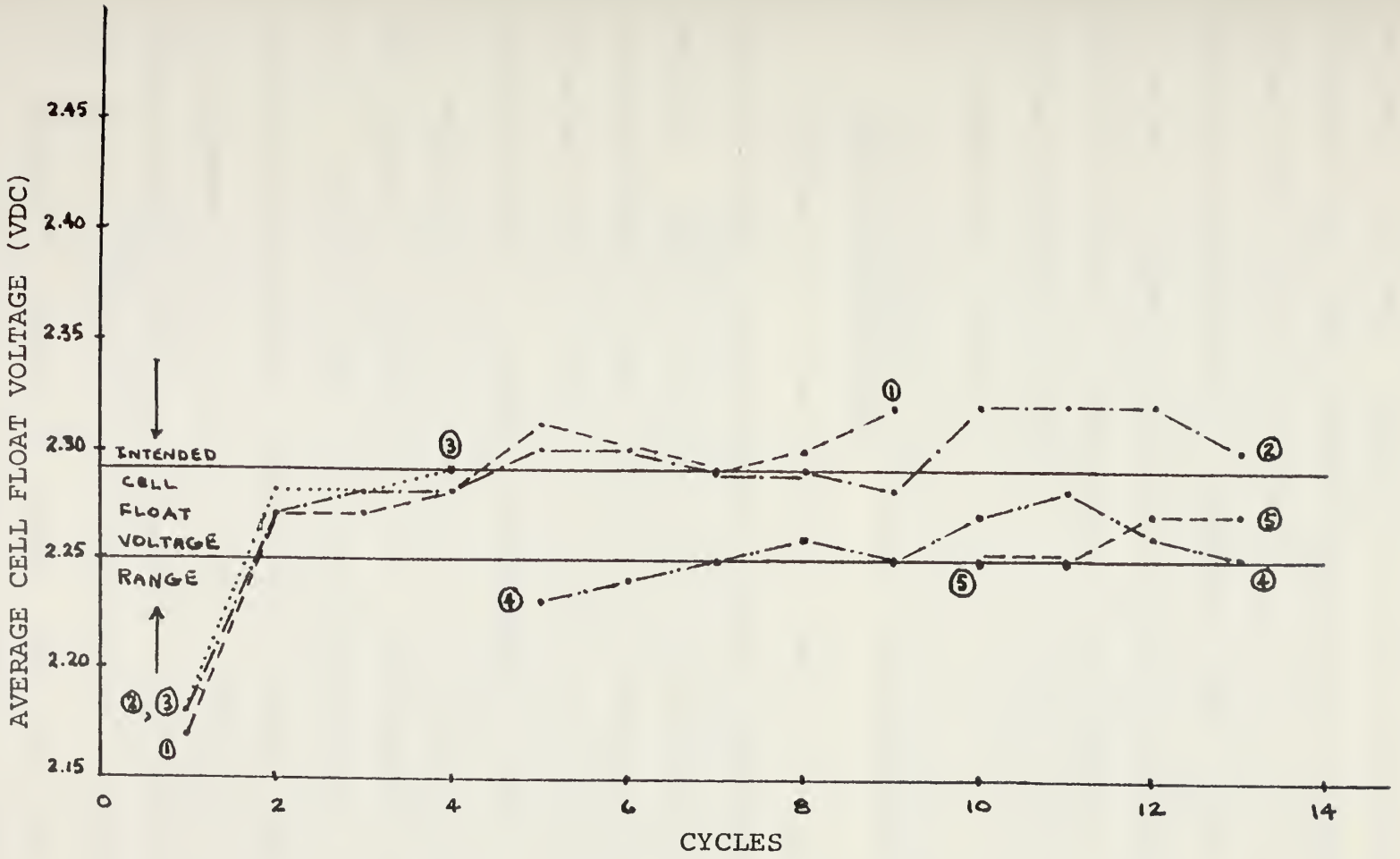

Figure 18 — Average cell float voltages vs cycles PbSb

regarding the service performance of trickle-discharged versus floated lead-calcium batteries, based on these tests, subjective at best. However, it is an established fact in submarine use, that floated lead-calcium batteries prematurely lose capacity and that the practice of trickle discharging circumvents this capacity loss. It is, therefore, intended to examine the morphological development of the positive plates in these batteries and attempt to characterize differences which may lead to the performance seen in operational service.

B. SCANNING ELECTRON MICROSCOPE (SEM) ANALYSIS OF POSITIVE PLATE MICROSTRUCTURE

Figures 19-23 show different views of the uncycled positive plate microstructure from the lead-calcium grid battery. Figure 19 shows a porous active material surface in what appears to be a continuous structural matrix. Figure 20 shows the structure to be composed of aggregates of small nodular masses. A similar photograph is shown in Ref. 24; the morphology can be described as a regular arrangement of PbO_2 grains on the surface of the electrode following formation. Figure 21 shows, at high magnification, the porous surface substructure of the nodular masses. This substructure appears to be a field of fine needlelike crystals. These crystals seem to be comrpised of at least two different forms. The majority are very short, on the order of a few tenths of a micron in length, fuzzy, and very hard to resolve in the SEM. In addition, there are some spiny

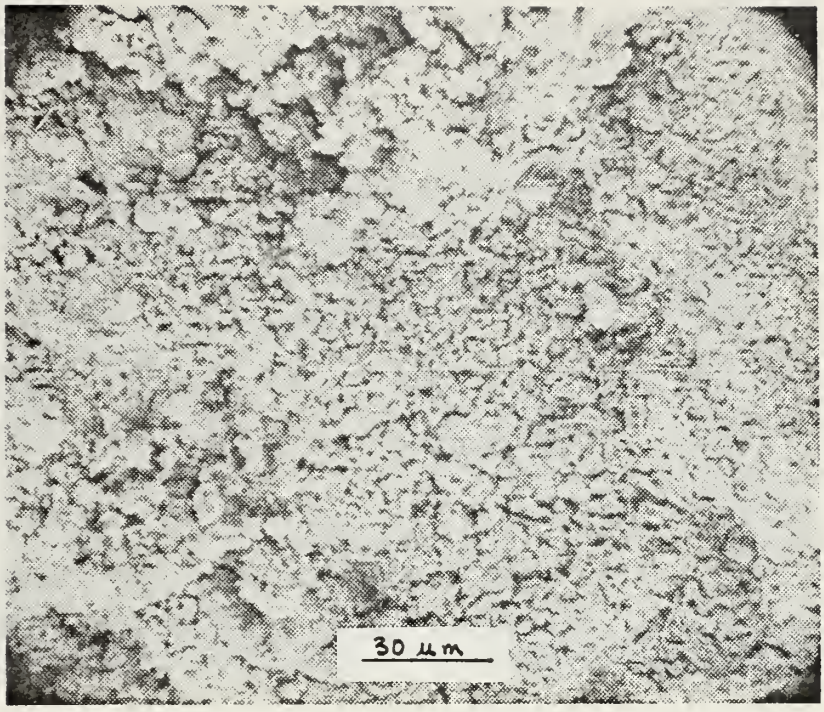

Figure 19 - Active material from 0-cycle lead-calcium alloy grid battery, 580x.

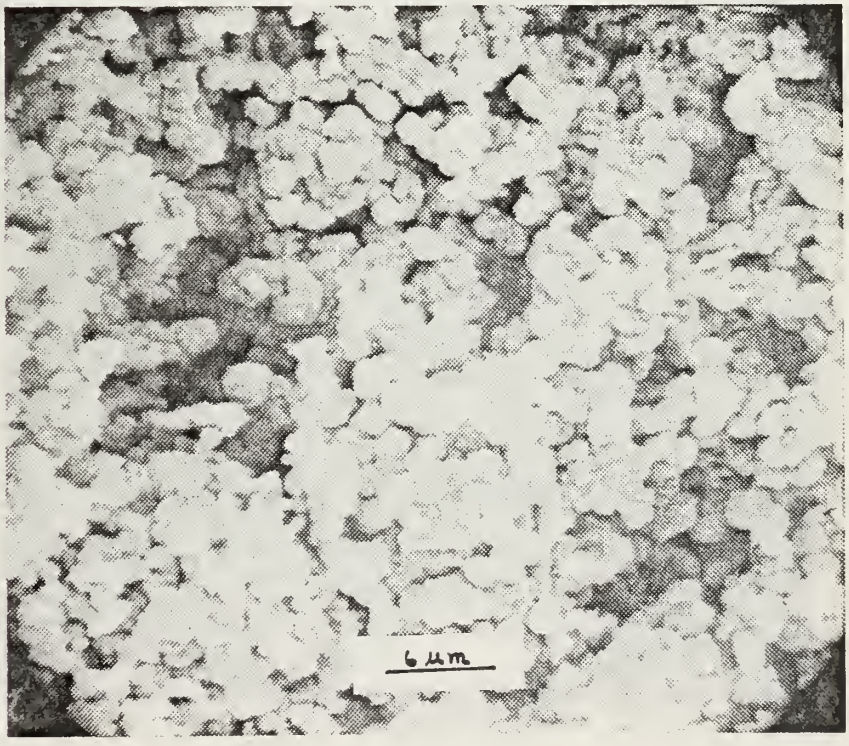

Figure 20 - Active material from 0-cycle lead-calcium alloy grid battery, 2400x.

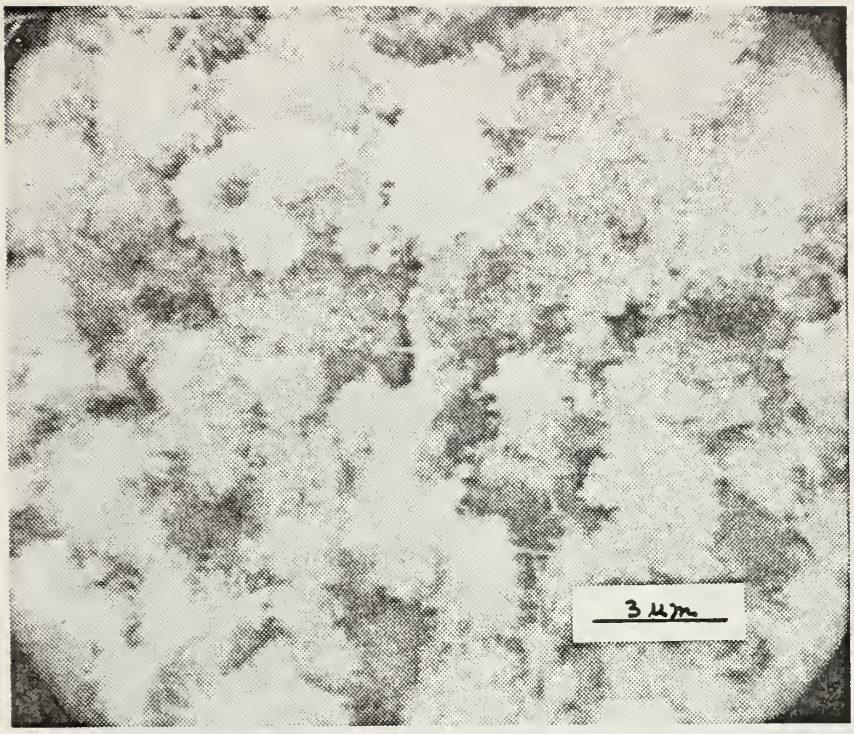

Figure 21 - Active material from 0-cycle lead-calcium alloy grid battery, 5800x.

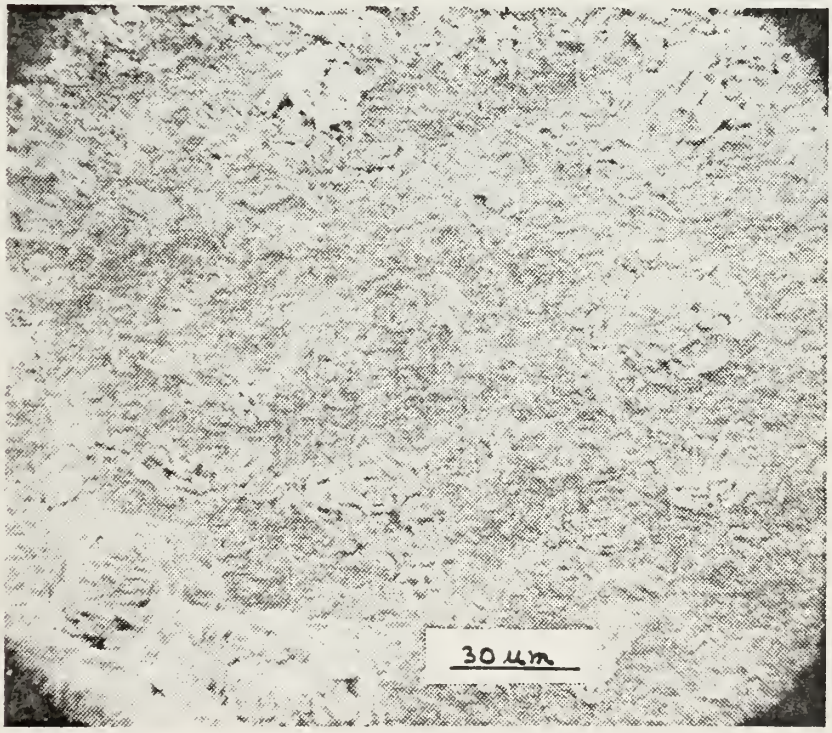

Figure 22 - External surface of a 0-cycle lead-calcium alloy grid, active material has been broken away, 570x.

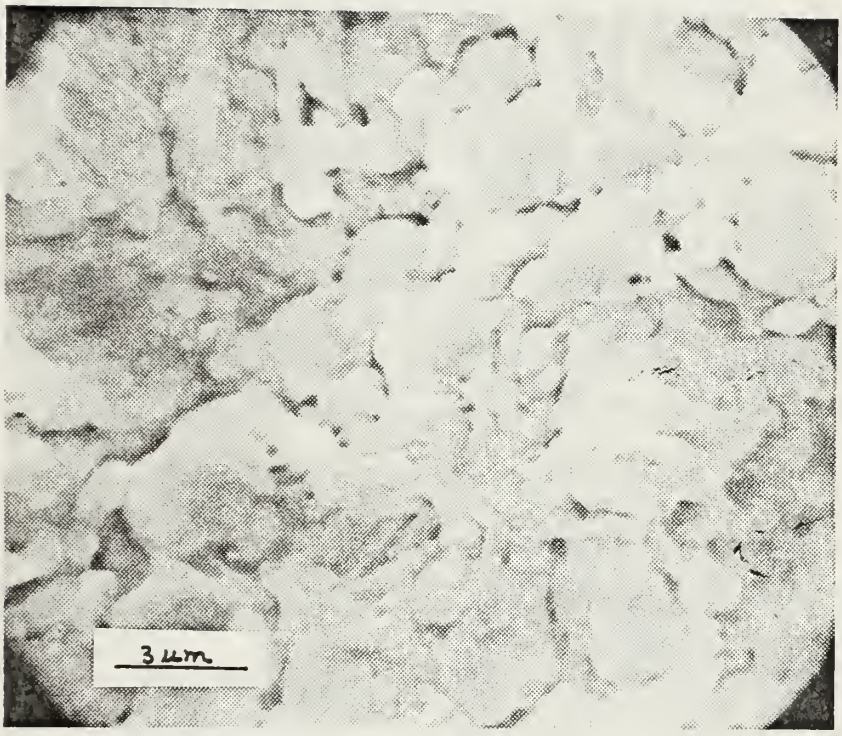

Figure 23 - External surface of a 0-cycle lead-calcium alloy grid, active material has been broken away. A small residual amount of active material still remains in evidence, 5700x.

projections which are very distinct. These are about 1.5 microns in length as determined by quantitative microscopy techniques. In the uncycled active material, these latter crystals are randomly distributed and are only a small fraction of the entire substructure.

This morphology is similar to that noted by Burbank and Ritchie [26] when they formed PbO_2 from three representative lead oxides. Branched prismatic crystals of PbO_2 were observed individually and clustered together in "Christmas tree" dendrites. In addition, aggregates, composed of compound spikes of dendritic growth, covered with so-called sessile crystallites of varying sizes, were seen.

Figure 22 shows the external surface of an uncycled lead-calcium grid bar where the active material has been broken away. The surface is uneven and at this magnification might appear to be porous. However, Figure 23 shows the detail of the surface; and as can be seen, the surface is not porous, appearing quite irregular, apparently the net result of casting and the plate formation process. This picture also shows some pieces of active material still attached to the grid surface. A significant feature to note about Figure 23 is the absence of a surface corrosion layer.

1. Trickle-Discharged Lead Calcium

Structural changes in the active material morphology for 5, 10, and 13 cycle PbCa plates, operated on the trickle discharge routine (PbCa #1), are shown in Figures 24 - 26.

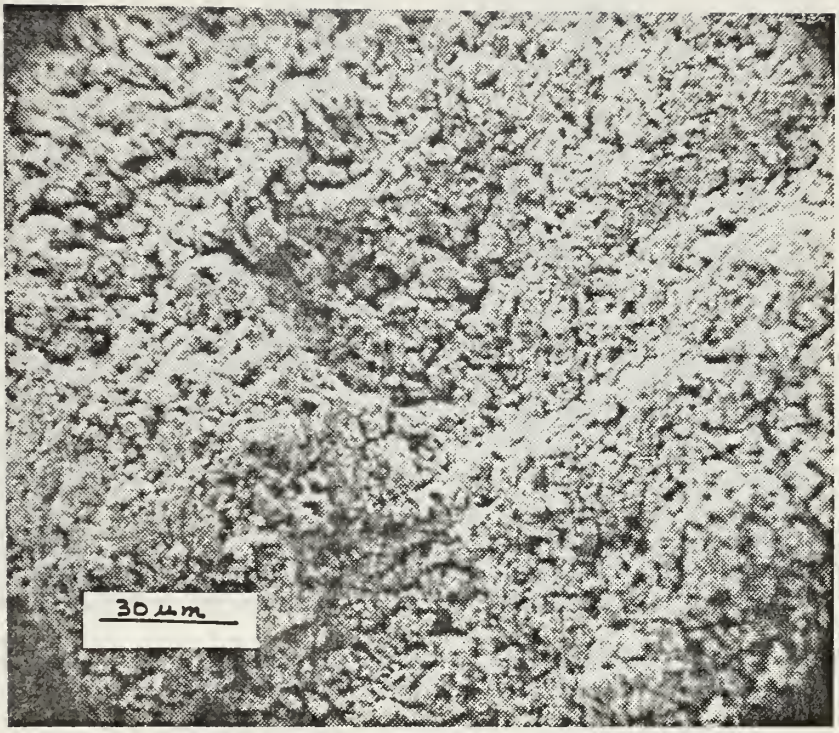

Figure 24 - Active material, 5 cycle PbCa positive plate, trickle-discharge routine, plate is fully charged, 600x.

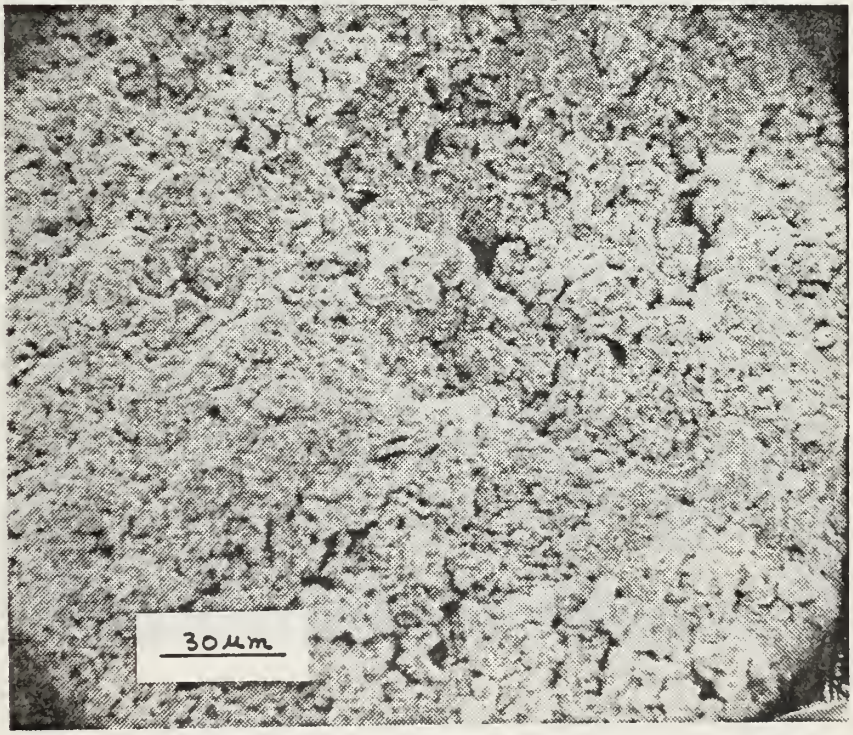

Figure 25 - Active material, 10 cycle PbCa positive plate, trickle-discharge routine, plate is fully charged, 550x.

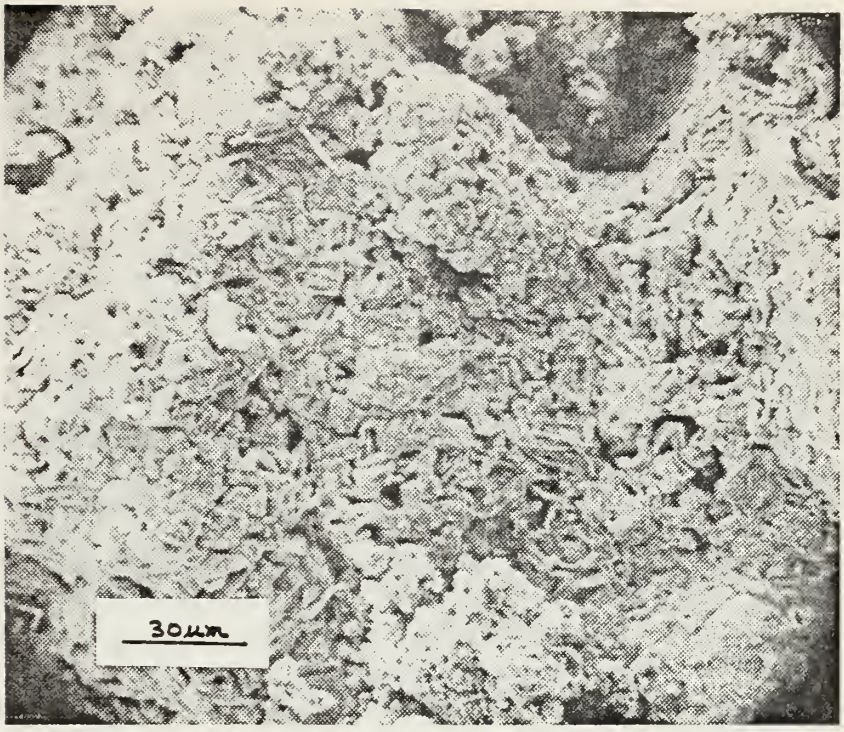

Figure 26 - Active material, 13 cycle PbCa positive plate, trickle-discharge routine, plate is fully charged, 550x.

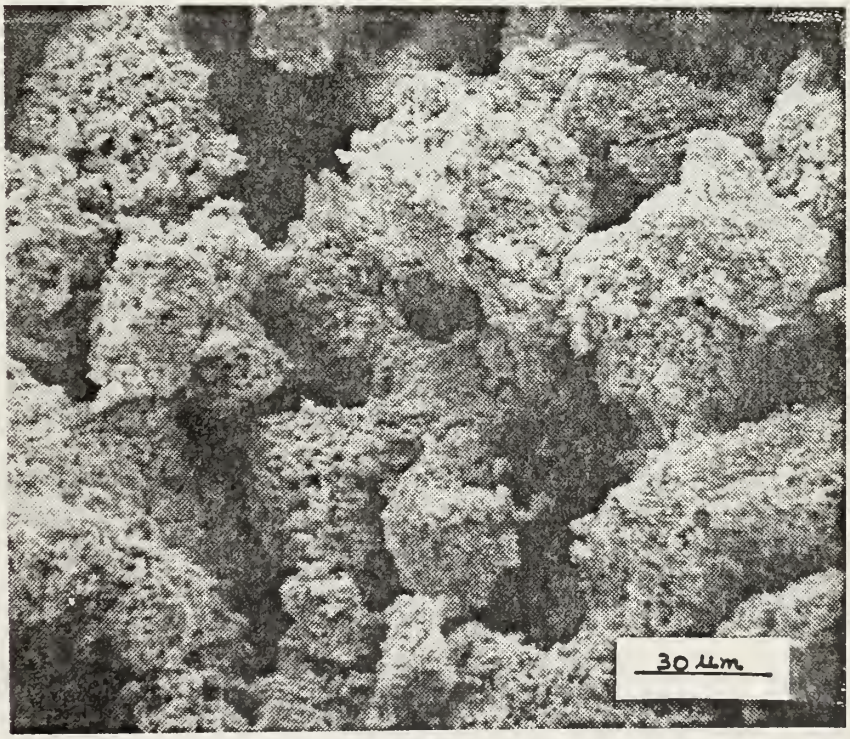

Figure 27 - Active material, coralloid structure in a PbCa positive plate after 60 continuous charge/discharge cycles.

The porous surface, seen in the 0-cycle plate (Figure 19), gradually disappears, and the underlying active material fuses together into a more compact structure containing some voids. Simon, Caulder and Stemmle studied the morphology of active material during continuous charge/discharge cycling and noted similar void formation as being incidental to the formation of a three dimensional so-called "coralloid" labrynth structure that developed after about 30 cycles [25]. It is felt that the structure seen in Figure 26 is an early stage in the formation of the coralloid network. Figure 27, obtained from a lead-calcium plate cycled by Pokorny [32], shows this structure after 60 charge/discharge cycles.

Another feature noted in the active material is shown in Figures 28 and 29; this shows what appears to be a very dense layer that coats the surface of the charged PbO_2 crystal shapes. This coating was found only in the middle thickness region of active material pellets. Figures 30 and 31 show the substructure of the layer at higher magnification. It appears to be made up of the same two crystalline forms seen in the 0-cycle active material (Figure 21); however, more of the longer, spiny crystals are evident, apparently developed into a branching dendritic network extensive enough to blanket the underlying nodular aggregates.

Perhaps the most distinctive feature of positive plate microstructure in the trickle discharge routine batteries is a patterned structure, made up on the fine scale, of a

Figure 28 - Active material, 10 cycle PbCa positive plate, trickle-discharge routine, dense surface layer, plate is fully charged, 550x.

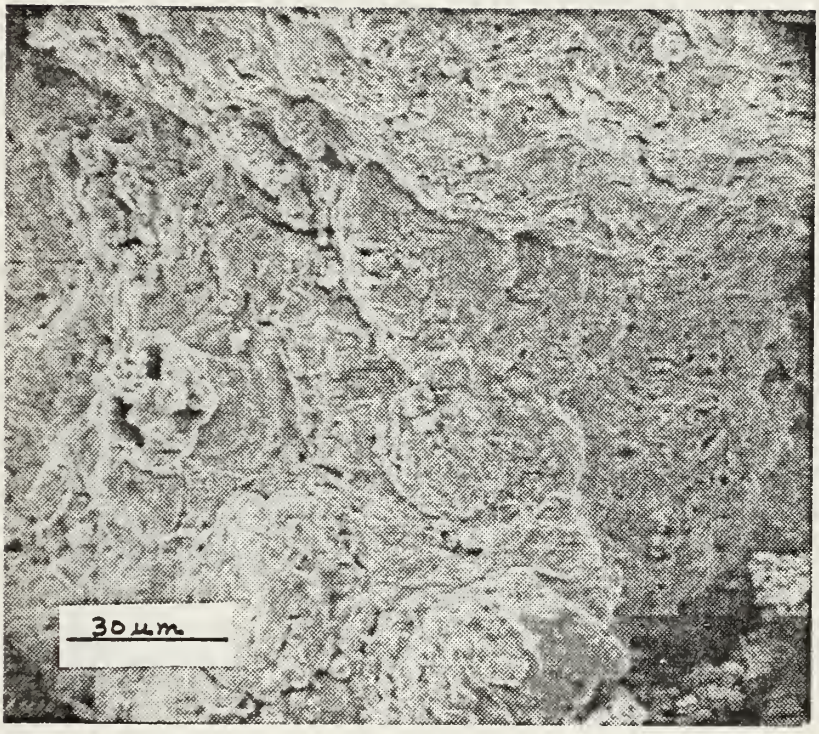

Figure 29 - Active material, 13 cycle PbCa positive plate, trickle-discharge routine, dense surface layer, plate is fully charged, 700x.

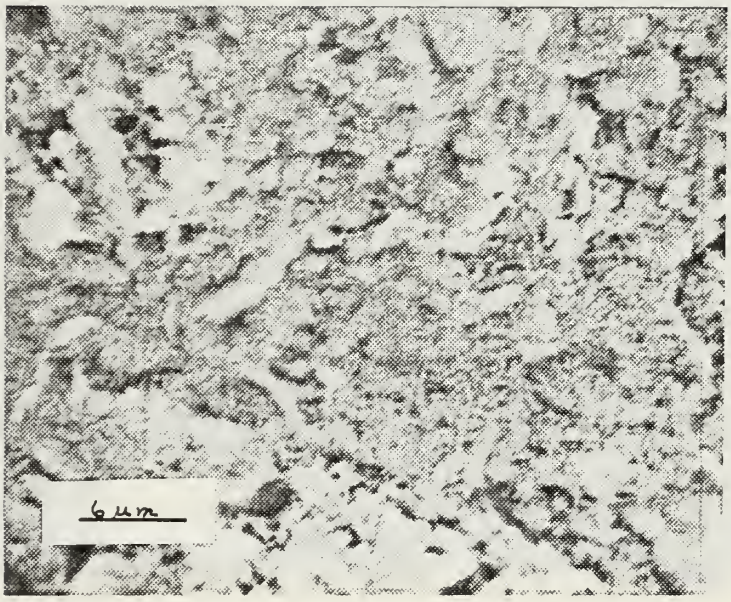

Figure 30 - Active material, 10 cycle PbCa positive plate, trickle-discharge routine, surface layer on PbO_2, plate is fully charged, 2350x.

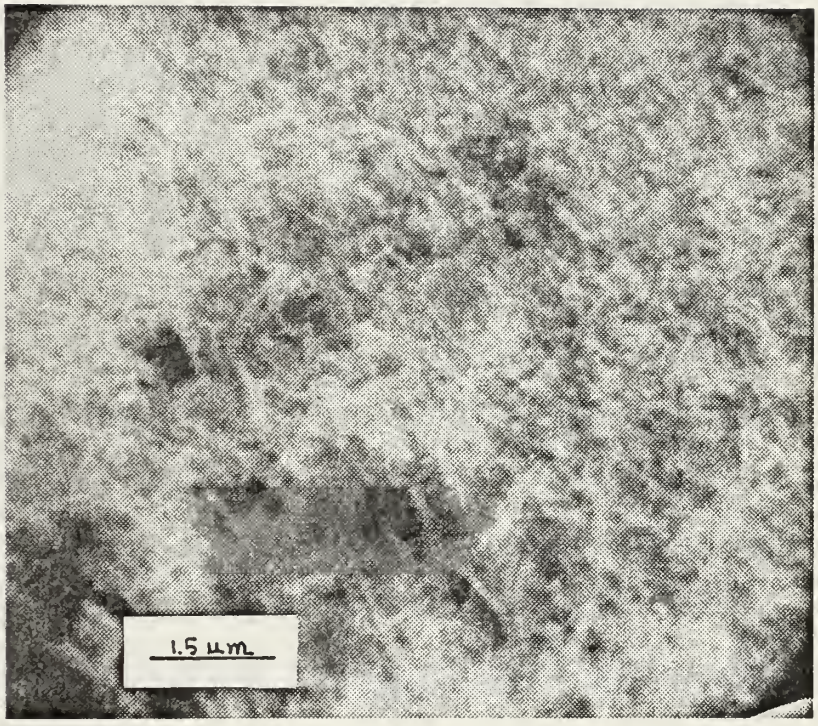

Figure 31 - Active material, 10 cycle PbCa positive plate, trickle-discharge routine, substructure of surface layer seen in Figure 28, plate is fully charged, 11,000x.

dendritic network similar to that described above; this is seen on the grid surface corrosion layer and on the dense central layer in the active material noted above. Figures 32-43 show this network and its substructure at various magnifications. At the lower manifications (600x - 1400x), it is seen as a white pattern in relief against the surface of either the grid corrosion layer or dense active material layer. At higher magnifications (5000x - 7000x), other features become more evident, such as the height of the "walls" of this structure, about 2 μm; and the linearity of some of the sides. In fact, the shape suggests that this network represents the outlines of large polyhedral crystals which have since transformed. Another observation is that the substructure of these walls consists of a network of spiny needlelike crystals similar to that just discussed. Figure 43, taken at 11,500x, shows the needles assembled together, projecting outward from a central trunk.

It is postulated that this dendritic network is composed of a dense weave of the spiny crystals, and extends throughout the plate in a pattern determined by the prior location and originating from the array of polyhedral lead sulfate crystals which have since transformed during charging.

Figures 44 and 45 show areas on the grid bar (after the active material has been broken away) where recharge has not been completed and $PbSO_4$ crystals remain in various

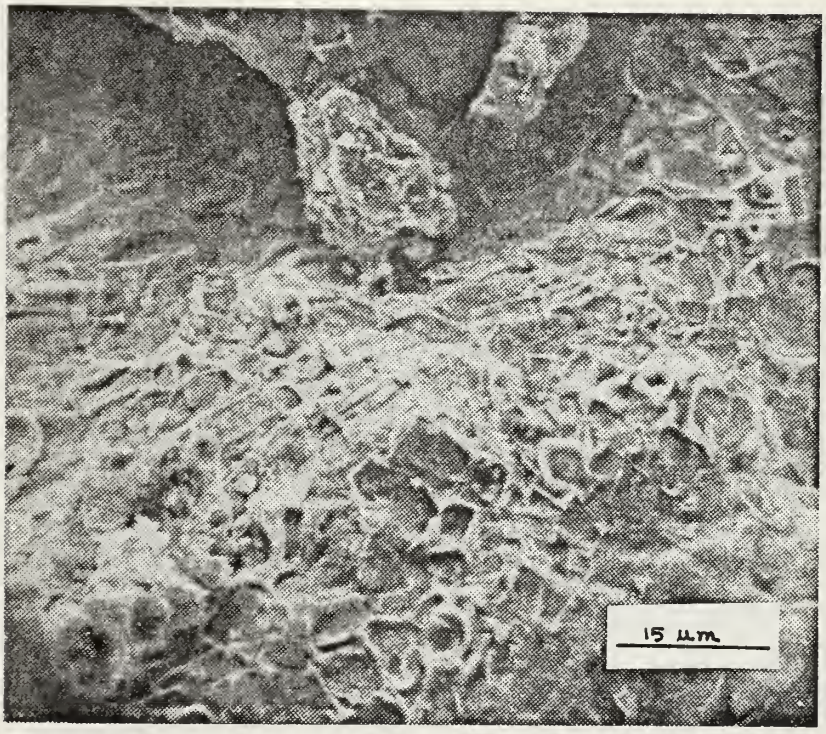

Figure 32 - Active material, 13 cycle PbCa positive plate, trickle-discharge routine, white dendritic structure on a dense surface layer covering the active material, plate is fully charged, 1350x.

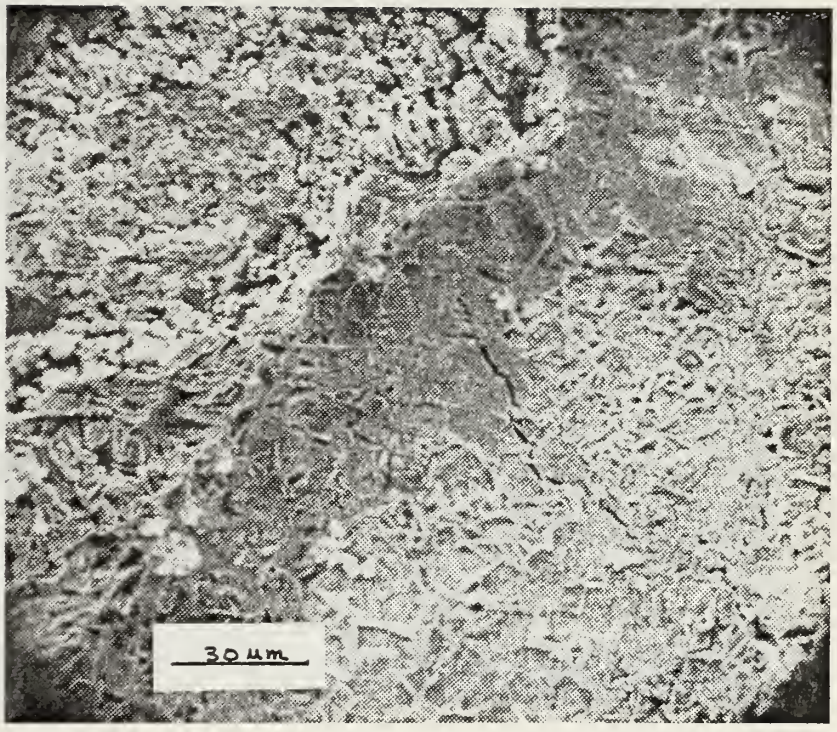

Figure 33 - Exterior of grid with active material broken away, 13 cycle PbCa positive plate, trickle discharge routine, dendritic network seen in relief against the grid surface corrosion layer, some active material remains on the left, some partially dissolved $PbSO_4$ crystals can be seen in the middle of the picture, plate is fully charged, 600x.

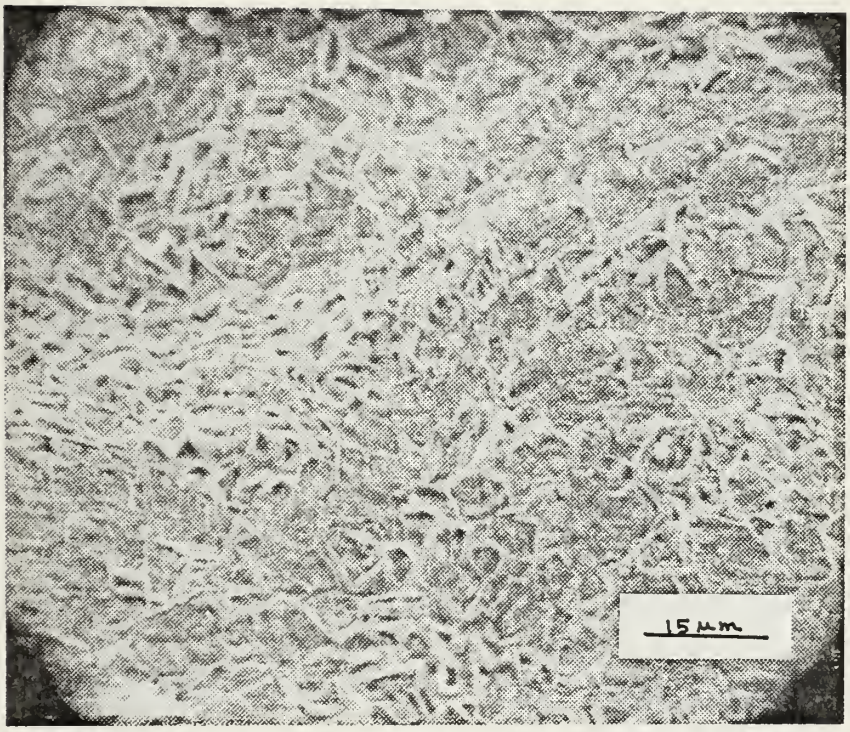

Figure 34 - Exterior of grid with active material broken away, 13 cycle PbCa positive plate, trickle discharge routine. Dendritic network seen in relief against the grid surface corrosion layer, plate is fully charged, 1100x.

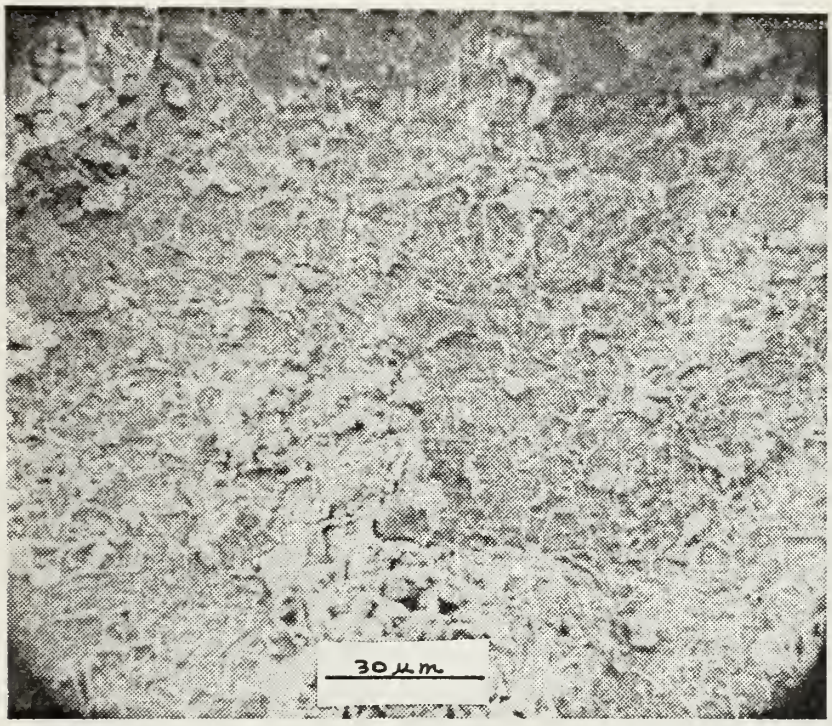

Figure 35 - Exterior of grid with active material broken away, 4 cycle PbCa positive plate, trickle discharge routine. Dendritic network seen in relief against the grid surface corrosion layer, some loose grains of PbO_2 remain scattered about, plate is fully charged, 700x.

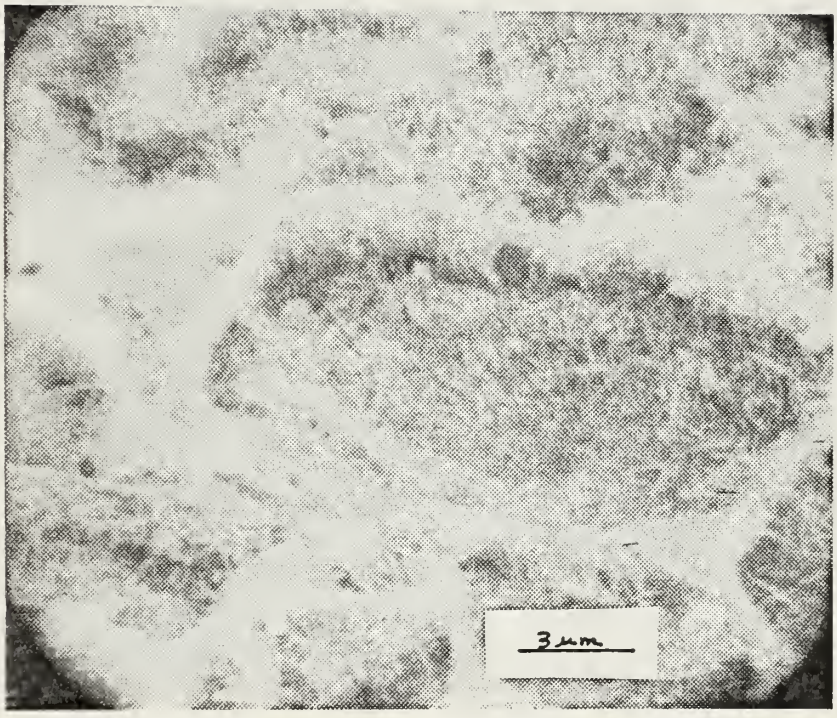

Figure 36 - Exterior of grid with active material broken away, 4 cycle PbCa positive plate, trickle discharge routine. Dendritic network. Height of structure is approximately 2µm, spiny crystals evident, plate is fully charged, 5100x.

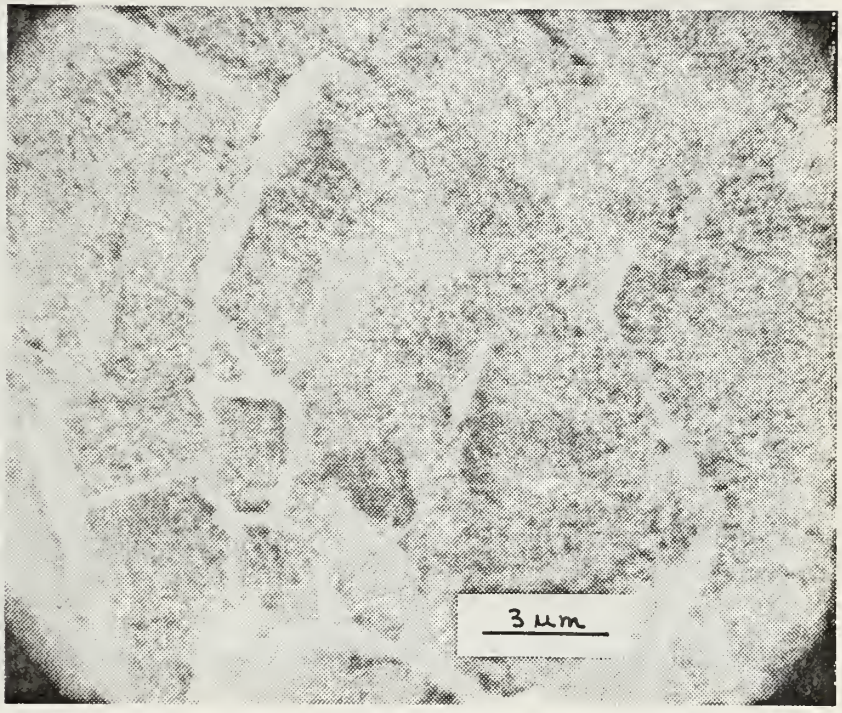

Figure 37 - Active material, 13 cycle PbCa positive plate, trickle discharge routine. Dendritic network seen on the surface of a dense layer on the active material, plate is fully charged, 5600x.

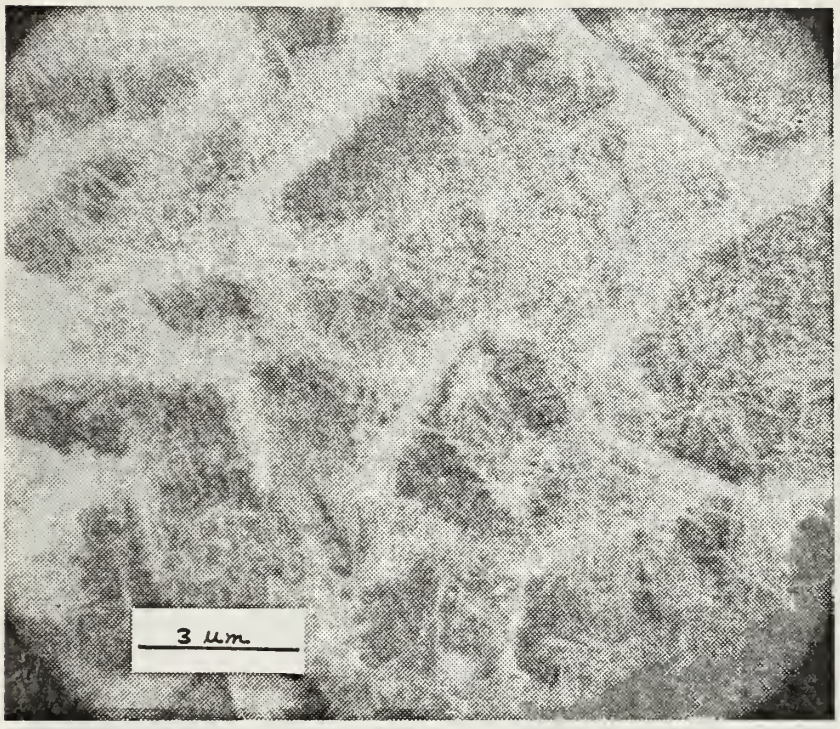

Figure 38 - Exterior of grid with active material broken away, 4 cycle PbCa positive plate, trickle discharge routine. Dendritic structure showing a large number of spiny crystals, plate is fully charged, 7000x.

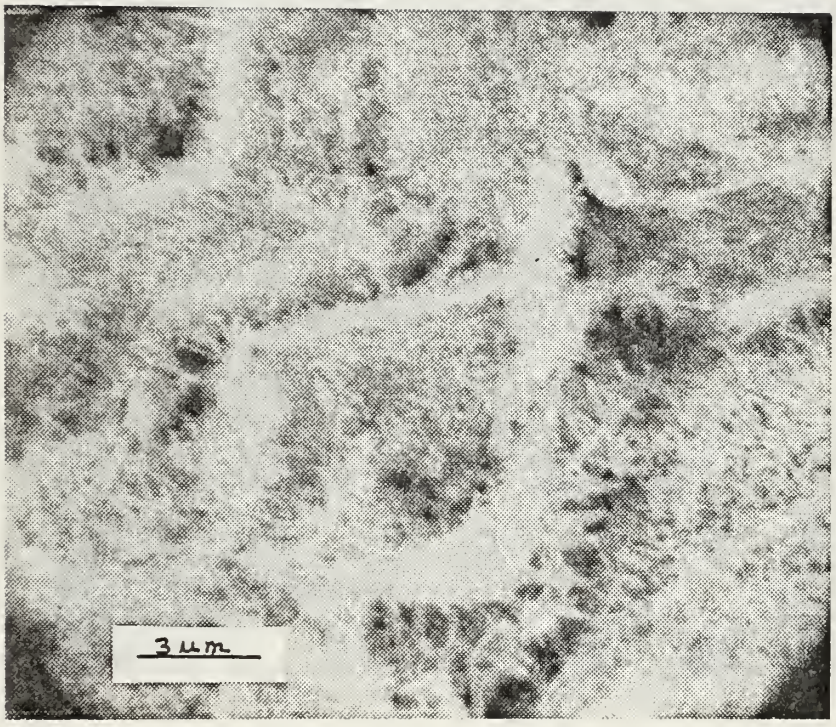

Figure 39 - Exterior of grid with active material broken away, 10 cycle PbCa positive plate, trickle discharge routine. Dendritic structure, spiny crystals are present, appears to be the outline of a rectangular or prismatic crystal, plate is fully charged, 5500x.

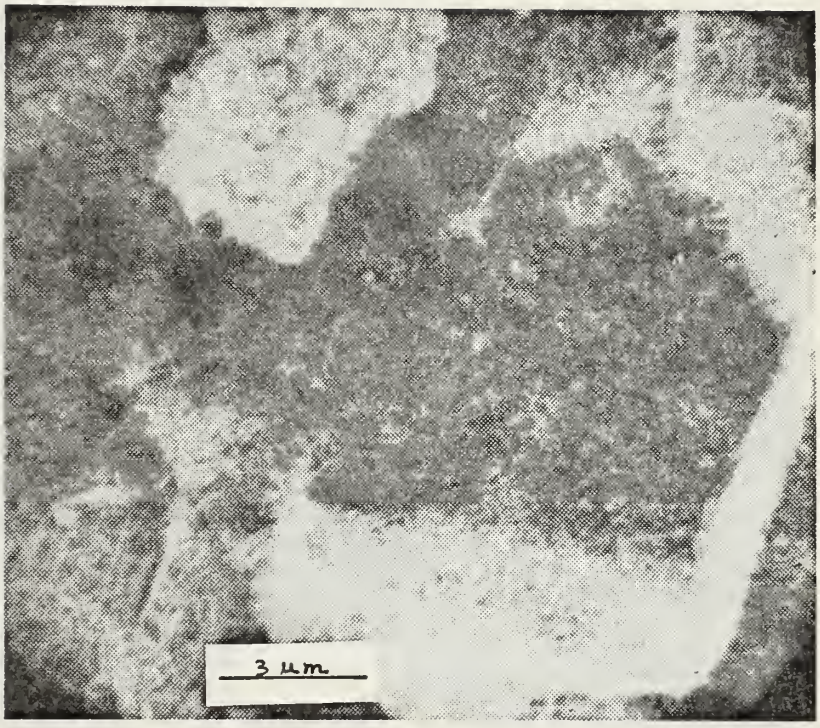

Figure 40 - Active material, 4 cycle PbCa positive plate, trickle discharge routine. Dendritic structure seen on region of dense layer over active material surface. The wall of the structure is much thicker than those seen against the grid bar surfaces, plate is fully charged, 6500x.

Figure 41 - Exterior of grid with active material broken away, 13 cycle PbCa positive plate, trickle discharge routine. Dendritic structure with many spiny crystals evident throughout, plate is fully charged, 5600x.

Figure 42 - Exterior of grid with active material broken away, 13 cycle PbCa positive plate, trickle discharge routine. Dendritic structure, plate is fully charged, 5650x.

Figure 43 - Exterior of grid with active material broken away, 13 cycle PbCa positive plate, trickle discharge routine. Spiny needle arrangement as substructure of dendritic network, plate is fully charged, 11,500x.

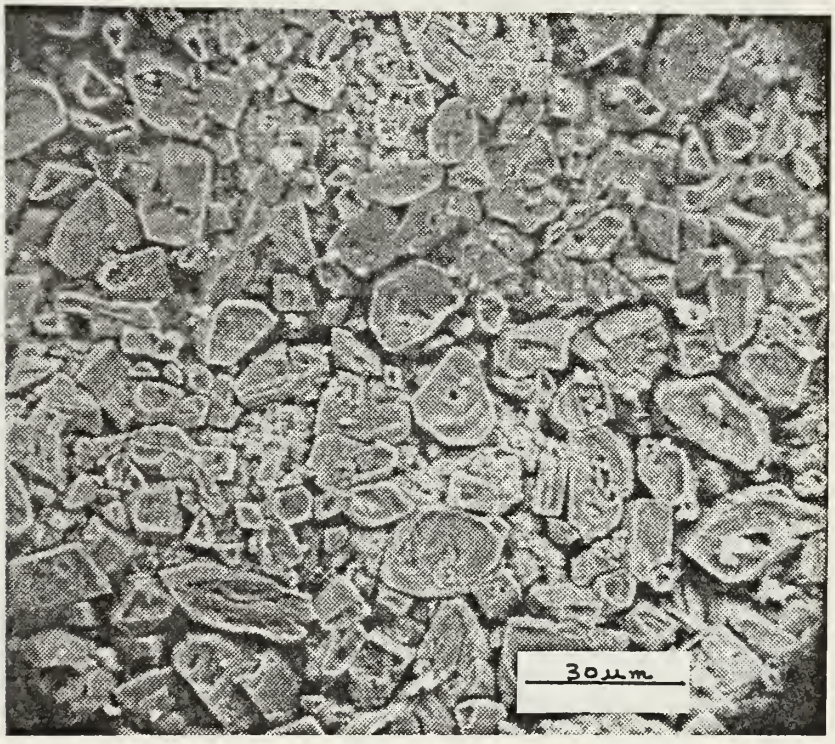

Figure 44 - Exterior of grid showing dense layer of lead sulfate crystals which were not transformed to lead dioxide during the final charge on this positive plate; 4 cycle PbCa positive plate, trickle discharge routine, 700x.

Figure 45 - Exterior of grid showing skeletons of partially dissolved lead sulfate crystals. The general shape of these crystals is similar to the walls of the dendritic structure seen in previous photographs; 5 cycle PbCa positive plate, trickle discharge routine, plate is in charged condition, 2250x.

stages of dissolution. A similarity is noted between the shape of these crystals and the patterned outline of the dendritic structure observed on the grid surface corrosion layer. The mechanism of formation of this pattern structure is not known but two possibilities will be mentioned. The first is that unreacted PbO_2 piles up next to the walls of the growing $PbSO_4$ crystals during discharge and remains when they are consumed upon recharge; in this model the large accumulation of the spiny crystals in the vicinity of these walls might indicate that these are an unreactive form of PbO_2; Simon et. al. [25] conclude that an inactive form of PbO_2, resistive to reduction to $PbSO_4$ but capable of acting as nucleii for the crystallization of active PbO_2, remains as a residue in the active material following discharge; they also observed this residue deeply imbedded within $PbSO_4$ crystals.

Another, more plausible, explanation for the formation of this patterned structure is that large $PbSO_4$ crystals, formed during the trickle discharge operation, are subsequently transformed by a preferred crystallographic mechanism. It is apparent that the $PbSO_4$ crystals edges dissolve more slowly than the planar faces, so that the interior of the crystals are eaten out, leaving behind a "framework" structure of the edges, which eventually convert, but to a denser network of spiny crystals arranged in a corresponding dendritic pattern. This pattern is seen as an imprint near the grid surface (Figures 34-36,

38,39,41-43) and within the active material mass particularly near the central region of pellets (Figures 32, 33, 37,40). Figures 45-47 suggest the mechanism just described. The genesis of the fine needlelike form which makes up these networks is unknown, but this is probably a preferred morphological form of PbO_2 associated with $PbSO_4$ transformation under certain electrochemical conditions of recharge. More will be said about the dendritic network and the spiny crystals after examining the floated positive plate morphology.

The final feature which will be noted for the trickle discharged positive plates is the layer that is formed on the exterior of the grid and which is seen under the patterned dendritic network in several earlier figures. A similar dense, tightly-woven structure was seen covering sections of the active material (Figures 28 and 29). This structure adhered to the grid and was seen to be nearly continuous over the metallic surface of the grid when the active material was broken away. Figures 48-53 show the appearance of the layer at various magnifications and Figure 54 shows an isolated section where the layer itself has broken away from the bare grid and can be seen in contrast against the uneven lead surface. This layer therefore represents the "corrosion layer" which has been studied extensively by many workers. A review of that research is contained in Ref. 9. At high magnification (Figures 50-53), many of the crystals are similar in appearance to those seen

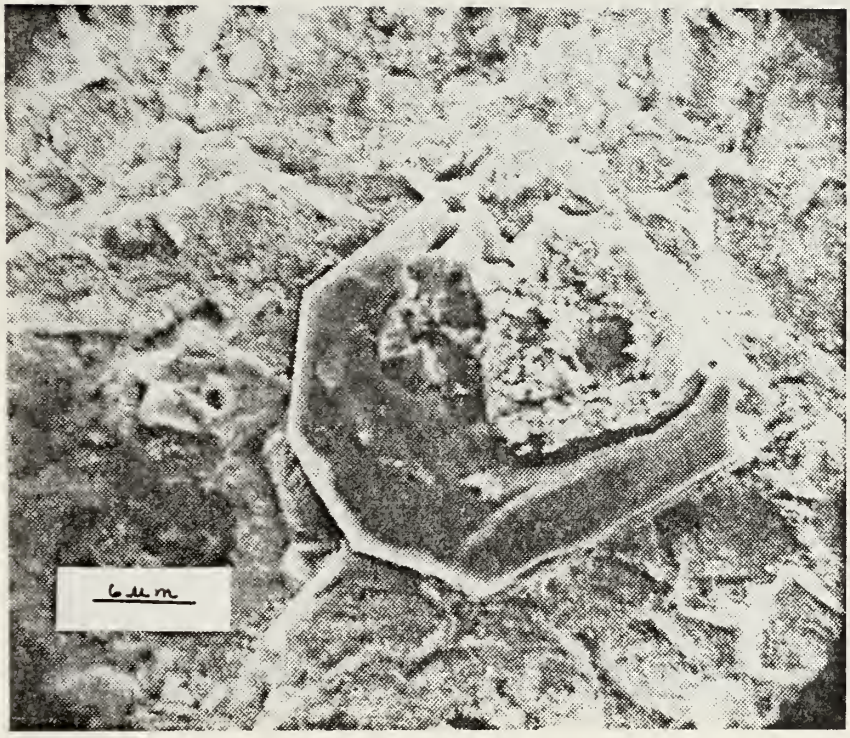

Figure 46 - Exterior of grid showing a partially transformed lead sulfate crystal. The lead dioxide appears to be growing from inside the $PbSO_4$; 13 cycle PbCa positive plate, trickle discharge routine, plate is in charged condition, 2250x.

Figure 47 - Exterior of grid showing a partially transformed lead sulfate crystal. The dendritic structure is seen around the periphery of the $PbSO_4$; 4 cycle PbCa positive plate, trickle discharge routine, plate is in charged condition, 2100x.

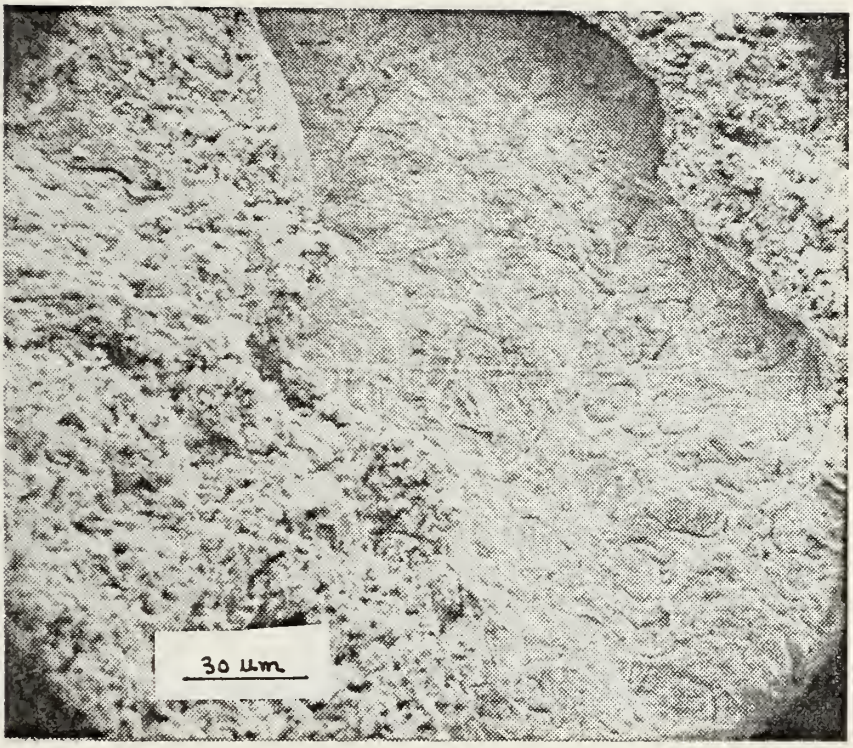

Figure 48 - Exterior of grid with active material partially broken away showing dense layer covering grid surface. 7 cycle PbCa positive plate, trickle discharge routine, plate is fully charged, 550x.

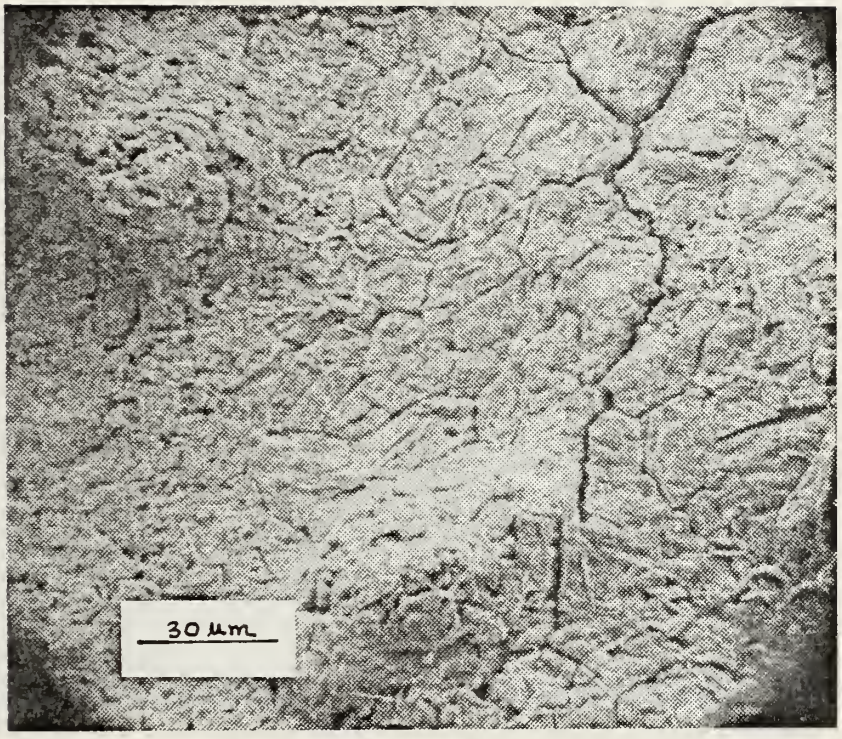

Figure 49 - Exterior of grid with active material broken away showing dense layer covering grid surface. 7 cycle PbCa positive plate, trickle discharge routine, plate is fully charged, 620x.

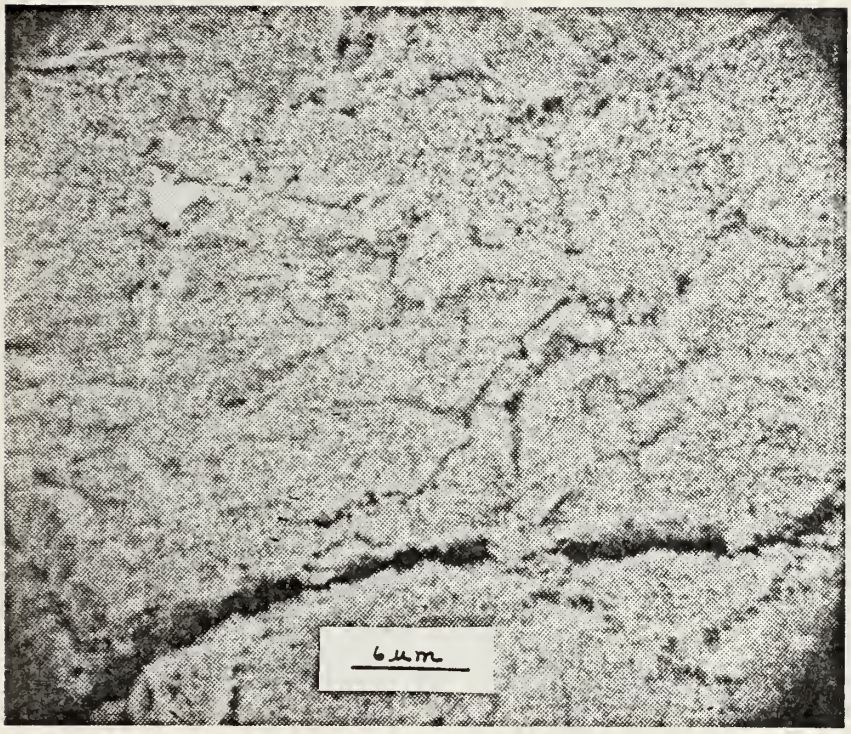

Figure 50 - Exterior of grid with active material broken away showing dense layer covering grid surface. 7 cycle PbCa positive plate, trickle discharge routine, plate is fully charged, 2600x.

Figure 51 - Exterior of grid with active material broken away showing dense layer covering grid surface; some dendritic structure shells are also visible. 10 cycle PbCa positivie plate, trickle discharge routine, plate is fully charged, 2200x.

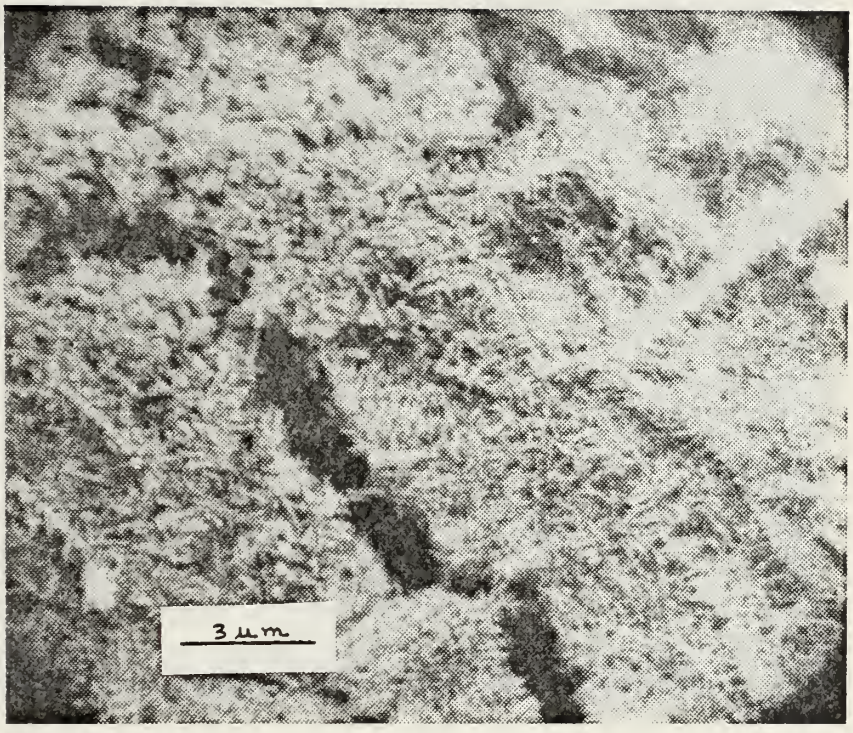

Figure 52 - Exterior of grid with active material broken away showing break in dense layer covering grid surface; spiny crystals and dendritic shells are visible. 13 cycle PbCa positive plate, trickle discharge routine, plate is fully charged, 5900x.

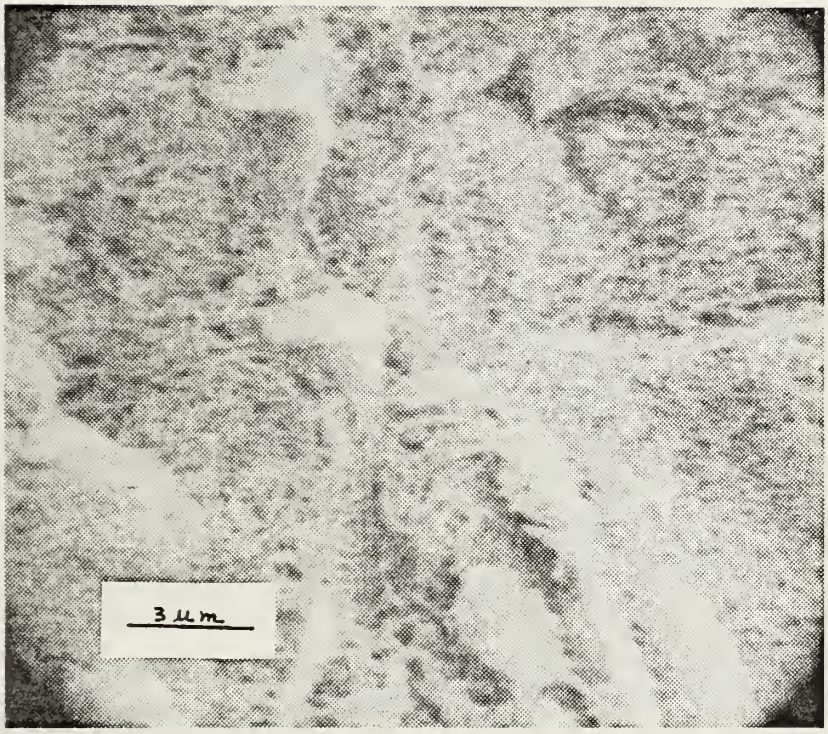

Figure 53 - Exterior of grid with active material broken away showing dense layer covering grid surface. 7 cycle PbCa positive plate, trickle discharge routine, plate is fully charged, 5500x.

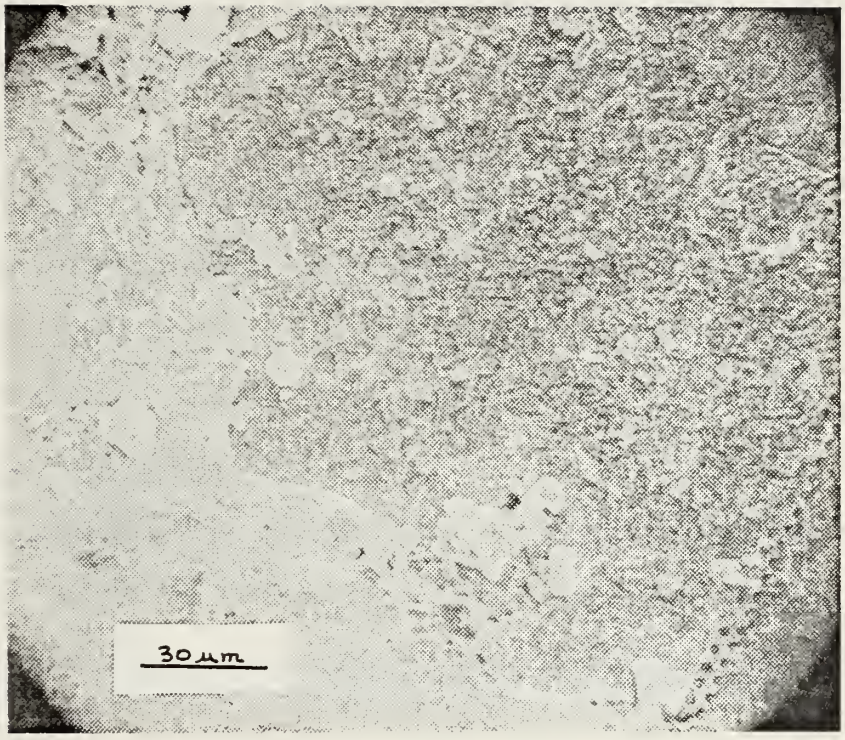

Figure 54 - Exterior of grid with active material broken away. Shows region where dense layer has been broken and bare grid is seen to the right of the layer; some grains of active material are also evident on the surface. 5 cycle PbCa positive plate, trickle discharge routine, plate is fully charged, 550x.

within the active material mass (i.e., short rounded and longer spiny forms). This suggests that PbO_2 is a major component of this corrosion layer. Reference 9, in discussing the work of Astakhov et. al., notes that they found the initial film formed during prolonged anodic polarization at constant current, consisted of mainly tetragonal PbO with some α-PbO_2. As the film thickness increased, the outer layer became more porous and was composed of α- and β-PbO_2. Figure 55, a light micrograph, shows the thickness of the layer seen in contrast between the grid and active material. This photograph was taken of the 13 cycle PbCa positive plate operated in the trickle discharge mode. The layer thickness ranges from about 20-25 μm.

2. Floated Lead Calcium.

In examining the morphology of the floated lead-calcium alloy positive plates, perhaps the most significant observation is the absence of the web-like dendritic structure seen in the trickle discharged plates. Figures 56-58 show the outer layer on grid bars where the active material has been broken away. A surface layer, similar to the corrosion layer seen on the trickle discharged plates, is evident; but the pattern and dendritic network structures are not seen. The morphology of this layer is different from that of the trickle discharged plates as seen in Figures 59-61. In these higher magnification views, it is noteworthy that long spiny crystals, such as seen in the trickle discharged plates, are generally not

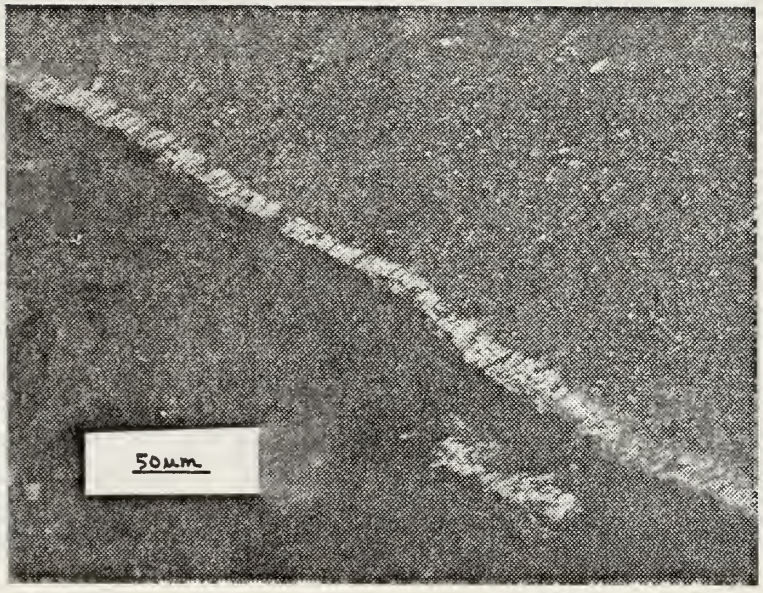

Figure 55 - Light micrograph of corrosion layer between the grid and active material, grid is at upper right. 13 cycle PbCa positive plate operated in trickle discharge routine, plate is fully charged, 200x.

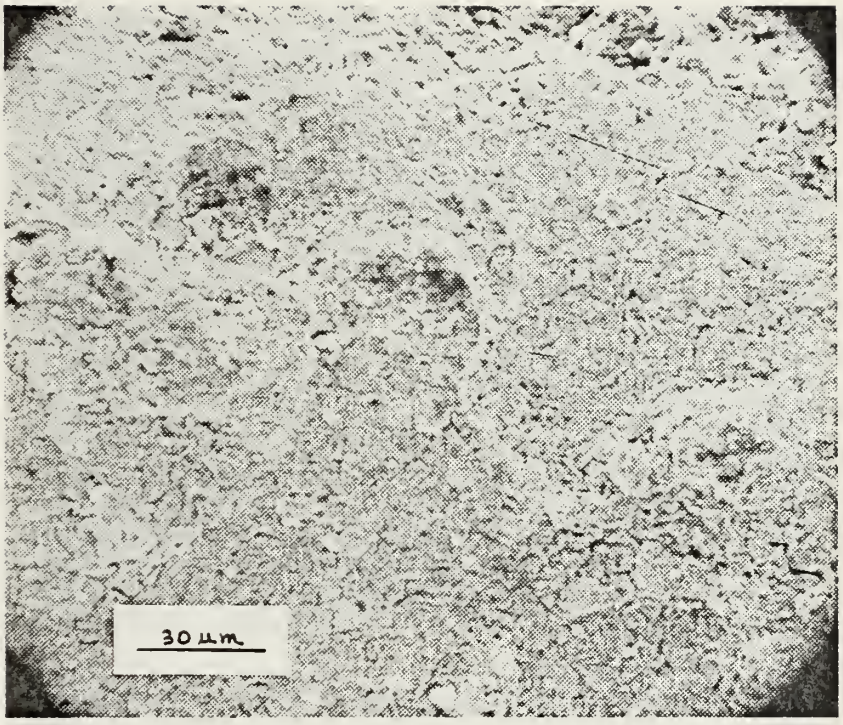

Figure 56 - Exterior of grid with active material broken away. Corrosion layer evident but the dendritic network is not seen. 10 cycle PbCa positive plate operated in float routine, plate is fully charged, 550x.

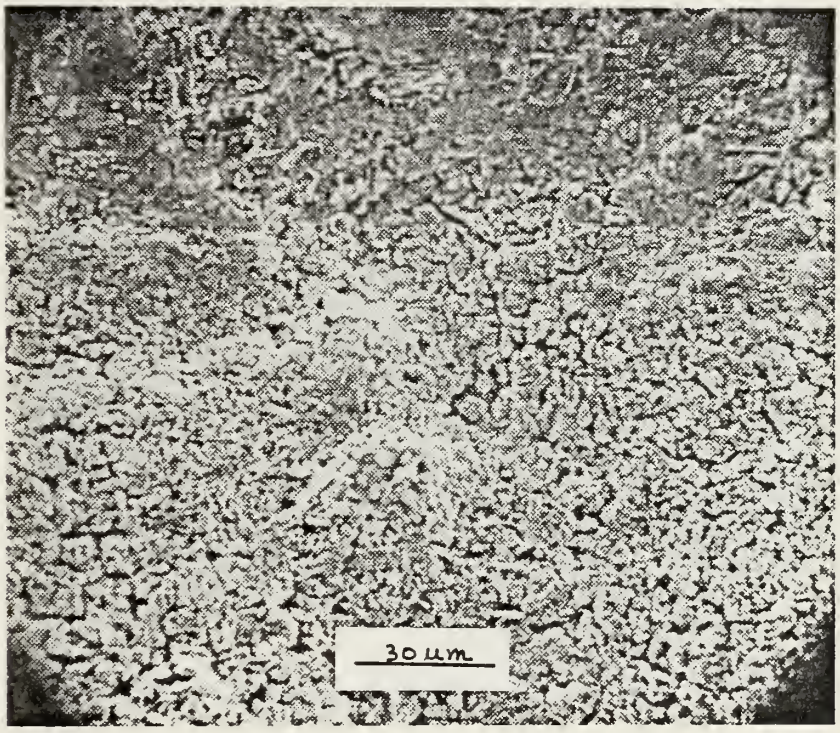

Figure 57 - Exterior of grid with active material broken away. Corrosion layer evident but the dendritic network is not seen. 12 cycle PbCa positive plate operated in float routine, plate is fully charged, 610x.

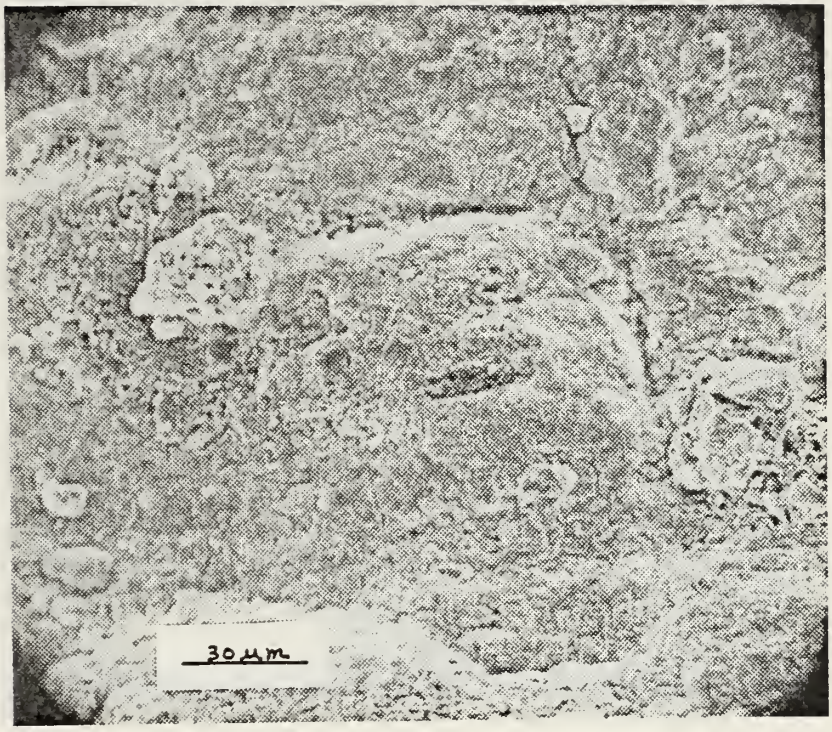

Figure 58 - Exterior of grid with active material broken away. Corrosion layer evident but the dendritic network is not seen. 16 cycle PbCa positive plate operated in float routine, plate is fully charged, 550x.

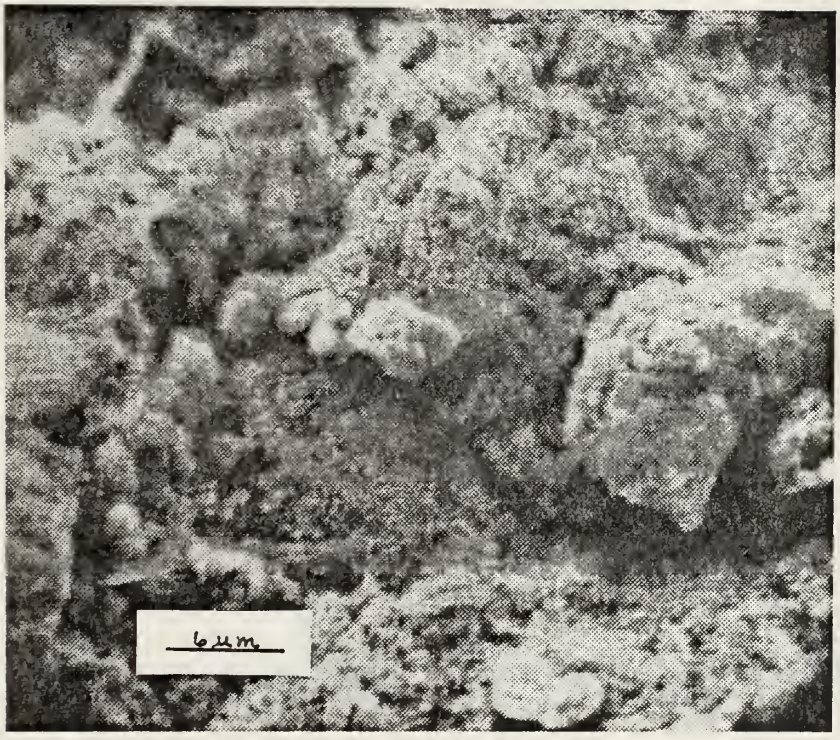

Figure 59 - Exterior of grid with active material partially broken away. Some pieces of active material and grid surface are covered by a layer of pebbly grains. 16 cycle PbCa positive plate operated in float routine, plate is fully charged, 2650x.

Figure 60 - Exterior of grid with active material broken away. Corrosion layer has fine pebbly grain morphology. 12 cycle PbCa positive plate operated in the float routine, plate is fully charged, 2500x.

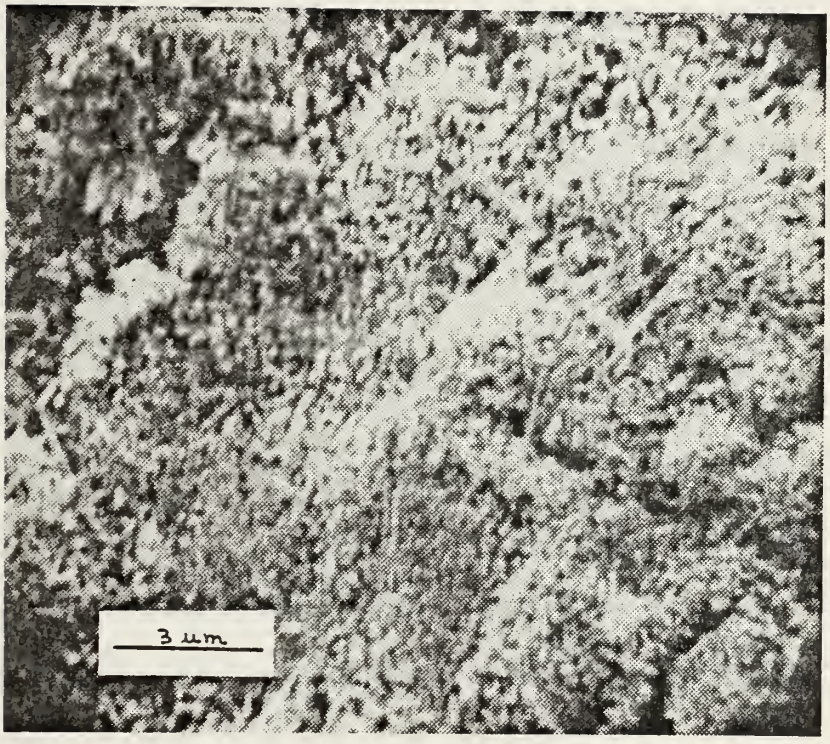

Figure 61 - Exterior of grid with active material broken away. Shows pebbly grains making up the corrosion layer. 16 cycle PbCa positive plate operated in the float routine, plate is fully charged, 6500x.

observed. The major component of this layer is an array of grains which are covered with very short fine asperities. Figure 62, a light micrograph, shows this layer to be about one-half the thickness of the layer seen on the trickle discharged plate of comparable service life.

There was one observed exception, however, to this morphology of floated PbCa plates. The positive plate from cell #5 of the floated lead calcium battery did show an array pattern of the spiny dendritic structure evident on the corrosion layer covering the grid; Figures 63 and 64 show these features. Referring back to Figure 17, the plot of average cell float voltages versus cycles for PbCa #2, it can be seen that this cell's float voltages were well below the cell float voltage range for much of its testing duration. It is believed that the period of low float voltage resulted in the plate experiencing some self discharge and taking on characteristics similar to those observed in the trickle discharged plates.

Floated cell active material morphology was also somewhat different from that seen in the trickle discharged plates. Figures 65-67 show the active material appearance at various stages of cycle life. Consolidated, void regions developed during initial cycles, and became more extensive as testing progressed, resulting in a more fragile and open active material structure. When compared with trickle discharge active material microstructure seen in Figures 24-26, the void development is more rapid in the floated plates.

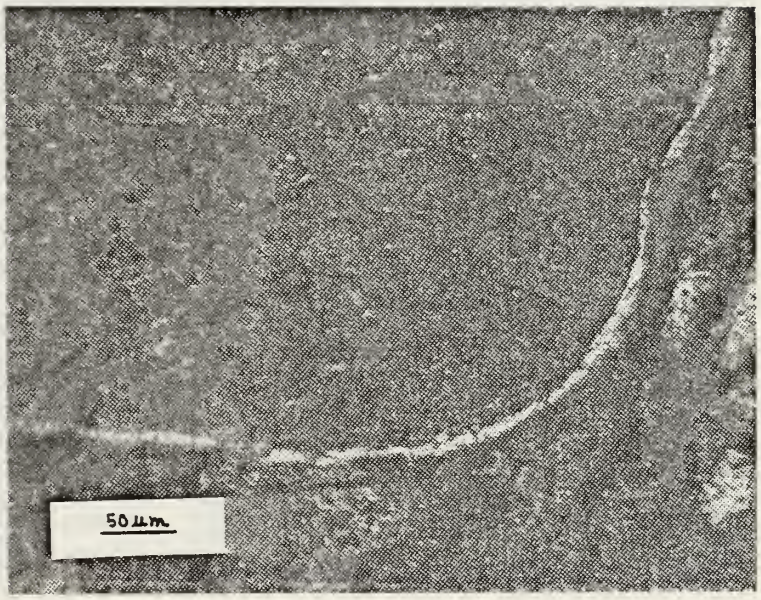

Figure 62 - Light micrograph showing corrosion layer between the grid (upper) and active material (lower). 16 cycle PbCa positive plate operated in float routine, plate is fully charged, 200x.

Figure 63 - Exterior of grid with active material broken away. Some dendritic network is visible on the corrosion layer. Spiny crystals are also evident. 6 cycle PbCa positive plate operated in the float routine at lowered cell voltage, plate is fully charged, 2650x.

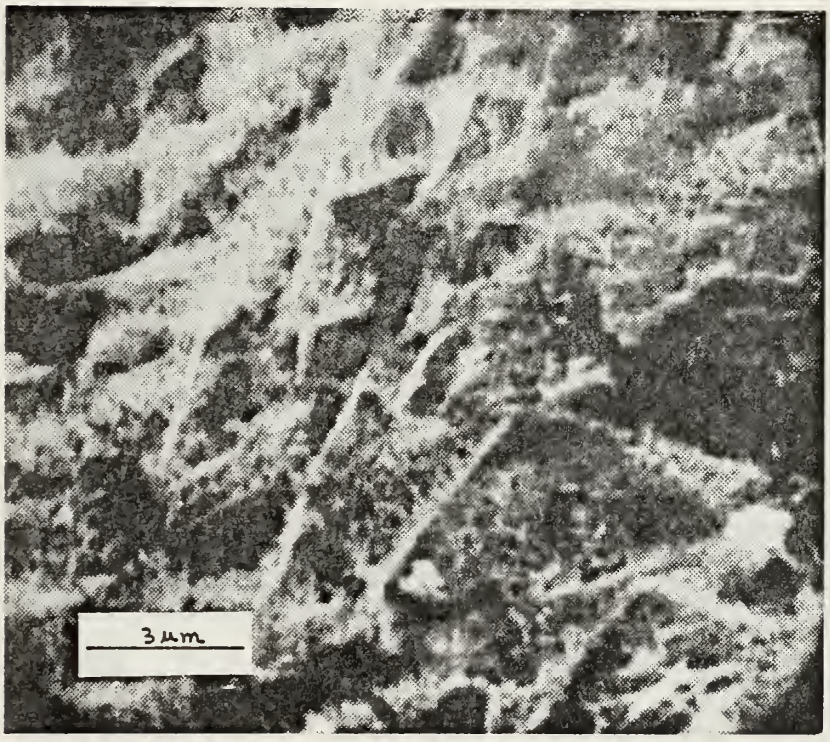

Figure 64 - Exterior of grid with active material broken away. Spiny crystals are evident in the corrosion layer. 6 cycle PbCa positive plate operated in the float routine at lowered cell voltages, plate is fully charged, 6900x.

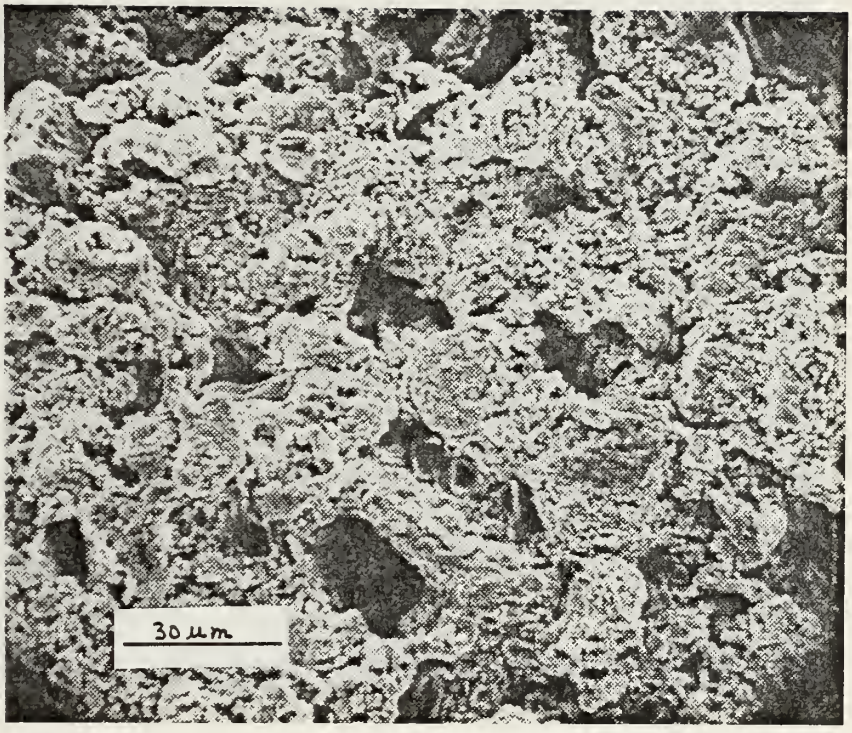

Figure 65 - Active material, 6 cycle PbCa positive plate operated in float routine, plate is fully charged, 610x.

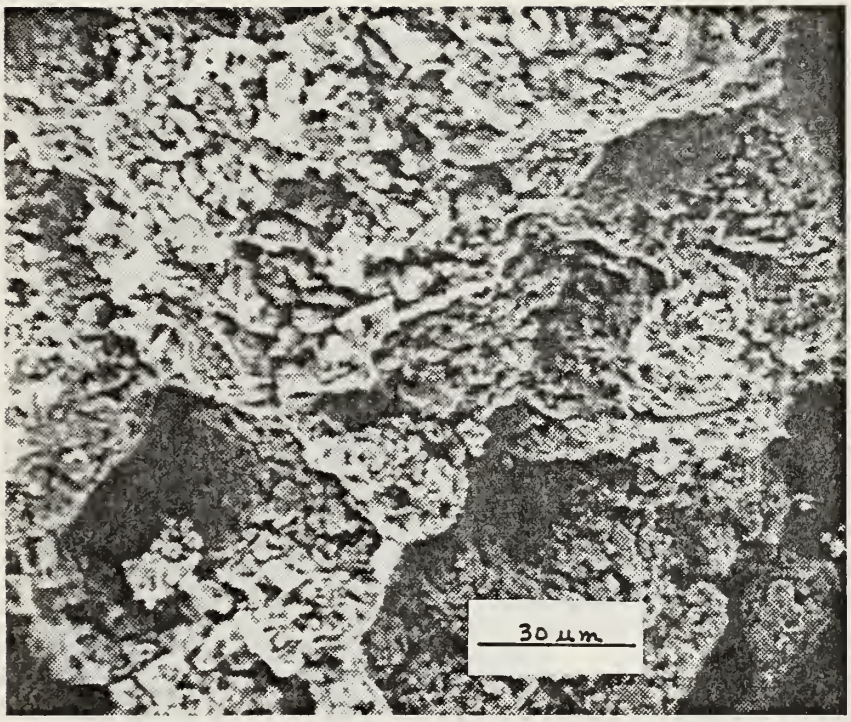

Figure 66 - Active material, 12 cycle PbCa positive plate operated in the float routine, plate is fully charged, 695x.

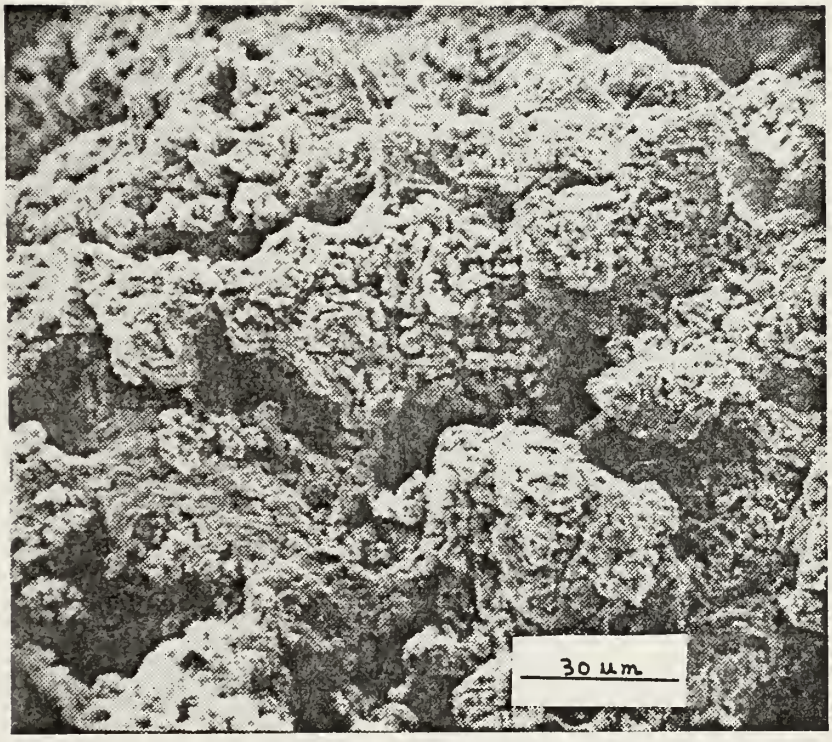

Figure 67 - Active material, 16 cycle PbCa positive plate operated in the float routine, plate is fully charged, 680x.

The active material substructure of floated plates was characterized by the asperity-covered grains previously noted in the corrosion layer. Figure 68 shows a high magnification picture of these grains. In comparison, Figure 69 shows the active material substructure from a trickle discharged plate and a difference in crystalline forms is noted. The trickle discharged plate contains larger linear spiny crystals in addition to some of the asperity-covered grains.

It has already been noted that the corrosion layer thickness in the floated plates is about one-half that of the trickle-discharged plate layer. The comparison between the two and a 0-cycle PbCa positive plate is shown in Figures 70-75. Figures 70 and 71 show a top view of breaks in the layer contrasted against the uneven surface of the grid. Figure 72 shows the clean grid surface of a 0-cycle PbCa grid. Figures 73-75 are light micrographs showing the grid/active material interface for the 0 cycle, 13 cycle trickle discharged, and 16 cycle floated PbCa positive plates. The corrosion layer is not evident for the 0-cycle plate (which confirms the SEM view in Figure 72), measures about 10-12 μm for the floated plate, and about 20-25 μm for the trickle discharged cell.

3. Floated Lead Antimony

Figures 76-83 reveal the morphology of the floated lead-antimony grid positive plates. Many similarities are noted between the PbSb and PbCa plates operated under the

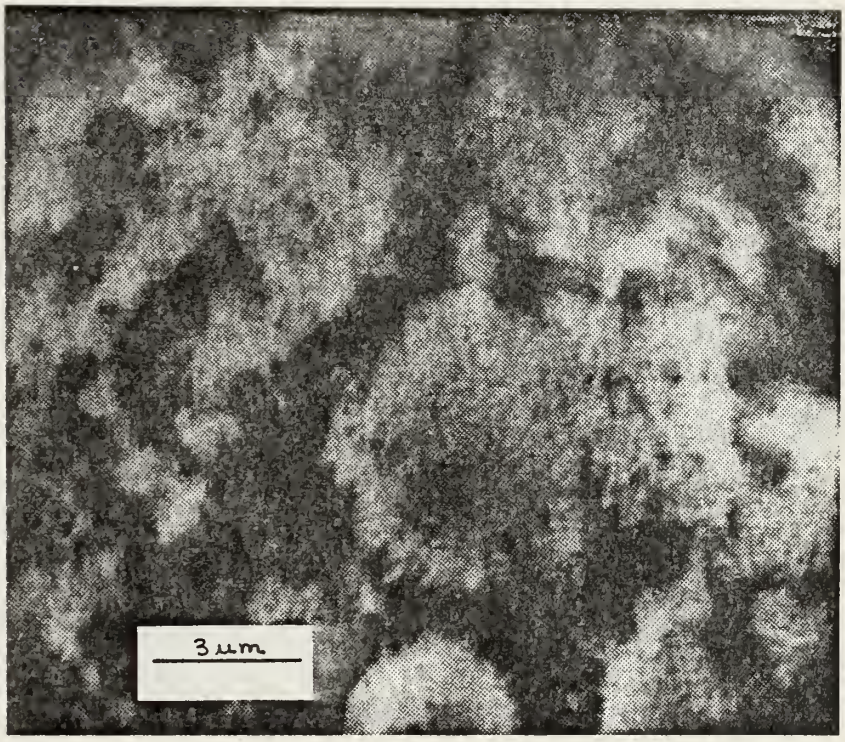

Figure 68 - Active material, 16 cycle PbCa positive plate operated in the float routine, plate is fully charged. Substructure of active material showing pebbly grains, 6400x.

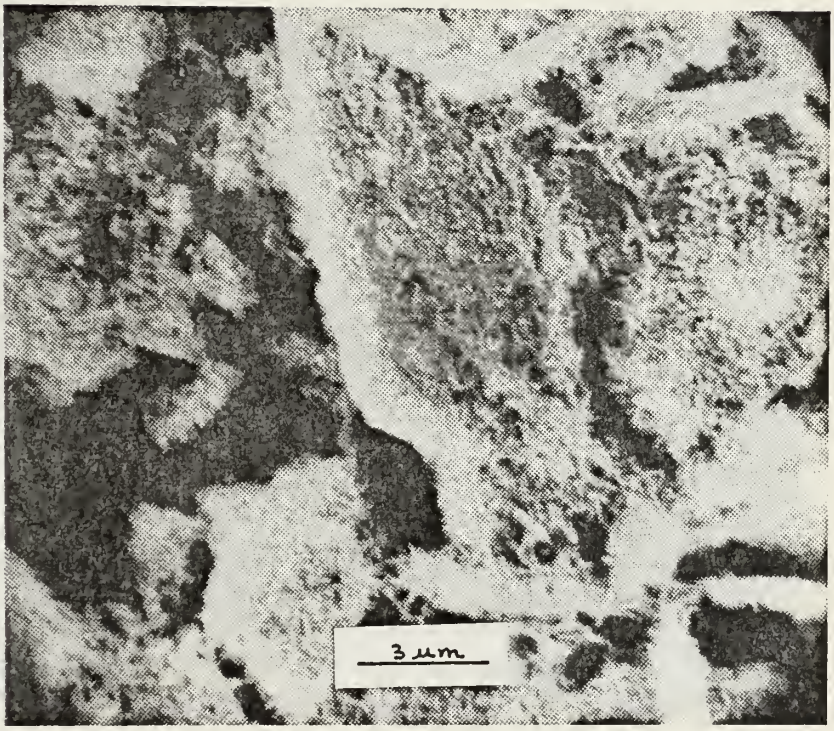

Figure 69 - Active material, 10 cycle PbCa positive plate operated in the trickle discharge routine, plate is fully charged. Substructure of active material showing spiny crystals and some pebbly grains, 5700x.

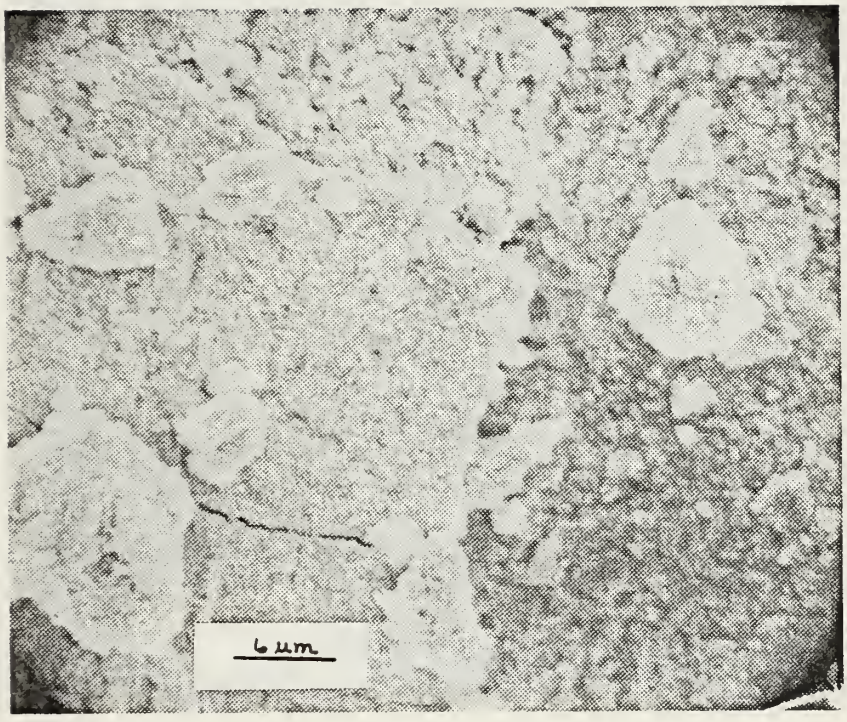

Figure 70 - Exterior of grid with active material broken away showing break in the dense corrosion layer covering the grid surface. 5 cycle PbCa positive plate operated in the trickle discharge routine, plate is fully charged, 2200x.

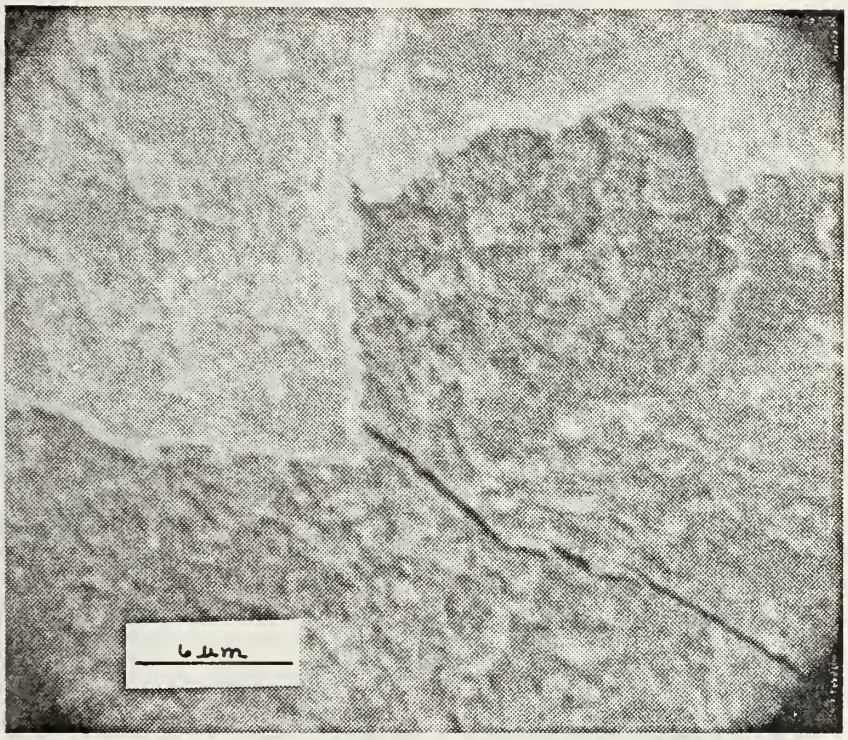

Figure 71 - Exterior of grid with active material broken away showing break in the dense corrosion layer covering the grid surface. A narrow crack in the grid metal surface is also evident. 12 cycle PbCa positive plate operated in the float routine, plate is fully charged, 3450x.

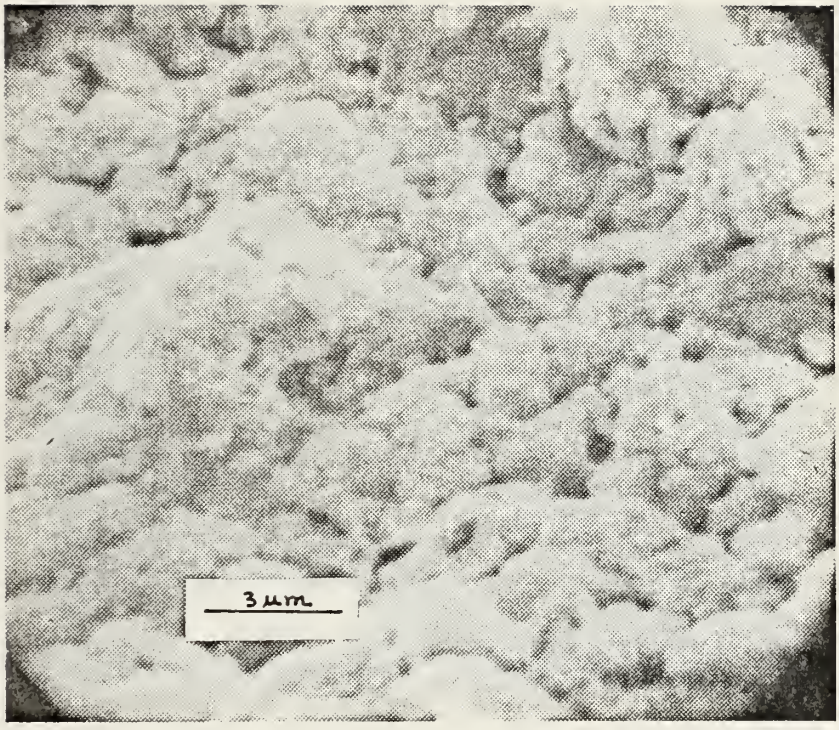

Figure 72 - Exterior of grid with active material broken away. No corrosion layer evident. 0-cycle PbCa positive plate, 6000x.

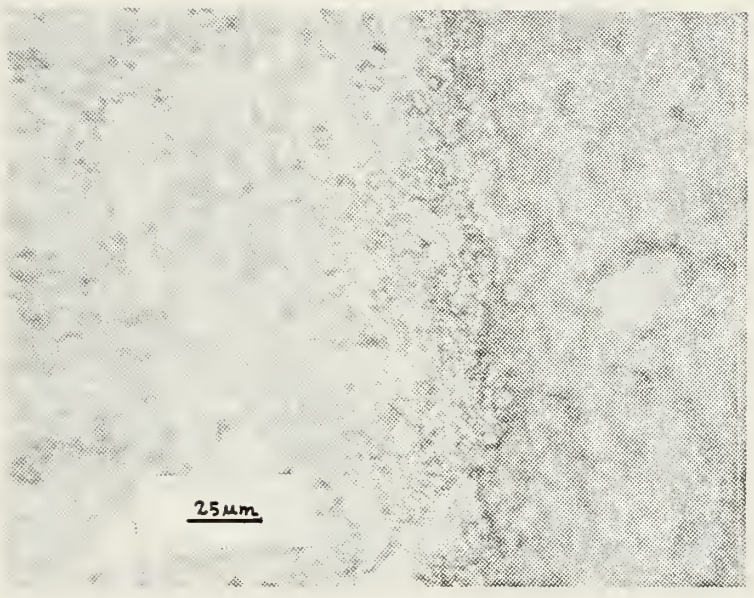

Figure 73 - Light micrograph of 0-cycle PbCa positive plate showing the grid (left)/active material (right) interface. No corrosion layer is evident, 400x.

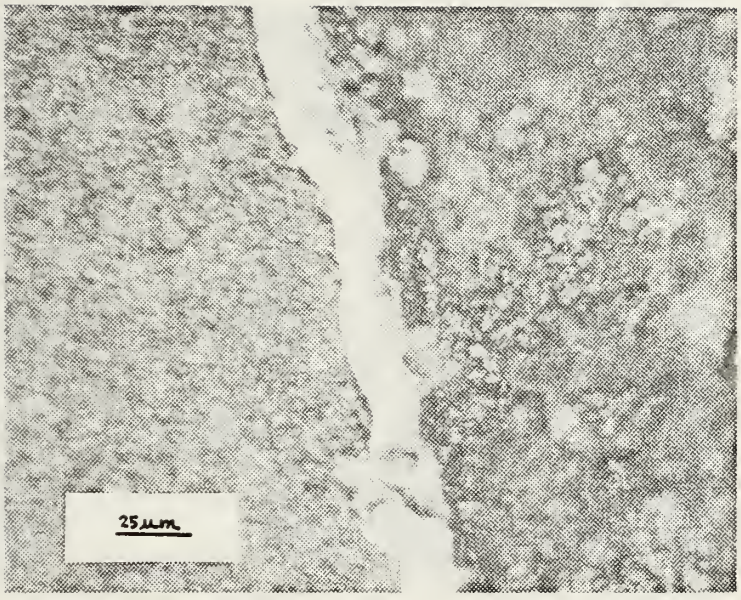

Figure 74 - Light micrograph of 13 cycle PbCa positive plate operated under trickle discharge routine showing the corrosion layer (white) between the grid (left) and the active material (right). Plate is fully charged, 400x.

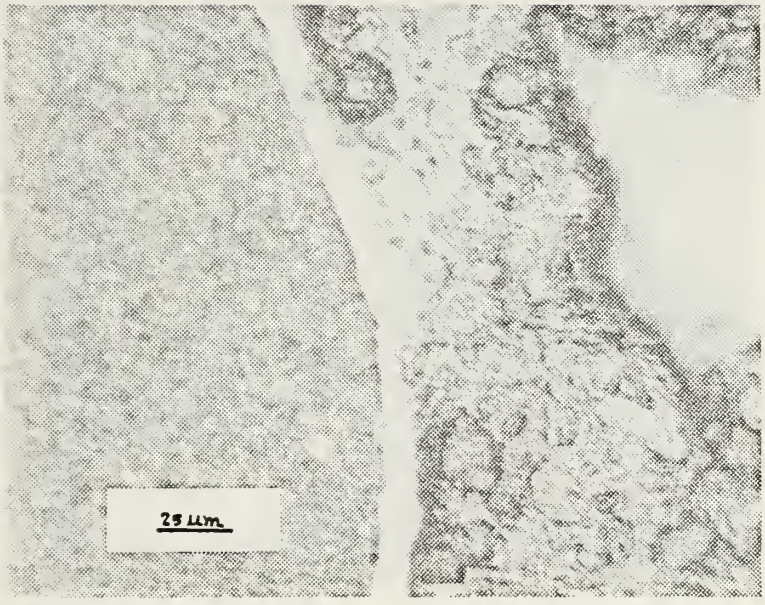

Figure 75 - Light micrograph of 16 cycle PbCa positive plate operated under the float routine showing the corrosion layer (white) between the grid (left) and the active material (right). Plate is fully charged, 400x.

Figure 76 - Exterior of grid with active material broken away. No corrosion layer evident. 0-cycle PbSb positive plate, 2300x.

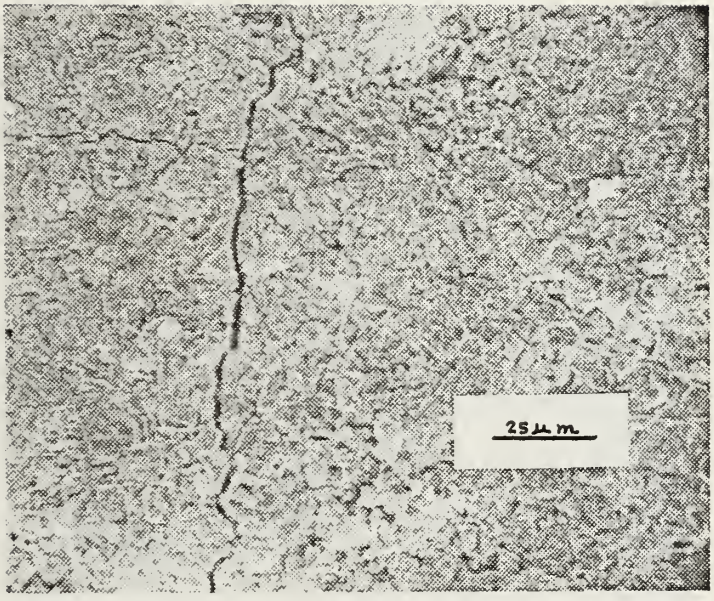

Figure 77 - Exterior of grid with active material broken away showing corrosion layer. 13 cycle PbSb positive plate operated under float routine, 550x.

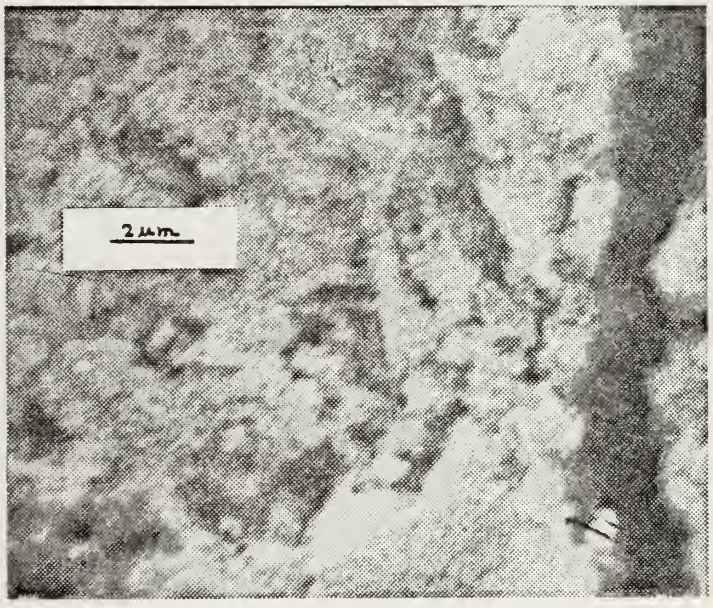

Figure 78 - Exterior of grid with active material broken away showing corrosion layer substructure. 13 cycle PbSb positive plate operated under float routine, 5500x.

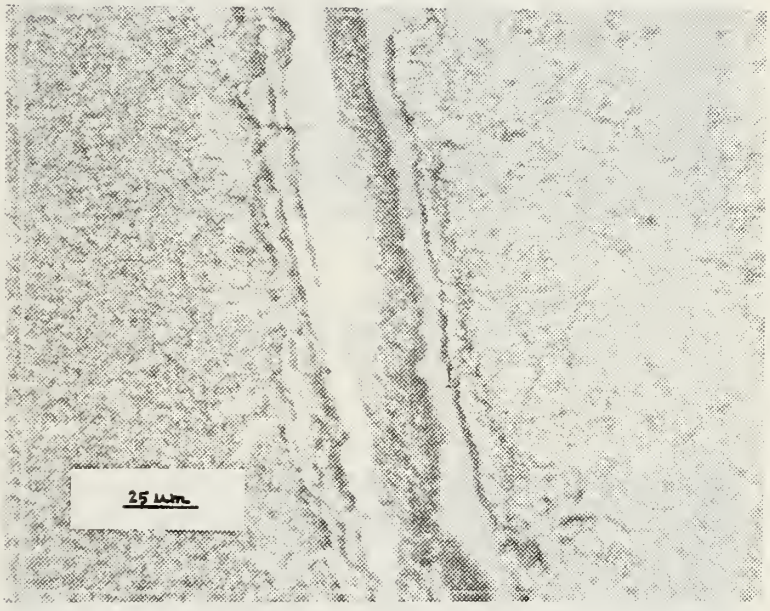

Figure 79 - Light micrograph of 13 cycle PbSb positive plate operated under the float routine showing a dished corrosion layer between the grid (left) and the active material (right). Plate is fully charged, 400x.

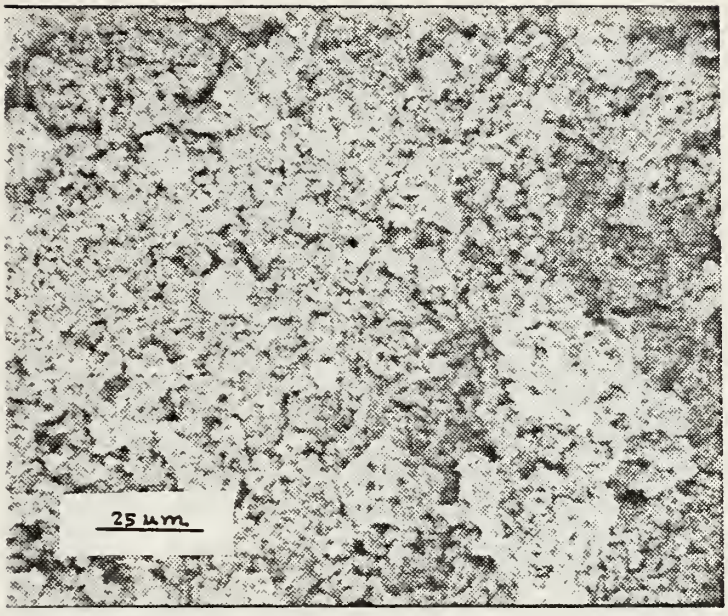

Figure 80 - Active material 0-cycle PbSb positive plate, 570x.

Figure 81 - Active material, 13 cycle PbSb positive plate operated under the float routine, plate is fully charged, 540x.

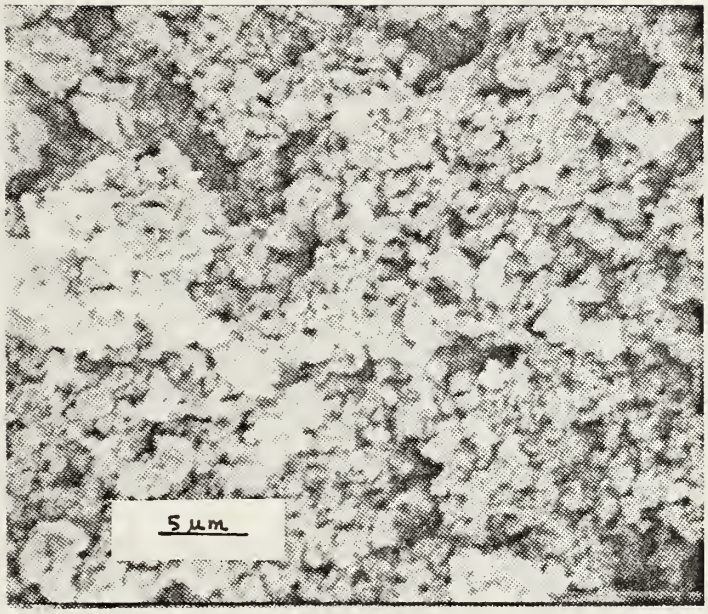

Figure 82 - Active material, 0-cycle PbSb positive plate, 2300x.

Figure 83 - Active material, 13 cycle PbSb positive plate operated under the float routine, plate is fully charged, 2200x.

float routine. The most notable difference appeared in the corrosion layer. The PbSb corrosion layer seen in Figures 77-79 was much thicker (about 45 μm) and was more easily removed from the grid surface than was the layer on either PbCa battery. When viewed under the light microscope the layer had a slightly dished appearance. It's substructure morphology was similar to that of the PbCa floated battery, being made up primarily of asperity-covered grains. There was no appearance of a dendritic network pattern or spiny crystals either on the corrosion layer or the active material.

The active material in the PbSb plates did undergo structural degradation. Several pellets blistered, and upon removal and macroscopic examination it was observed that the active material, through the thickness of the pellet, had lost surface contact with itself and could easily be peeled open. It was this condition of the active material which evidently caused the declining capacity in cell #2 at the end of the test.

In comparing the 0 cycle active material morphology of the PbCa and PbSb positive plates (Figure 20 and Figure 82), the nodular masses of the PbCa plate appear to be much larger than for those of the PbSb plate. An additional observation concerning the active material is that, although large pores do open up in the aggregate masses of these nodules, as they do in the PbCa plates, the distinct nodular shape of the PbO_2 grains is retained. In the

PbCa plates there is a tendency for the active material to agglomerate as seen in Figures 84 and 85.

C. X-RAY DIFFRACTION ANALYSIS OF ACTIVE MATERIAL

X-ray diffraction patterns were run on representative samples of active material from lead-calcium and lead-antimony grid positive plates. CuK_{α} radiation was utilized in obtaining these diffraction patterns. Figure 86 shows the location of prominent peaks for $PbSO_4$, α-PbO_2 and β-PbO_2, as determined by ASTM Hanawalt Card File data. Figures 87-91 reduce the data collected for 0-cycle PbCa and PbSb plates, 13 cycle trickle discharged PbCa, 16 cycle floated PbCa, and 13 cycle floated PbSb. As can be seen, all samples showed β-PbO_2 as the predominant compound present with some $PbSO_4$ detected in the 13 cycle trickle discharged positive plate. No α-PbO_2 was detected. The latter was not unexpected, but does not constitute prima facie evidence that α-PbO_2 is not present. Reference 9, in discussing x-ray analysis of mixtures, notes that in standard mixtures of α- and β-PbO_2, the α-PbO_2 diffraction pattern is weaker than it should be relative to its composition in the mixture. Two reasons are suggested for this; (a.) the α-PbO_2 is coated over by the soft β-PbO_2 during grinding or, (b.) recrystallization to stable β-PbO_2 takes place in the superficial layers of the metastable crystals of α-PbO_2. The results do indicate that, if α-PbO_2 is present, it makes up a small percentage of the mixture. The presence

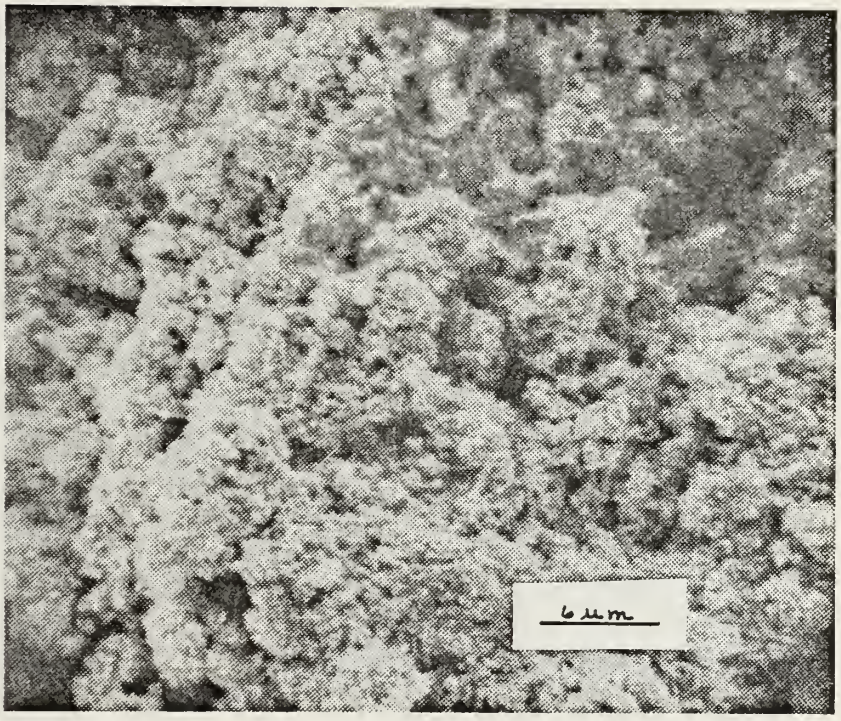

Figure 84 - Active material, 13 cycle PbCa positive plate operated under the trickle discharge routine, plate is fully charged. Shows tendency of PbO_2 to agglomerate in PbCa plates, 2600x.

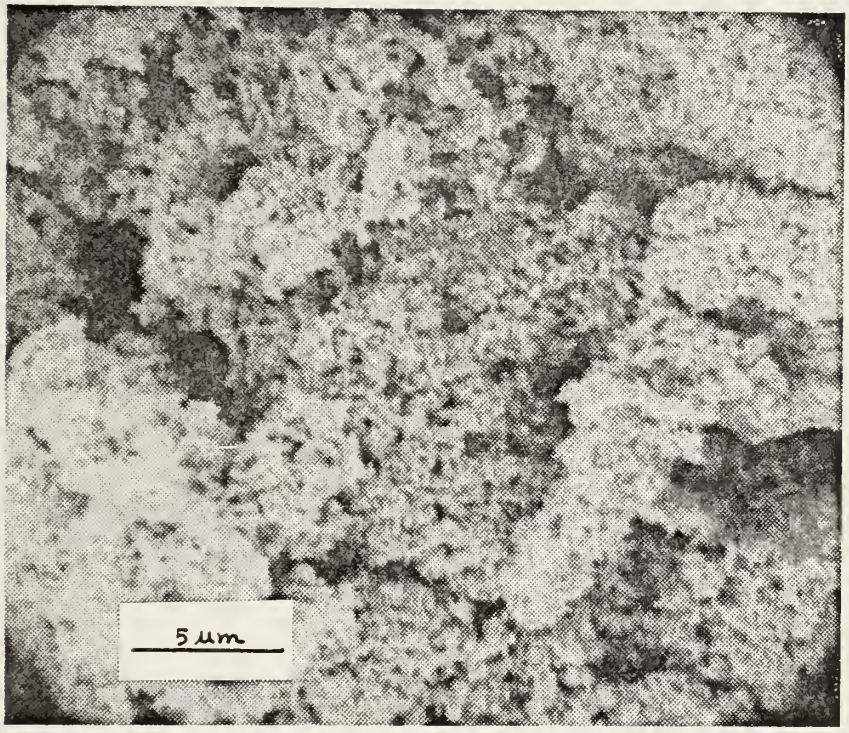

Figure 85 - Active material, 12 cycle PbCa positive plate operated under the float routine, plate is fully charged. Nodular grains of PbO_2 has agglomerated into large active material clusters, 4000x.

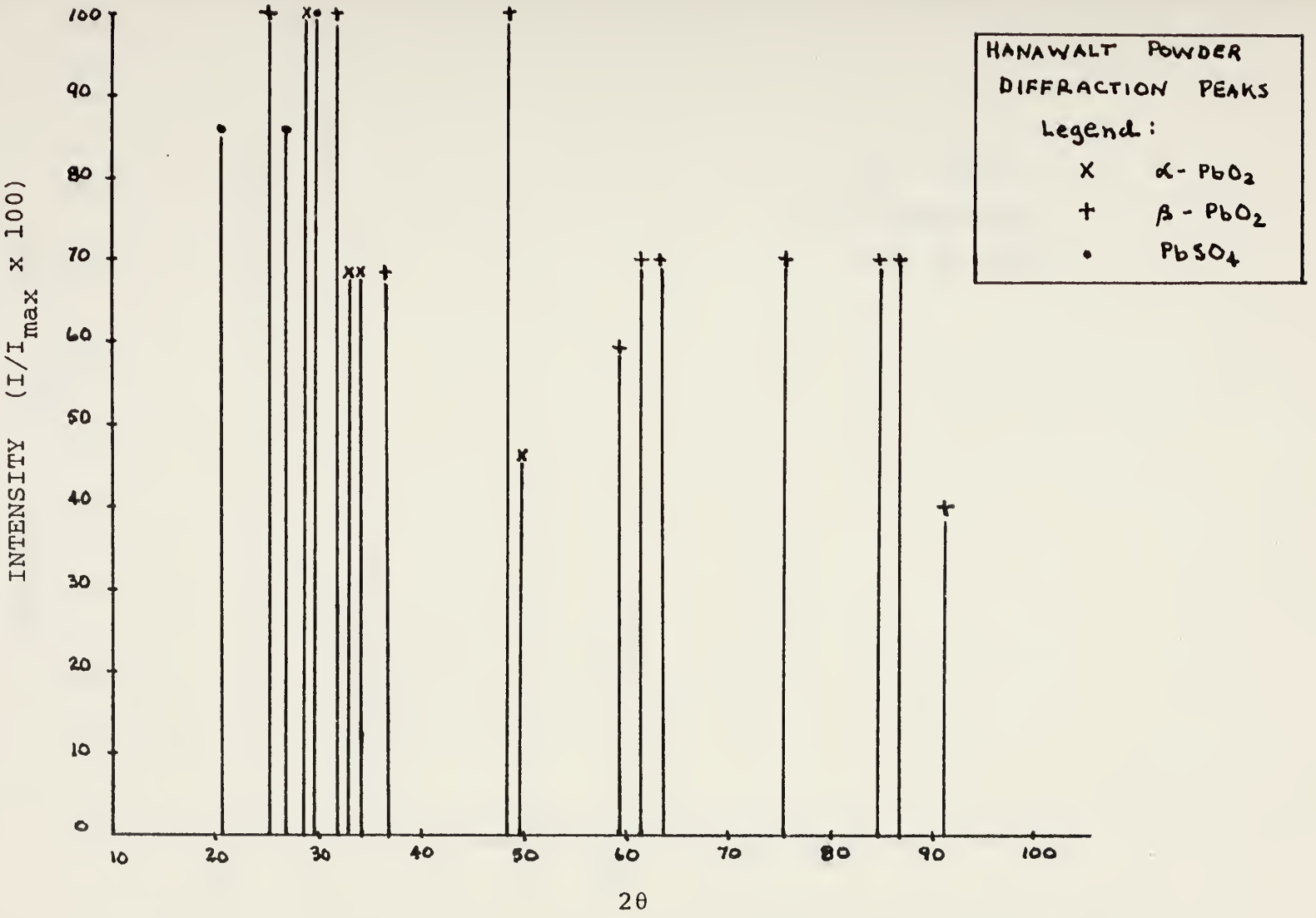

Figure 86 — Relative intensity vs. 2θ for major x-ray diffraction peaks of α - PbO_2 , β - PbO_2 , and $PbSO_4$

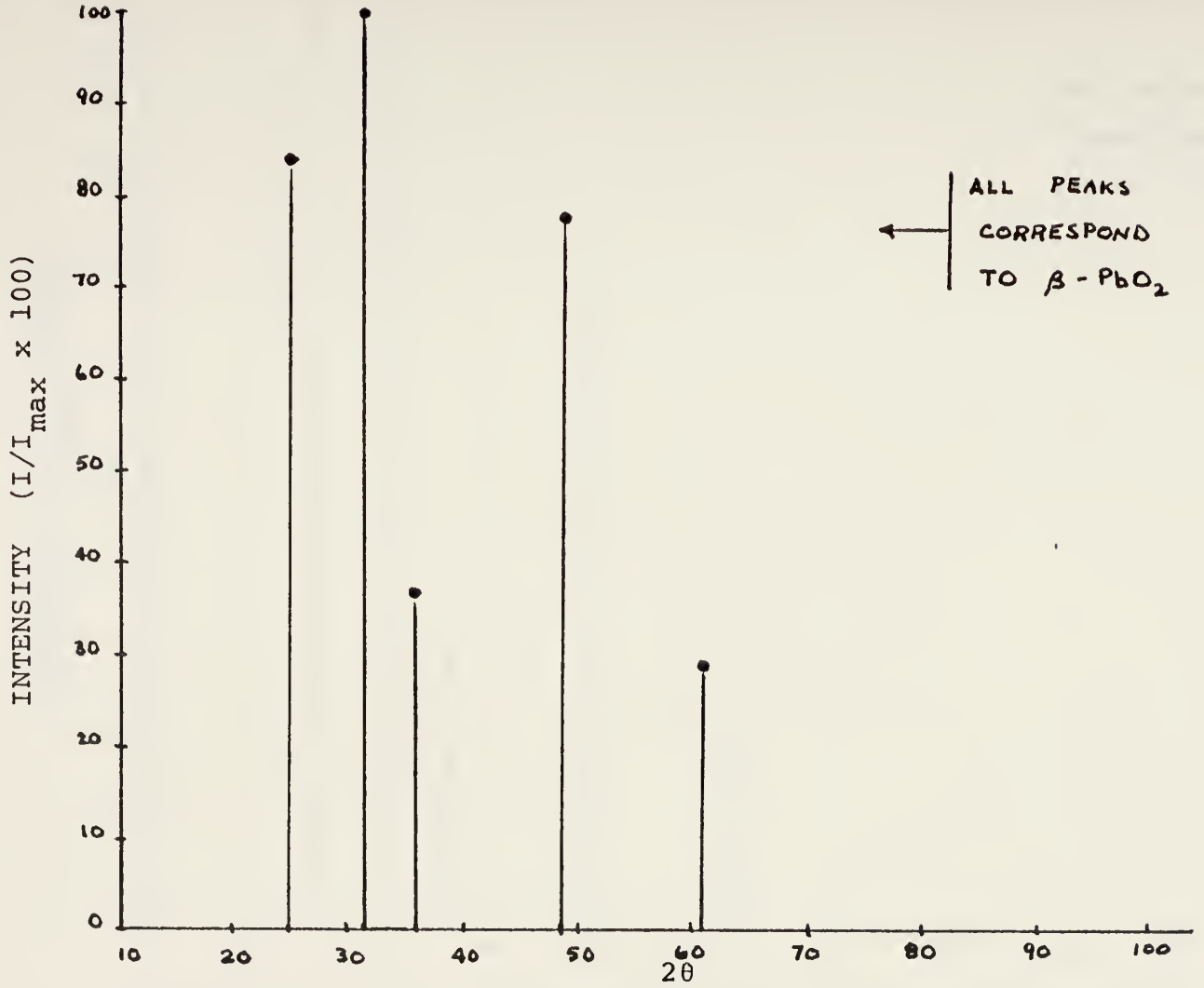

Figure 87 — X-ray diffraction plot of relative intensity vs. 2θ
Active material 0-cycle PbCa positive plate

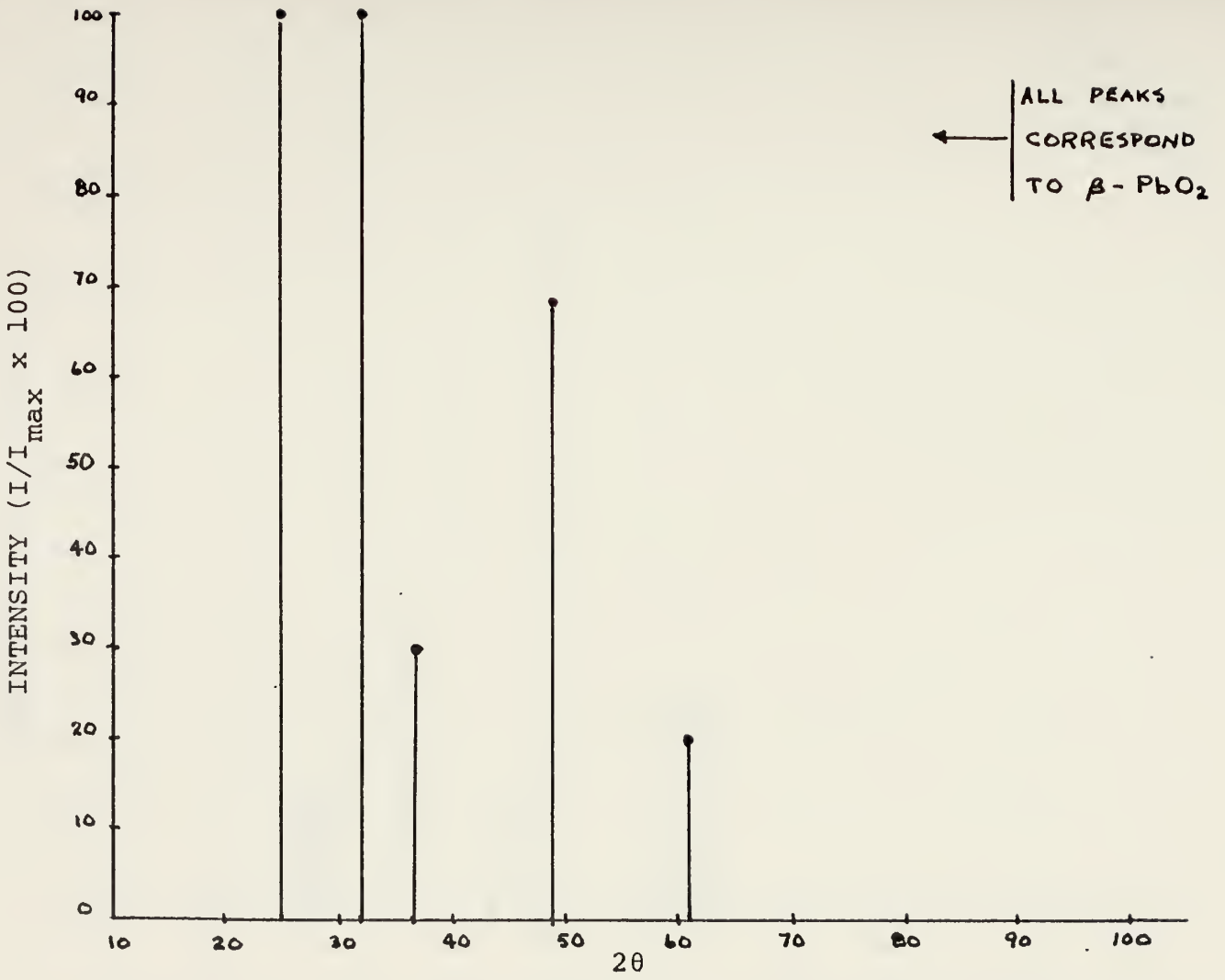

Figure 88 — X-ray diffraction plot of relative intensity vs. 2θ
Active material, 0-cycle PbSb Positive Plate

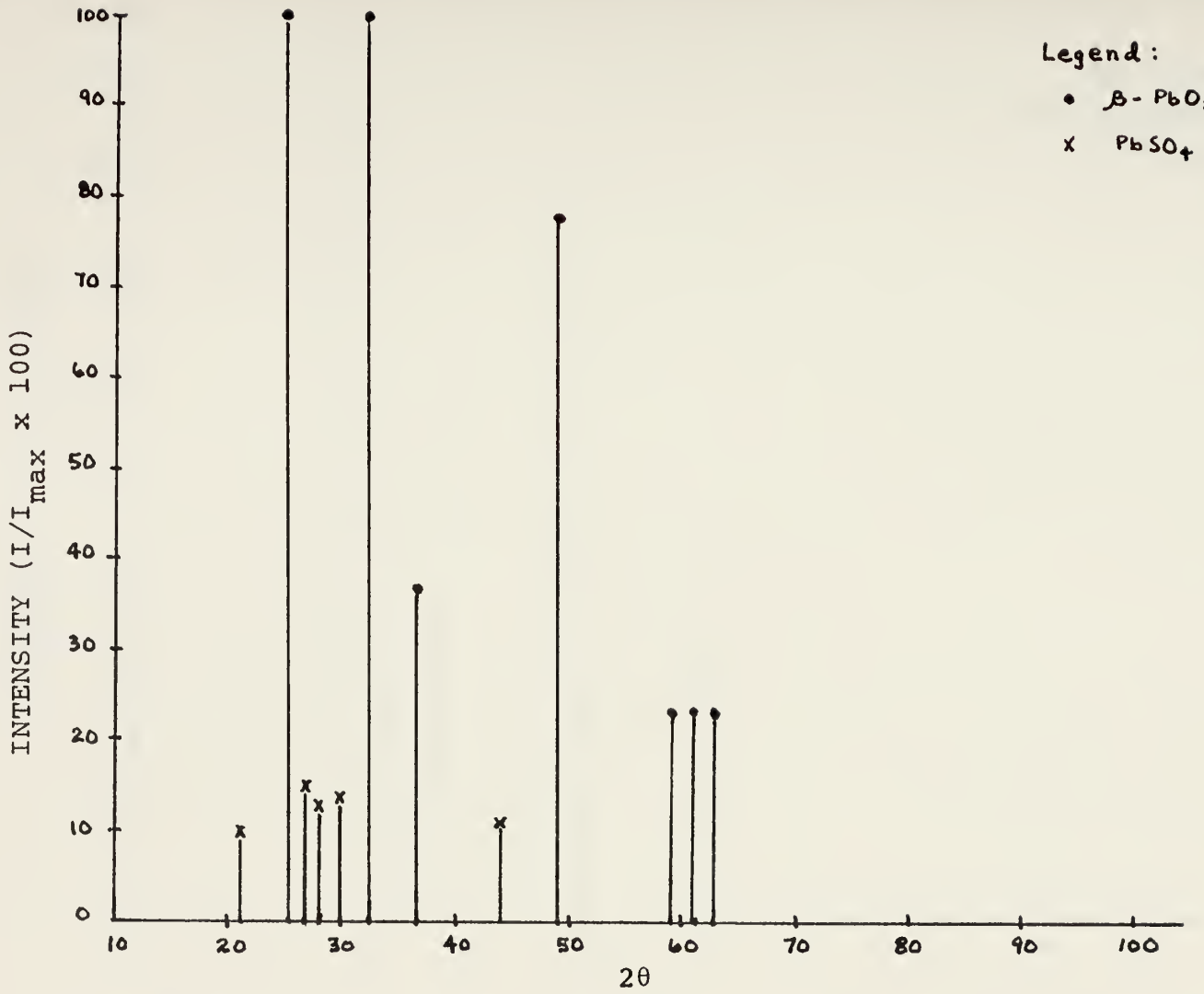

Figure 89 — X-ray diffraction plot of relative intensity vs. 2θ
Active material, 13 cycle PbCa Trickle Discharge Positive Plate

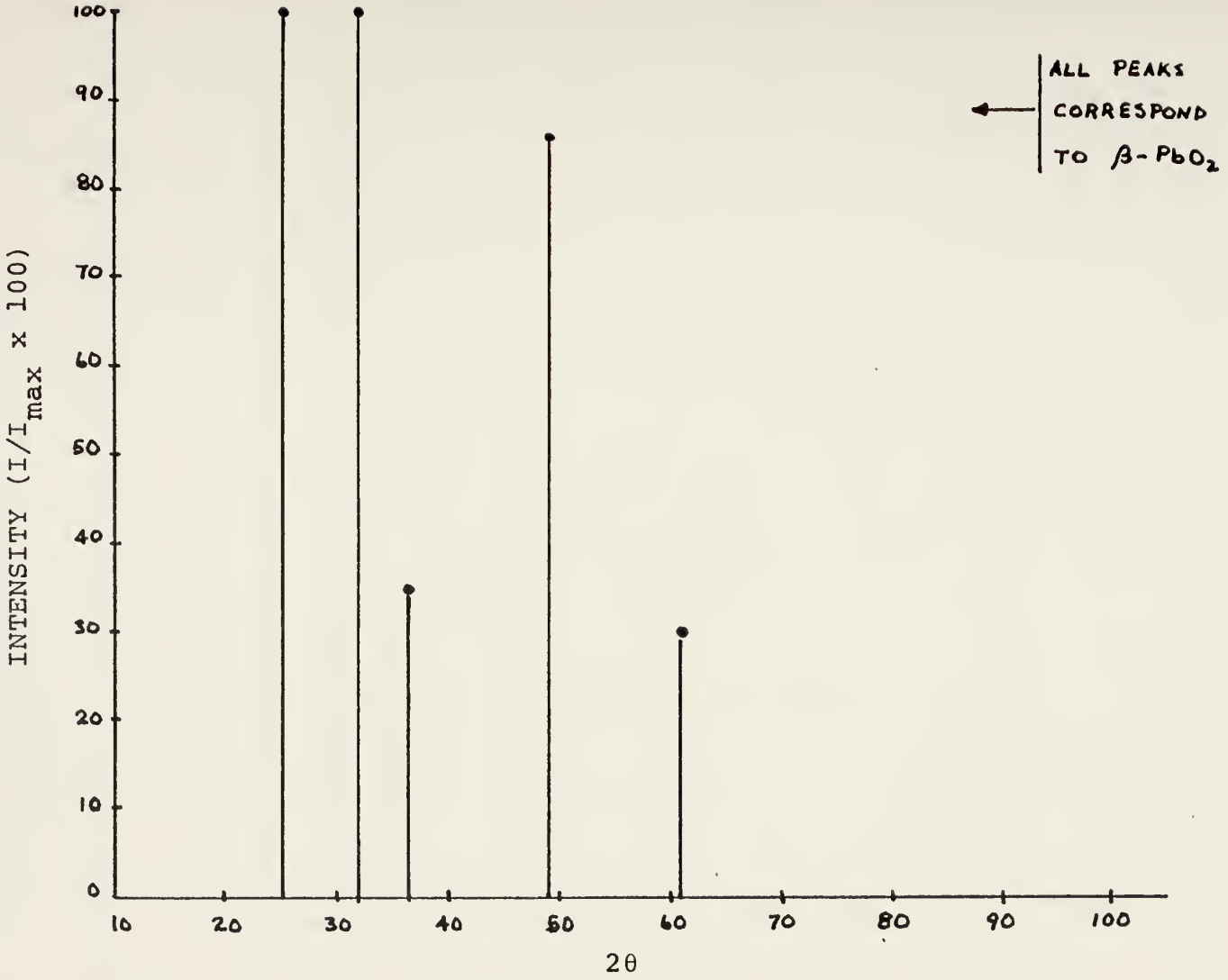

Figure 90 — X-ray diffraction plot of relative intensity vs. 2θ
Active material, 16 cycle PbCa Floated Positive Plate

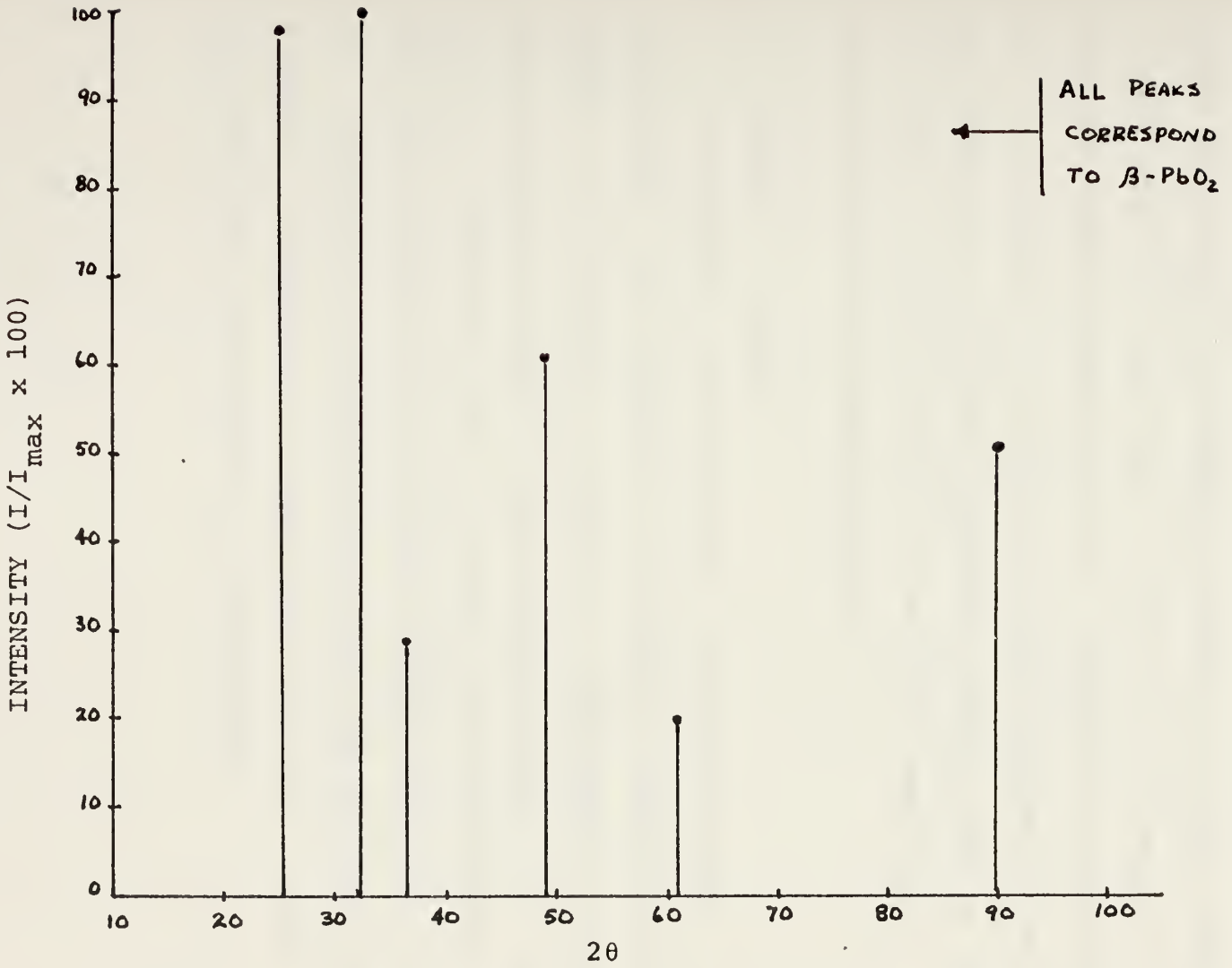

Figure 91 — X-ray diffraction plot of relative intensity vs. 2θ
Active material, 13 cycle Floated PbSb Positive Plate

of $PbSO_4$ in the 13 cycle PbCa trickle discharged plate is interesting in light of the fact that little of the standard morphologies described extensively in the literature [25,27,28] for $PbSO_4$, was seen during visual exploration of this plate using the SEM. It will be recalled that this plate did contain the dendritic network of spiny crystals on the corrosion layer next to the grid surface and in the reported dense coating layer over regions of active material. In general the x-ray diffraction information was not as conclusive as had been expected, but did seem to indicate that no dramatic change in compound composition occurred during the testing period.

D. SUMMARY OF RESULTS

In evaluating the myriad data obtained from SEM, light microscopy, x-ray analysis, and review of service performance, it is difficult to provide a comprehensive explanation which correlates all the observed results. As noted earlier, a bona-fide loss of capacity was not obtained for the PbCa batteries, while the PbSb battery did appear to be in a condition of inexorable decline. The following table presents a comparison of significant features in plate microstructure development and performance:

TABLE III. Comparison of Significant Features of Lead-Calcium and Lead-Antimony Cells

Feature	PbCa #1	PbCa #2	PbSb
A. Routine	Trickle Discharge	Float	Float
B. Capacity	Increasing	Steady	Declining
C. Active material (SEM)	1) Some voids developing in oldest plate and some areas covered with dense layers (500-700x)	1) Large voids develop early in plate life (500-700x)	1) Large voids have developed early in plate life (500-700x)
	2) Nodular masses have agglomerated into larger clumps (2000-3000x)	2) Nodular masses have agglomerated into larger clumps (2000-3000x)	2) Nodular masses retain distinct morphology. Nodules are smaller than seen in PbCa plates (2000-3000x)
	3) Substructure consists of many more spiny crystals than seen in the 0-cycle morphology (5000-7000x)	3) Substructure comprised of small asperity-covered crystal grains. Needles are generally not present (5000-7000x)	
	4) Patterned dendritic network of spiny crystals seen on coating over some regions of active material		

TABLE III (Continued)

Feature	PbCa #1	PbCa #2	PbSb
D. Grid Corrosion Layer (SEM/LM)	1) 13 cycle thickness 20-25 μm (LM)	1) 16 cycle thickness 10-12 μm (LM)	1) 13 cycle thickness 40-45 μm; has dished appearance (LM)
	2) Fine network weave containing many spiny crystals (5000-7000x)	2) Mass of asperity-covered grains similar to active material substructure, but layered, not clumped. Virtually no spiny crystals except in plate which floated at low voltage (5000-7000x)	2) Mostly fine, asperity-covered pebbly grains compacted together. (5000-6000x)
	3) Tenacious adherence to the grid surface.	3) Tenacious adherence to the grid surface.	3) Easily removed from grid surface by mechanical shock.
	4) Patterned dendritic network of spiny crystals on surface of top layer of corrosion product.		

The formation mechanism of the patterned dendritic structure of spiny crystals noted in the trickle discharged plates has been discussed earlier. The other significant differences in plate morphology, as delineated in Table 2, relate to corrosion layer thickness, corrosion layer substructure, and active material void formation as a function of service life.

Both the corrosion layer thickness and its substructure are related to the positive plate voltage maintained during the trickle discharge and float periods. Much research has been done to establish the chemical properties of the anodic layer as a function of plate voltage [29,30,31]. In the voltage range of the floated plate α- and β-PbO_2 are the principal constituents of the layer, while in the trickle discharge voltage range, tetragonal PbO and $PbSO_4$ are also present. The layer seen in the SEM analysis of the trickle discharged plates does not appear to contain $PbSO_4$ since it was evidently converted to PbO_2 during the final charge prior to removing the plates from service. The layer thickness is explained by the fact that the PbO_2 produced from conversion of $PbSO_4$ has a greater volume than PbO_2 formed from the oxidation of lead, hence the fully charged layer of the trickle discharged plate is thicker than that of the floated plate.

It is believed that the active material morphology can be explained by the nature and size of the $PbSO_4$ crystals formed in the plates during the different phases of service.

In Reference 24 Simon analyzed the differences in $PbSO_4$ crystal development for varying rates of discharge. He observed that, for slow discharge rates, the crystals of $PbSO_4$ grew to a large size, while the PbO_2 in their vicinity dissolved. Discharge terminated when the remaining undissolved PbO_2 was encapsulated by the growing $PbSO_4$ crystals. Recharge of these crystals proceeded by two separate mechanisms. First, nucleation and growth occurred in exposed PbO_2 remaining at the end of discharge, producing small PbO_2 crystals deposited as a dense and non-porous layer upon the PbO_2 already there. Such a layer was noted in the active material of the trickle discharged plates (Figures 28 and 29). The second growth mechanism involved encapsulated PbO_2 which acted as nuclei for further PbO_2 crystallization, slowly increasing in size and spreading across the faces of the crystals in a porous layer. Concurrent $PbSO_4$ dissolution resulted in a very delicate and porous PbO_2 structure. In contrast, high rate discharges produced a dense layer of smaller, hard (i.e., no PbO_2 encapsulation, $PbSO_4$ all the way through) $PbSO_4$ crystals over the surface of unreacted PbO_2. Discharge terminated when the PbO_2 became isolated from the electrolyte due to the extent of this passivation by the $PbSO_4$ layer. The recharge process was characterized by formation of a compact surface layer of PbO_2 in the area where the small $PbSO_4$ crystals were located. Subsequent high rate discharges refined this structure, with the layer becoming more compact

and less reactive with each successive cycle. In Reference 25, Simon et. al., explain this phenomenon as resulting from the fact that the $PbSO_4$ crystals become more uniform in size and are arranged in a tightly interlocked, non-porous layer on the PbO_2. As the active material mass becomes more compact, a branched network or coralloid structure becomes evident and large voids form around its interconnected arms.

The trickle discharged plates, operated in the manner established for these tests, experienced both types of $PbSO_4$ crystal growth; the large crystals growing during trickle discharge and the small ones during test discharge. As a result, the active material did not develop a "memory" pattern such as it does in a plate subjected to continual high rate cycles. For this reason the active material resisted taking on a definite shape. Although some voids were opening in the active material mass of the 13 cycle trickle discharged plate (Figure 26), these were not nearly as extensive as those seen in the floated plates (Figures 65-67) which only were discharged at high rates. This is believed to be one of the reasons for the success of the trickle discharge operation in retaining cell capacity. It also tends to explain how capacity is regained in a floated plate which has failed then subjected to trickle discharge operation. In this case the compact structure refinement, caused by repeated high rate discharges of the floated plate, leads to apparent loss of capacity when the

small, uniform sized, passivating $PbSO_4$ crystals rapidly cover the PbO_2 during discharge. The trickle discharge routine introduced at this stage will interfere with the uniform size $PbSO_4$ development, eventually producing PbO_2 by the two mechanisms described earlier for recharging after a slow rate discharge.

The refined network is also structurally inferior to the more coherent active material mass seen in the trickle discharged plates. It is this fact which probably leads to active material shedding and loss in floated plates, eventually resulting in ultimate failure when the structure can no longer sustain the stresses of cycling operation. Mechanical strength of the active material is also influenced by the morphology of the substructural crystals. The trickle discharged plates had a large number of spiny crystals interlocked together (Figure 69) whereas the floated plates were composed primarily of fine pebbly crystals agglomerated into larger clumps (Figure 68). Although it is a subjective opinion, it is believed that the trickle discharged substructure gives greater mechanical cohesion.

Although the existence and possible formation mechanisms of the needlelike networks and pattern of spiny crystals, noted in the active material and on the grid surface corrosion layer of the trickle discharged plates has been discussed, the possible effects on cell performance have been reserved for the final portion of this section. There is no supporting data to confirm a helpful or deleterious

effect of these structures. It is a fact they exist, prominently in trickle discharged plates (and in the one plate floated at low cell voltage). The appearance of these structures does not suggest a mechanism harmful to plate performance, while several possible beneficial effects come to mind. First, these networks may comprise extensive current-conducting paths between the active material and the grid. If these structures are resistant to transformation during cycling, they may serve as conducting paths of current to $PbSO_4$ crystals upon recharge; however, this is completely unconfirmed at present. Subsequent research is recommended to determine behavior of these structures during discharge/charge sequences. Another possible function of these structures is to impart mechanical strength to the active material mass. Although it appears too fragile to support high stresses such as imposed when physically removing the active material from the grid in sample preparation, it does. It is not clear what structural integrity it might lend to a plate in service. It is obvious that a fairly efficient bond exists between the supporting surface (grid corrosion layer or dense layer in active material) and the network.

In Reference 18 Simon discusses a so-called reticulate structure found in the active material of some positive plates. He suggested it might act as a "microgrid" to lend support to the active material. He noted that the structure was arranged in a cell-like network with generally rectilinear

sides. He also correlated this with the electron microscope work of Burbank [33] which showed prismatic, branched crystals in satisfactorily floated plates, whereas unsatisfactory plate crystal structure was nondescript. Simon noted that these small prismatic crystals accompanied the reticulate structure in all plates tested. He concluded by stating that two characteristics appear desirable for good paste retention: (a.) reticulate structure of α-PbO_2 and (b.) a prismatic, branched structure in the crystals of β-PbO_2 which are enclosed by the reticulate structure of α-PbO_2. Although Simon's work was done with light microscopy, there is considerable similarity in appearance between his reticulate structure and the dendritic network seen with the SEM in the trickle discharged plates.

The complexities of establishing a viable testing routine and marrying it to the comprehensive analytical techniques at the Naval Postgraduate School is a manifold task. In retrospect, a more efficient and representative program of testing and evaluation is now apparent. It is hoped, however, that subsequent investigators can benefit from both the errors and the positive aspects of this research.

V. CONCLUSIONS

The following conclusions have been reached as a direct result of this study:

1. Trickle discharge operation of a lead-calcium alloy grid battery results in the formation of a patterned dendritic network of spiny crystals in regions of the positive plate active material and in the corrosion layer on the external surface of the grid bar. The appearance of a similar network in a floated positive plate, which happened to be operated at a voltage well below its normal float voltage range, implies that positive plate voltage is a particular parameter which influences its formation.

2. The active material morphology of lead-calcium grid positive plates is characterized by the development of large voids early in cycle life. Void formation appears to proceed at a slower rate in the active material of comparable trickle discharged plates. Although no failures occurred during this testing, actual submarine service performance, showing trickle-discharge operation to be superior to float for retaining capacity, and the exhaustive research of Burbank et. al., which correlated active material shedding with capacity loss [5], indicates that this void filled structure might not be able to withstand mechanical stresses of discharge/charge cycling.

3. An "apparent" loss of capacity has been experienced by several workers [5,19] in floated lead-calcium grid

batteries. This loss, which is recoverable upon shifting to a trickle-discharge routine, may be caused by the morphology of the active material in a floated plate which is subjected to periodic high rate discharges. The arms of the void filled structure noted in the active material of these plates became more compact with increasing numbers of cycles, suggesting a refinement of the $PbSO_4$ crystal development upon discharge. This type of plate behavior was noted by Simon [24] in studies of plate morphology during high rate discharges and is believed to be related to the manner in which $PbSO_4$ nucleates and grows as a function of discharge rate. It is postulated that, as the degree of refinement progresses, the reversible $PbO_2/PbSO_4$ transformation occurs more rapidly, and discharge duration decreases. It is tentatively concluded that trickle discharging interferes with this process by producing different sizes of $PbSO_4$ crystals by high and low rate growth mechanisms.

4. The corrosion layer formed on the external surface of the trickle discharged lead-calcium plate grid is thicker than the layer formed on the floated lead-calcium grid. The corrosion layer morphologies are also different. The trickle discharged layer consists of spiny, needlelike crystals whereas the floated plate layer is made up of asperity-covered grains.

5. The floated lead-antimony plate corrosion layer is thicker than either trickle-discharged or floated lead-calcium layers and is more easily removed by mechanical means.

6. The major component of positive plate active material throughout life is β-PbO_2. This applies to both lead-calcium and lead antimony grid plates.

VI. RECOMMENDATIONS

The results of this study represent an initial step in evaluating submarine lead-acid battery performance at the Naval Postgraduate School, utilizing the scanning electron microscope (SEM) as the primary research instrument. More work is necessary in this field and the following are suggested as possible areas for future research:

1. A distinct possibility exists that the patterned dendritic network of spiny crystals observed in the trickle-discharged positive plates is the same as the so-called "reticulate" structure seen by Simon in light microscopic evaluations of successfully floated lead-calcium plates [18]. It is recommended that further correlations be performed to confirm this hypothesis. Since it is felt that formation is dependent upon plate voltage, and that present float voltages (for the specific gravity used in the TLX-39B) are too high to support its development, this might lead to the adoption of lower float voltages for submarine service use which could result in capacity retention.

2. In order to gain a better understanding of positive plate morphology as a function of discharge rate, it is recommended that plate microstructure be examined at various rates of discharge.

3. $PbSO_4$ crystal development appears to be an integral part of the plate morphology and performance. $PbSO_4$ crystal formation and growth should be characterized as a function of discharge rate, discharge duration, and plate lifetime (i.e., do they become more uniform with increasing cycles?).

4. Recognizing that the quality of testing undertaken in this research was fraught with the inconsistencies associated with procedural and technique development, it is highly recommended that these tests be repeated in whole or in part to confirm the validity of the results.

5. In order to obtain a bona-fide failure of a floated cell within the time constraints of student research at the Naval Postgraduate School, it is recommended that accelerated life testing procedures specified in Reference 34 be undertaken.

APPENDIX A

The following discussion addresses features and operating characteristics of the two channel voltage controlled generator and programmable constant current discharge unit used in testing and was written by the designer of the apparatus.

2 CHANNEL VOLTAGE CONTROLLED CURRENT GENERATOR

AND

PROGRAMMABLE CONSTANT CURRENT DISCHARGE UNIT

T. Christian
Department of Mechanical Engineering
Naval Postgraduate School, Monterey, CA

This device (Figures 92 and 93) is a three channel unit each channel of which is separate and independent although they are all referenced to the same ground and share a common raw DC power supply for circuit power. In the case of the voltage controlled current generators charging power is derived from the raw DC supply as well. In no case can any channel be put in series or parallel with any other channel.

The voltage controlled current generators are identical in specifications and design. Each has two ranges, 0 to 7.5 milliamp and 0 to 75 milliamp. By joining the yellow and green connectors together a 0 to 7.5 volt regulated supply configuration capable of sourcing 100 milliamps can

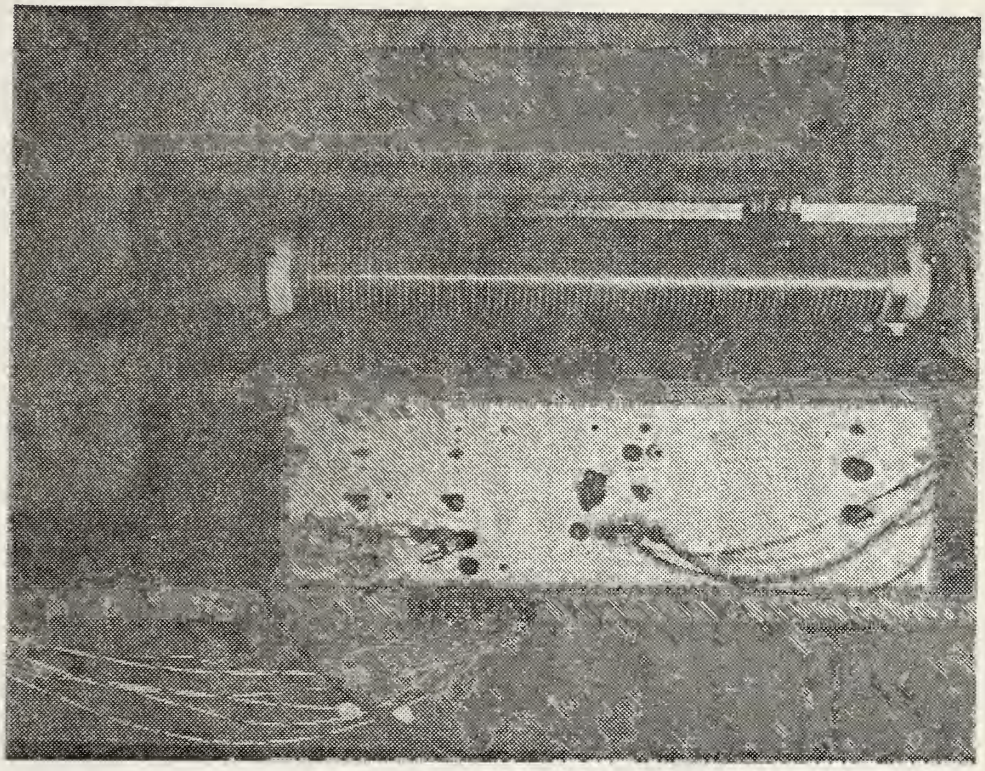

Figure 92 - 2-channel voltage controlled current generator (left) and programmable constant current discharge unit (right). Slide wire resistor mounted on top.

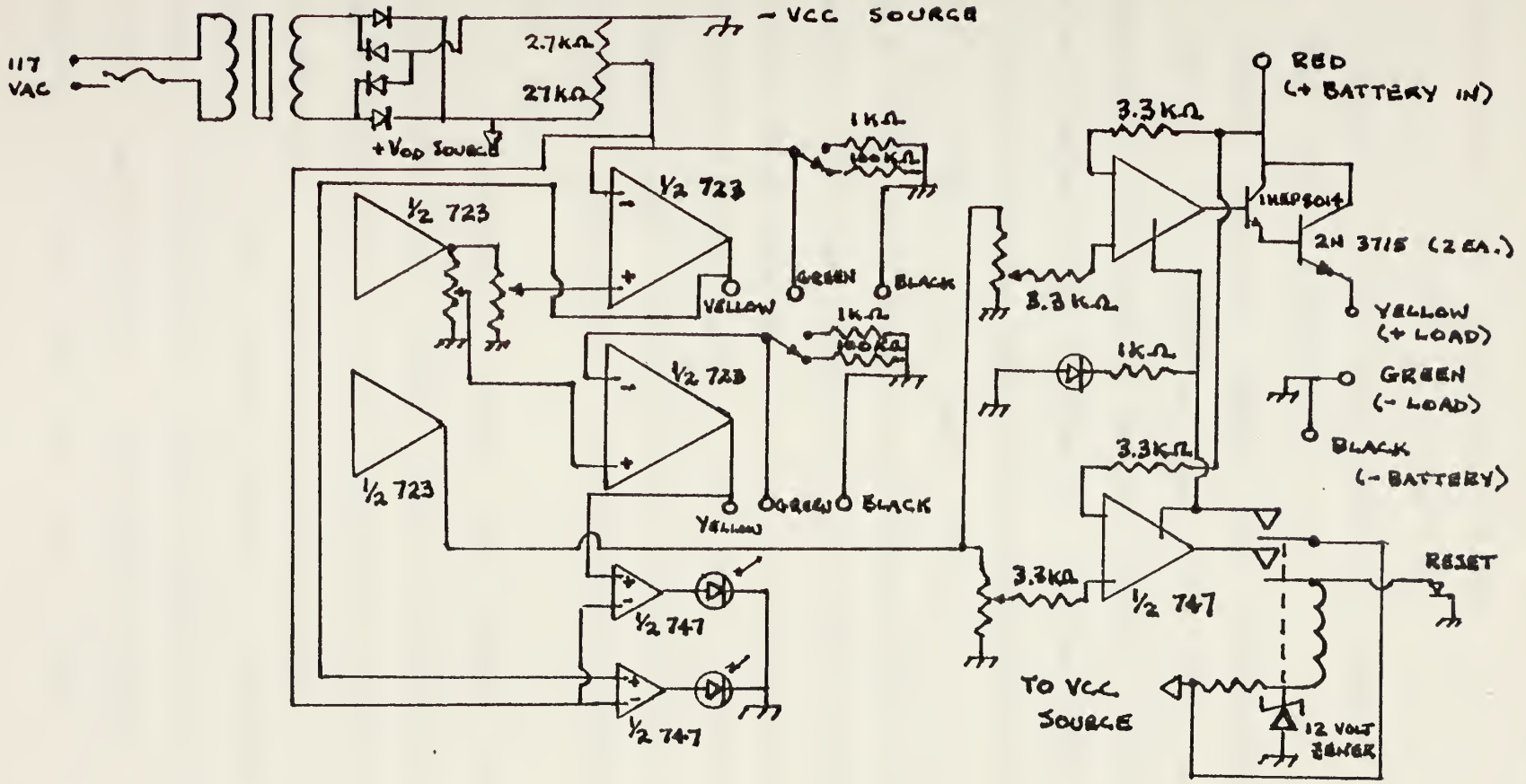

Figure 93 — Circuit drawing for 2-channel voltage controlled current generator and programmable constant current discharge unit

be realized from either channel as well. The primary design was, however, controlled current and the following specifications are for that configuration.

Voltage: 2.00 to 27 Volts DC

Current: to 75 milliamps in 2 ranges

Regulation: better than .1%

Dynamic response: better than 15 microseconds

The load is connected between the yellow and green connectors. The current can be measured either by a series ammeter or by reading the voltage between the GREEN and BLACK connectors and dividing by 100 for RANGE 2 or 1000 for RANGE 1. The control elements in each channel are actually regulating the voltage across a precision resistor (100 Ohms in RANGE 2, 1000 Ohms in RANGE 1). The load is in series with that precision resistor and since the current is the same in all parts of a series circuit (Kirchoff's Law) the current is regulated and controlled by the E/R relationship of the precision resistor (Ohm's Law).

Since the control elements must adjust the voltage across the load it follows that if the load resistance becomes very high, a high voltage will be required (Ohm's Law) in order to maintain constant current. The raw DC supply can provide about 30 VDC but in the event the voltage required is excessive, a voltage comparator has been included in each channel. The reference point of the comparators is 90% of available supply voltage and the sense

point is the current source point. If the voltage rises above the 90% reference point, the comparators activates the LED (light emitting diode) on each channel to alert the operator that the control element is in an unstable state and cannot be considered reliable.

The constant current discharge channel is basically a voltage controlled current generator with theory identical to the previously discussed channels with the exception of the precision resistor being replaced by a load resistor or load bank and the current source is external to the control circuit. The external current source (battery) is connected in series with the control element and load resistor (or load bank). The voltage across the load is maintained constant, thereby regulating the current. Voltage and current can be measured using the same methods previously discussed. Needless to say the operator must select a load resistor (or load bank) which will be within the limitations of the control element.

A dropout feature has been incorporated in the design which will cause the control element to be disabled when the source voltage (battery) falls below a present point selected by the operator. In addition a LED (light emitting diode) is energized when the control element is active to alert the operator of a stable control condition. When drop out occurs, the LED is extinguished. The control element will <u>not</u> restart regardless of the voltage at the

source point until the device is manually reset by the operator.

The following specifications apply to the constant current discharge channel.

Voltage: 2.00 to 5.5 VDC

Current: to 4.5 amps

Regulation: better than .1%

Dynamic Response: better than 15 microseconds

*Headroom: .6 to .9 Volts DC

Drop Out Differential: better than 5 millivolts

* Headroom is defined as the maximum voltage differential between the source voltage and the voltage across the load resistor.

APPENDIX B

TRICKLE DISCHARGE AND FLOAT OPERATION DATA

PbCa #1 Trickle Discharge Data

Cycles	Cells	Voltage			Specific Gravity			Battery
		High	Low	Average	High	Low	Average	Ave. Temp.
1	1	2.14	2.08	2.10	1.272	1.249	1.264	70° F
	2	2.13	2.07	2.09	1.268	1.247	1.260	
	3	2.13	2.08	2.10	1.270	1.250	1.261	
2	1	2.14	2.10	2.11	1.276	1.267	1.271	69° F
	2	2.13	2.09	2.11	1.267	1.260	1.265	
	3	2.13	2.10	2.12	1.271	1.264	1.268	
3	1	2.13	2.11	2.12	1.278	1.272	1.276	71° F
	2	2.12	2.10	2.11	1.272	1.264	1.269	
	3	2.12	2.11	2.11	1.274	1.266	1.271	
4	1	2.13	2.11	2.11	1.285	1.275	1.279	70° F
	2	2.12	2.11	2.11	1.277	1.269	1.272	
	4	2.12	2.09	2.10	1.266	1.258	1.261	
5	3	2.11	2.08	2.10	1.278	1.268	1.274	72° F
	2	2.12	2.10	2.11	1.276	1.265	1.271	
	4	2.11	2.09	2.10	1.270	1.253	1.260	
6	3	2.13	2.11	2.12	1.277	1.272	1.274	73° F
	2	2.12	2.11	2.12	1.276	1.268	1.272	
	4	2.12	2.10	2.11	1.265	1.258	1.261	
7	3	2.13	2.12	2.12	1.282	1.276	1.279	76° F
	2	2.12	2.11	2.11	1.277	1.271	1.274	
	4	2.11	2.10	2.11	1.268	1.262	1.266	

PbCa #1 - Trickle Discharge Data

Cycles	Cells	Voltage			Specific Gravity			Battery
		High	Low	Average	High	Low	Average	Ave. Temp.
8	3	2.13	2.11	2.12	1.280	1.267	1.275	72° F
	2	2.13	2.10	2.11	1.275	1.263	1.271	
	4	2.12	2.09	2.10	1.272	1.256	1.263	
9	5	2.11	2.10	2.10	1.272	1.260	1.266	71° F
	2	2.12	2.11	2.11	1.280	1.268	1.275	
	4	2.11	2.10	2.10	1.272	1.261	1.267	
10	5	2.13	2.10	2.11	1.282	1.261	1.272*	70° F
	2	2.13	2.11	2.12	1.279	1.274	1.276	
	4	2.12	2.11	2.11	1.280	1.269	1.271	
11	5	2.13	2.10	2.11	1.276	1.267	1.271	70° F
	2	2.14	2.12	2.13	1.282	1.276	1.279	
	4	2.13	2.11	2.12	1.278	1.271	1.274	
12	5	2.12	2.11	2.11	1.271	1.265	1.267	72° F
	2	2.13	2.11	2.12	1.278	1.274	1.275	
	4	2.12	2.11	2.11	1.273	1.268	1.270	
13	5	2.13	2.10	2.12	1.276	1.265	1.271	72° F
	2	2.14	2.11	2.12	1.282	1.273	1.277	
	4	2.13	2.11	2.12	1.277	1.268	1.272	

* Leak occurred during cycle and cell was refilled with lower S.G. electrolyte

PbCa #2 Float

Cycles	Cells	Average Voltage	Average Specific Gravity	Battery Average Temperature
1	1	2.29	1.271	70° F
	2	2.28	1.272	
	3	2.30	1.272	
2	1	2.34	1.271	69° F
	2	2.31	1.273	
	3	2.34	1.272	
3	1	2.35	1.272	71° F
	2	2.31	1.273	
	3	2.33	1.274	
4	1	2.35	1.272	71° F
	2	2.32	1.273	
	3	2.34	1.273	
5	4	2.28	1.268	71°F
	2	2.35	1.273	
	3	2.37	1.274	
6	4	2.30	1.268	72° F
	2	2.33	1.273	
	3	2.34	1.274	
7	4	2.31	1.271	72° F
	2	2.33	1.274	
	3	2.34	1.275	
8	4	2.31	1.272	74° F
	2	2.32	1.275	
	3	2.34	1.276	

PbCa #2

Cycles	Cells	Average Voltage	Average Specific Gravity	Battery Average Temperature
9	4	2.31	1.274	71° F
	2	2.32	1.278	
	3	2.34	1.279	
10	4	2.32	1.276	72° F
	2	2.32	1.279	
	3	2.34	1.281	
11	4	2.38	1.276	68° F
	5	2.16	1.274	
	3	2.39	1.280	
12	4	2.35	1.278	69° F
	5	2.19	1.279	
	3	2.36	1.284	
13	4	2.36	1.281	71° F
	5	2.20	1.282	
	3	2.34	1.286	
14	4	2.36	1.281	72° F
	5	2.26	1.283	
	3	2.32	1.285	
15	4	2.36	1.282	72° F
	5	2.28	1.284	
	3	2.31	1.286	
16	4	2.37	1.282	73° F
	5	2.30	1.284	
	3	2.33	1.286	

PbSb Float

Cycles	Cells	Average Voltage	Average Specific Gravity	Battery Average Temperature
1	1	2.17	1.253	69° F
	2	2.18	1.252	
	3	2.18	1.251	
2	1	2.27	1.252	70° F
	2	2.27	1.250	
	3	2.28	1.251	
3	1	2.27	1.252	69° F
	2	2.28	1.251	
	3	2.28	1.251	
4	1	2.28	1.253	71° F
	2	2.28	1.252	
	3	2.29	1.252	
5	1	2.31	1.254	72° F
	2	2.30	1.253	
	4	2.23	1.254	
6	1	2.30	1.254	72° F
	2	2.30	1.252	
	4	2.24	1.254	
7	1	2.29	1.255	76° F
	2	2.29	1.253	
	4	2.25	1.255	
8	1	2.30	1.259	72° F
	2	2.29	1.255	
	4	2.26	1.256	

PbSb

Cycles	Cells	Average Voltage	Average Specific Gravity	Battery Average Temperature
9	1	2.32	1.263	71° F
	2	2.28	1.258	
	4	2.25	1.256	
10	5	2.25	1.254	69° F
	2	2.32	1.258	
	4	2.27	1.258	
11	5	2.25	1.257	69° F
	2	2.32	1.260	
	4	2.28	1.256	
12	5	2.27	1.259	72° F
	2	2.32	1.260	
	4	2.26	1.259	
13	5	2.27	1.259	72° F
	2	2.30	1.260	
	4	2.25	1.261	

APPENDIX C

CAPACITY TEST DISCHARGE RESULTS

PbCa #1 (Trickle Discharge) - Record of Test Discharge

Cycles	Cells	Specific Gravity Start	Finish	Duration Hrs:Min	Limiting Cell
2	1	1.281	1.233	3:26	#3
	2	1.275	1.234		
	3	1.278	1.230		
4	1	1.283	1.248	3:34	#4
	2	1.278	1.240		
	4	1.268	1.234		
5	3	1.275	1.243	3:37	#3
	2	1.273	1.241		
	4	1.265	1.239		
7	3	1.281	1.249	3:53	#3
	2	1.276	1.244		
	4	1.268	1.233		
8	3	1.276	1.248	3:52	#4
	2	1.277	1.239		
	4	1.273	1.238		
9	5	1.274	1.240	3:42	#5
	2	1.283	1.251		
	4	1.274	1.240		

PbCa #1 (Continued)

Cycles	Cells	Specific Gravity Start	Finish	Duration Hrs:Min	Limiting Cell
10	5	1.275	1.240	3:44	#5
	2	1.282	1.248		
	4	1.277	1.240		
12	5	1.277	1.243	3:59	#5
	2	1.283	1.246		
	4	1.280	1.243		
13	5	1.275	1.238	4:13.5	#5
	2	1.280	1.248		
	4	1.277	1.241		

PbCa #2 (Float) - Record of Test Discharge

Cycles	Cells	Specific Gravity Start	Finish	Duration Hrs:Min	Limiting Cell
0	1	1.266	1.240	2:44	#1
	2	1.270	1.235		
	3	1.270	1.238		
1	1	1.273	1.247	2:40	#1
	2	1.275	1.248		
	3	1.274	1.247		
3	1	1.273	1.250	2:52	#1
	2	1.275	1.245		
	3	1.276	1.247		
4	1	1.275	1.246	2:45	#1
	2	1.276	1.252		
	3	1.276	1.250		
5	4	1.270	1.242	3:10	#3
	2	1.274	1.246		
	3	1.276	1.244		
6	4	1.268	1.244	3:15	#3
	2	1.275	1.242		
	3	1.277	1.242		
7	4	1.271	1.252	3:15	#3
	2	1.275	1.242		
	3	1.277	1.240		
8	4	1.272	1.248	3:19	#3
	2	1.278	1.248		
	3	1.278	1.246		

PbCa #2 (Continued)

Cycles	Cells	Specific Gravity Start	Finish	Duration Hrs:Min	Limiting Cell
9	4	1.275	1.243	3:22	#3
	2	1.279	1.243		
	3	1.281	1.245		
10	4	1.277	1.243	3:30	#3
	2	1.281	1.249		
	3	1.283	1.248		
11	4	1.276	1.248	3:24	#3
	5	1.276	1.248		
	3	1.280	1.253		
12	4	1.281	1.247	3:29	#3
	5	1.279	1.242		
	3	1.283	1.251		
13	4	1.282	1.254	3:36	#3
	5	1.285	1.254		
	3	1.286	1.261		
14	4	1.280	1.253	3.29	#3
	5	1.282	1.253		
	3	1.284	1.249		
15	4	1.282	1.249	3:37	#3
	5	1.283	1.247		
	3	1.285	1.247		
16	4	1.282	1.250	3:36	#3
	5	1.285	1.254		
	3	1.286	1.252		

PbSb (Float) - Record of Test Discharge

Cycles	Cells	Specific Gravity Start	Specific Gravity Finish	Duration Hrs:Min	Limiting Cell
0	1	1.253	1.204	5:25	#2
	2	1.250	1.200		
	3	1.250	1.204		
1	1	1.252	1.198	5:39	#2
	2	1.252	1.203		
	3	1.252	1.199		
2	1	1.251	1.210	5:06	#2
	2	1.249	1.208		
	3	1.249	1.206		
3	1	1.253	1.204	5:29	#2
	2	1.251	1.202		
	3	1.251	1.201		
4	1	1.253	1.219	5:32	#2
	2	1.251	1.219		
	4	1.251	1.219		
5	1	1.255	1.233	5:46	#2
	2	1.253	1.238		
	4	1.254	1.236		
7	1	1.256	1.221	5:50	#2
	2	1.255	1.220		
	4	1.256	1.220		
8	1	1.259	1.224	5:22	#2
	2	1.255	1.218		
	4	1.257	1.219		

PbSb (Continued)

Cycles	Cells	Specific Gravity Start	Specific Gravity Finish	Duration Hrs:Min	Limiting Cell
9	1	1.263	1.230	5:18	#2
	2	1.260	1.223		
	4	1.257	1.223		
10	5	1.258	1.220	5:15	#2
	2	1.259	1.223		
	4	1.259	1.224		
11	5	1.258	1.223	5:11	#2
	2	1.260	1.228		
	4	1.259	1.228		
12	5	1.259	1.228	5:06.5	#2
	2	1.262	1.232		
	4	1.260	1.227		
13	5	1.261	1.229	5:05	#2
	2	1.262	1.234		
	4	1.262	1.230		

LIST OF REFERENCES

1. Vinal, G.W., Storage Batteries, 4th ed., Wiley, New York, 1955.

2. Hoffman, W., Lead and Lead Alloys, English Translation of the 2nd Revised German Ed., Springer-Verlag, New York, 1970.

3. Naval Ships' Technical Manual, Chapter 9623, Submarine Lead-Acid Storage Batteries, 1 June 1973.

4. Willinghanz, E., "How to Get More Out of Your Float Battery Plant," Telephony, January 17, 1972.

5. Naval Research Laboratory Report 5773, The Lead Calcium Battery: Part 3 - Submarine Cells, by J. Burbank and C.P. Wales, 29 May 1962.

6. Smith, G., Storage Batteries: Including Operation, Charging, Maintenance and Repair, Pitman & Sons, London, 1964.

7. International Lead Zinc Research Organization, Inc. Final Report on ILZRO Projects LE-82 and LE-84, Pastes and Grids for the Lead-Acid Battery, by Stephenson, H.B., and others representing Eagle-Picher Industries, Inc. and ILZRO, 31 December 1971.

8. Mao, G.W., Larson, J.G., and Rao, P., "The Microstructure of Lead Based Alloys," Metallography, v. 1, p. 399-423, January, 1969.

9. Burbank, J., Simon, A.C., and Willinghanz, E., The Lead-Acid Cell, from Advances in Electrochemistry and Electrochemical Engineering, Vol. 8, (ed. P. Delahay and C.W. Tobias), Wiley, 1971.

10. Mao, G.W., Larson, J.G., and P. Rao, "Recent Results on Lead-Calcium Alloys as Grid Materials for Lead-Acid Batteries," Journal of the Electrochemical Society, v. 120, p. 11-17, January, 1973.

11. Burbank, J., "Morphology of PbO_2 in the Positive Plates of Lead Acid Cells," Journal of the Electrochemical Society, v. 111, p. 765-768, July, 1964.

12. Naval Research Laboratory Report 5693, The Lead Calcium Battery: Part 1 - Introduction and Background, by J. Burbank and C.P. Wales, 22 November 1961.

13. Milner, P.C., "Float Behavior of the Lead-Acid Battery System," The Bell System Technical Journal, v. 49, p. 1321-1334, September, 1970.

14. Naval Research Laboratory Report 5770, The Lead Calcium Battery: Part 2 - Small Portable Cells, by J. Burbank and C.P. Wales, 2 May 1962.

15. Naval Research Laboratory Report 6078, The Lead Calcium Battery: Part 4 - Comparison of Lead Calcium and Lead Antimony Cells in Float, by J. Burbank, 10 June 1964.

16. Tudor, S., Weisstuch, A., and Davang, S.H., "Positive Plate Sulfation Processes in Thin- and Thick-Plate Pb-Ca Grid Batteries," Electrochemical Technology, v. 5, p. 21-25, Jan-Feb 1967.

17. Ruetschi, P., Capacity Loss of Ca-Pb Alloy Cells On Float, comments on Eidensohn's observations relating to Pb-Ca Alloy Cells on Float (SE/CGG - 4/7/59) Yardley, Penna., 11 May 1959.

18. Naval Research Laboratory Report 6292, Active Material Retention in the Lead-Acid Battery - The Role of $PbSO_4 \cdot 4PbO$ and α-PbO_2, by A.C. Simon, 24 June 1965.

19. Hart, A., Daniels, E.L., and Horner, W.J., Photo-Micrographic Examinations Preliminary Investigations, a preliminary report in conjunction with Electric Storage Battery Project 1356, Lead Calcium Submarine Battery Investigation, February 27, 1963.

20. Naval Sea Systems Command Manual 0962-073-4010, Service Manual for U.S. Submarine Main Storage Battery Guppy 1 Mod C Type TLX-39-B, 30 April 1973.

21. Gould, Inc., letter AJP/276/14 of 27 February 1976.

22. Gould, Inc., Instruction Sheets for the Gould Type TPX-61-E, April 1967.

23. Cambridge Scientific Instruments Limited, Manual TL 1116-OM-96118-0002, Stereoscan S4-10 Scanning Electron Microscope, Issue 1.

24. International Lead Zinc Research Organization, Inc., ILZRO Lead Research Digest, No. 31, 1973.

25. Simon, A.C., Caulder, S.M., and Stemmle, J.T., "Structural Transformations of the PbO_2 Active Material During Cycling," Journal of the Electro-Chemical Society, v. 122, pp. 416-466, April, 1975.

26. Burbank, J. and Ritchie, E.J., "PbO_2 in the Lead-Acid Cell," Journal of the Electrochemical Society, v. 116, pp. 125-130, January, 1969.

27. Burbank, J., "Crystallization of $PbSO_4$ on Anodes of Lead-Antimony Alloy," Journal of the Electrochemical Society, v. 118, pp. 525-529, April, 1971.

28. Naval Research Laboratory Report 7256, Anodic Crystallization on Pure and Antimonial Lead in Sulfuric Acid, by J. Burbank, 24 May 1971.

29. Burbank, J., "The Anodic Oxides of Lead," Journal of the Electrochemical Society, v. 106, pp. 369-375, May, 1959.

30. Pavlov, D., Poulieff, C.N., Klaja, E., and Iordanov, N., "Dependence of the Composition of the Anodic Layer on the Oxidation Potential of Lead in Sulfuric Acid," Journal of the Electrochemical Society, v. 116, pp. 316-319, March, 1969.

31. Burbank, J., "Anodization of Lead and Lead Alloys in Sulfuric Acid," Journal of the Electrochemical Society, v. 104, pp. 693-701, December, 1957.

32. Pokorny, J.L., Study of the Cyclic Performance of Submarine Type Lead-Acid Storage Batteries by Examination of the Positive Plate Structures, MSME - Mechanical Engineer Thesis, Naval Postgraduate School, (in publication, 1976).

33. Burbank, J., "Positive Plate Characteristics in the Floating Lead Calcium Cell," in Batteries, Research and Development in Non-Mechanical Electrical Power Sources, Proceedings of 3rd International Symposium held at Bournemouth, Oct. 1962, London: Pergamon Press, p. 43, 1963.

34. Maskalick, N.J., "Accelerated Life Testing of Lead-Acid Industrial Motive Power Cells," Journal of the Electrochemical Society, v. 122, pp. 19-25, January, 1975.

35. COMSUBLANT Instruction 9620.10G, "Operation and Maintenance of Submarine Main Storage Batteries," 17 March 1975.

INITIAL DISTRIBUTION LIST

		No. Copies
1.	Defense Documentation Center Cameron Station Alexandria, Virginia 22314	2
2.	Library, Code 0212 Naval Postgraduate School Monterey, California 93940	2
3.	Department Chairman, Code 59 Department of Mechanical Engineering Naval Postgraduate School Monterey, California 93940	2
4.	Professor A.J. Perkins, Code 59Ps Department of Mechanical Engineering Naval Postgraduate School Monterey, California 93940	5
5.	LCDR M. T. Coyle, USN Engineering Duty Officer School Class 4-76B Mare Island Vallejo, California 94592	5